Study of a pulse tube refrigerator by direct measurement of working gas velocity and temperature

１９９７年３月

瀬尾和哉

Abstract

It has been recognized that in order to understand the refrigeration mechanism of a pulse tube refrigerator the in-situ measurement of the thermo-fluid dynamic state of the interior gas such as the velocity, the temperature and the pressure is strictly necessary as well as the measurement of the wall temperature as obtained in the previous researches. We made a in-situ measurement of the velocity and the temperature of gas inside a pulse tube simultaneously with a hot wire anemometer as well as the measurement of the pressure in the state where the pressure and the temperature dynamically vary in the ranges of the pressure from 0.1 MPa to 1.5 MPa and of the temperature from 220 K to 320 K for helium gas. As a result, it becomes first possible to draw a realistic P-V diagram on the basis of the measurement data of the gas velocity in addition to the pressure and temperature variations measured in the radial and longitudinal directions. The discussion is focused on the difference among the refrigeration performance of each type of a pulse tube refrigerator, that are a basic, an orifice and a double inlet types. It is first experimentally confirmed that the P-V work is mostly produced owing to the viscous effect in the basic type. In the case of the orifice and double inlet types the P-V work is far larger than that of the basic type by the fluid dynamic effect of the orifice valve-reservoir combination. This is the explanation why the refrigeration performance is improved in the orifice and double inlet types as compared with the basic type. Moreover, the dependence of the performance on the driving frequency and the valve opening are discussed.

Contents

Chapter 1

Introduction

1.1 Introduction.

The need for cryogenic cooling in satellite applications has brought about a strong requirement for high reliability refrigerators [1], [2]. Figure 1-1 shows the temperature range and the mission duration for a number of current cryogenic cooling techniques. A space cryogenic cooling system should be reliable without any maintenance during a whole mission for 3～5 years. The refrigeration power in an earth observation mission, for example, requires about several W in 70～100 K range. In this temperature range a radiator is available, but the refrigeration power is limited to a small value and the cooled elements hardly reach below 80 K. Moreover, its refrigeration power strongly depends on the attitude and the geometrical configuration of a satellite. To reach below 80 K, a stored cryogen, such as liquid helium, has been utilized. The total amount of cryogen is limited by the launching capability of a rocket, and thus the life time of a mission cooled by stored cryogen is limited not so long. From a view point of long term mission, closed-cycle cryogenic cooling system, that is a small refrigerator, is the most adequate for space cryogenics in the temperature range at least above 70 K.

A simple approach to higher reliability in the application of a small refrigerator is to eliminate some moving parts in a mechanical refrigerator. A Stirling refrigerator which has been frequently used for cooling infrared sensors has two mechanically moving parts, pistons in the compression and expansion spaces. In 1963, Gifford and Longsworth invented a refrigerator based on a Stirling refrigerator in which a displacer was replaced with a hollow tube [3]. They named this new type refrigerator a Pulse tube (PT) refrigerator. The technology is led to a small refrigerator which has the potential for lower cost, higher reliability and less vibration at the cold end, but with a penalty of low efficiency. However, the efficiency is now significantly improved to be competitive with that of Stirling refrigerators. It seems that PT refrigerators are now at the beginning to replace Stirling refrigerators in particular in space applications.

1.2 Development of a Pulse tube refrigerator.

Several variations of PT refrigerators have been developed for higher performance. A schematic of three types of PT refrigerators is shown in figure 1-2. The type (a) is now called a basic PT refrigerator which is an original PT refrigerator first developed by Gifford and Longsworth [4], [5]. Types (b) and (c) are named an orifice and a double inlet PT refrigerators according to the structural configuration around the hot end. The orifice type is characterized by a reservoir connected to a pulse tube via an orifice valve. In the double inlet type, a pipe is added to the orifice

type between a hot end and an entrance of the regenerator. Table 1-1 shows the chronology of PT refrigerators. The improvement of minimum attainable temperature are plotted against time in figure 1-3. Gifford and Longsworth reached a temperature of 124 K with a single-stage design, 79 K with a double stage model and 30 K by operating from 65 K at a hot end [6]. It is seen from figure 1-3 that after the initial development phase of basic PT refrigerators no innovations were attempted for twenty years owing to low performance. However, since Mikulin et al. [7] developed an orifice PT refrigerator in 1983, remarkable development has been done. Radebaugh et al. [8] were able to achieve a low temperature of 60 K with a modified version of Mikulin's work in 1987. Zhu et al. [9] achieved 49 K refrigeration with a double inlet PT refrigerator. The current lowest record of 3.6 K was established by Matubara and Gao with a three-stage refrigerator [10], [11], [12]. Now many laboratories around the world are involved in the investigation of PT refrigerators.

The refrigeration performance of a PT refrigerator, mostly focused on the attainable lowest temperature, have been improved by cut and try method [13], [14], [15]. It is, however, necessary to make clear the refrigeration mechanism further to improve the refrigeration performance. Several researchers have attempted to explain the PT refrigeration mechanism in terms of the surface heat pumping mechanism [16],[17], the enthalpy flow model [18],[19] or the thermo-acoustic theory [20],[21], [22]. Though the present enthalpy flow model and the thermo-acoustic theory fairly well agree with the experimental results qualitatively, quantitative agreement is rather

poor. One of the major reason for the quantitative discrepancy is that the thermo-fluid dynamic gas motion is in fact far from small amplitude variation which is inherently assumed in the theories.

1.3 Working principle of a Pulse tube refrigerator.

The refrigeration mechanism of the Stirling refrigerator is explained on the basis of the thermodynamic cycle shown in figure 1-4. The cycle is composed of four thermodynamic processes, $1 \rightarrow 2$; isothermal compression, $2 \rightarrow 3$; isochoric process, $3 \rightarrow 4$; isothermal expansion and $4 \rightarrow 1$; isochoric process. The working gas rejects heat Q_h at the hot end during isothremal compression process, and then its temperature decreases from T_h to T_c by the heat exchange between the working gas and the regenerator materials during isochoric process. After that the working gas absorbs heat Q_c at the cold end during isothrmal expansion process, and last its temperature increases from T_c to T_h during isochoric process. It should be noted that the control of the relative movement of two pistons in the compression and the expansion spaces generates a suitable phase difference in the oscillating motions between the pressure and the volume. As a result, P-V work is produced, and accordingly refrigeration is provided. In PT refrigerators, what produces the phase difference? It is considered that the viscous delay in the oscillating boundary layer flow generates the phase difference in the basic PT refrigerator. In fact, the refrigeration power is rather small because the phase delay in a dissipative process is

made use of. On the other hand, in the orifice and the double inlet PT refrigerators, the combination of an orifice and a reservoir, or of the double inlet valve are positively utilized to generate the phase difference. It should be noted that the way to generate the phase difference in the orifice and the double inlet PT refrigerators is more efficient than that of the basic PT refrigerator.

In order to understand the refrigeration mechanism in a PT refrigerator, let's consider a compression and a subsequent expansion processes during a steady operation. When a rapid compression process occurs, the gas element originally occupying the tube at low pressure is compressed isentropically while being displaced towards the closed end (hot end) of the tube. The temperature resulted from isentropic compression is considerably higher than the average gas temperature. The degree of displacement and compression experienced by a gas element will depend on the initial location of the element at the low pressure. The temperature becomes higher as the initial location is close to the closed end. A gas element flowing into a pulse tube from a regenerator just after the onset of compression process experiences considerable temperature rise while an element which enters the tube when the pressure is close to equilibrium state undergo little temperature rise. Accordingly, at the end of compression process a significant temperature gradient develops in the gas of a pulse tube. In the high pressure period, the temperature of the gas element near the wall falls as a result of heat transfer to the surroundings. In the expansion process the gas temperature drops further. If the expansion process isentropically

proceeds, the gas temperature drops below that at the onset of the compression process, that is to say, below ambient one. At this stage the temperature becomes lower towards the cold end. Some heat is absorbed in the cold end section as a refrigeration action. Consequently a refrigeration is accomplished, in which heat is absorbed in the cold end section, displaced towards the hot end side during compression process, and is exhausted at higher temperature as a result of gas compression in the hot end section.

1.4 Objectives of the present research.

It is recognized in order to understand the refrigeration mechanism both qualitatively and quantitatively the in-situ measurement of the thermo-fluid dynamic state of the interior gas such as the velocity, the temperature and the pressure is strictly necessary as well as the measurement of the wall temperature as obtained in the previous researches. This is thus the very objective of the present study. We directly measure the velocity, the temperature and the pressure of interior gas inside a pulse tube. The discussion is focused on the difference among the refrigeration performance of each type of PT refrigerator. Moreover, the difference of the performance on the driving frequency and valve openings are discussed.

1.5 Scope of this thesis.

In the following chapter 2, the experimental apparatus, in which the

velocity, the temperature and the pressure variations are measured in the PT refrigerator, will be explained. A method of calibration of a hot wire anemometer in the state where the pressure and the temperature dynamically vary in the ranges of the pressure from 0.1 MPa to 1.5 MPa and of the temperature from 220 K to 320 K for helium gas is discussed. The experimental procedures for the experiment of a start-up behavior and the steady state experiment are also described.

In chapter 3, a start-up behavior of a PT refrigerator is investigated by measuring the transient temperature variation. The point of this experiment is to investigate whether the wall temperature distribution along the pulse tube is essential or not for the refrigeration. The results can be summarized as follows. In first several cycles, the remarkable temperature difference between the cold end and the hot end appears in gas, so that the gas temperature difference is produced by only the gas motion, and does not rely on the wall temperature distribution along the pulse tube essentially to a fundamental refrigeration mechanism.

In chapter 4, the refrigeration mechanism for the basic type is investigated on the basis of the thermodynamics discussion. The reason why the P-V work is produced is investigated from the radial distributions of the velocity. It is confirmed that the phase difference between the pressure and the displacement of the gas element is generated near the wall owing to the viscous effect. Moreover, the effect

of the driving frequency for the performance is also discussed.

In chapter 5, the refrigeration mechanism for the orifice type is discussed. It is found that the phase difference between the pressure and the displacement in the orifice type approaches 90 degree compared to the basic type. Moreover, the amplitude of the displacement variation becomes larger than the basic type. Therefore, P-V work are quite larger than that of the basic type. In addition, the effect of the orifice valve openings for the performance are also discussed.

In chapter 6, the refrigeration mechanism for the double inlet type is discussed by taking account into the difference from the orifice type. It is found that P-V work in the double inlet type becomes smaller than that of the orifice type because of the decrease of the amplitude of the displacement variation compared to the orifice type, though the performance of the double inlet type is improved.

In chapter 7, the refrigeration mechanism for a PT refrigerator will be organized.

Chapter 2

Experiment

2.1 Experimental apparatus.

The schematic of the experimental apparatus is shown in figure 2-1. It is designed primarily for the direct measurement of the velocity, the temperature and the pressure of working gas at several points along the pulse tube refrigerator. Accordingly, the pulse tube and the regenerator are only wrapped with polyurethane thermal insulator instead of installing them in a vacuum chamber for thermal isolation from the atmospheric environment at the room temperature. A commercially available helium compressor unit designed for a Gifford-Macmahon refrigerator (SRD-208, Sumitomo Heavy Industries) and a rotary valve are employed to generate prescribed pressure variation in the pulse tube unit. The frequency of the pressure variation can be varied from 0 to 20 Hz. The pressure ratio between the high and low pressures can be changed from 1 to 3.4 by adjusting the opening of the bypass valve connecting the high pressure exit to the low pressure inlet of the compressor. The regenerator is composed of a stainless steel housing and a bakelite tube, 35 mm in diameter by 160 mm long , packed with 865 discs of 100 mesh stainless steel screen.

The pulse tube is made of stainless steel, 15.6 mm in inner diameter, 1.7 mm in wall thickness and 288 mm long. Two short pieces of copper tube with a length of 26 mm and 33 mm are soldered to the stainless steel tube at both ends as heat exchangers. One at the hot end is kept at the room temperature with a forced flow of cooling water. The heat rejection rate from it, denoted as the heat-out, is evaluated from the temperature rise of cooling water and the mass flow rate. The other functions as the cold head. Two capillary tubes are connected to the hot end of the pulse tube, one leading to the reservoir having a volume of 603 cm^3 through the orifice valve, V_o, and the other returning to the entrance of the regenerator through the double inlet valve, V_d. A particular type of pulse tube refrigerator can be selected by opening V_o for the orifice type, V_o and V_d for the double inlet type. A number of branch tubes are also welded to the refrigerator at the cold end, the middle point and the hot end as feedthroughs for hot wire probes and thermocouples as shown in figure 2-1.

The gas pressure is measured with a strain gauge type pressure transducer at the entrance of the regenerator and in the reservoir, and the gas temperature by an E-type (Chromel/Constantan) sheathed thermocouple of 150 μm in diameter. The thermoelectric power of thermocouples, amplified by 500 times with an amplifier, is acquired with a personal computer with the aid of a 16 bit-DMA A/D converter board (ADXG-16, Canopus). The thermoelectric power is converted to temperature on the basis of the JIS thermocouples table (JIS C 1602). The nominal response times of the pressure transducer and the thermocouple are about 0.25 msec (4 KHz) and 5

msec (200 Hz), respectively. However, a practical response time of the thermocouple is found to be 15 msec (70 Hz) in the working gas. T-type (Copper/Constantan) thermocouples are also soldered on the outer surface of the pulse tube at seven points to measure the wall temperature. These data are acquired with a multi-channel digital recorder and then are transferred and stored with a personal computer via GP-IB.

The probe for velocity measurement is composed of a set of hot wire element of 25 μm diameter of platinum wire and an E-type sheathed thermocouple of 150 μm in diameter, attached to one end of a 4 mm diameter stainless steel tube (see Figure 2-2). By the use of this probe it becomes possible to measure the velocity and temperature variations simultaneously at the same position. Owing to the simultaneous measurement, the velocity of working gas, of which temperature varies in a wide range, can be measured with a hot wire. The correction of the temperature and pressure effects to the hot wire output is made with the aid of an in-house software on a personal computer. The probe is tightened by Swage Locks with Teflon rings for the sake of easy traversing.

2.2 Calibration of a hot wire anemometer.

As mentioned above, in the present study it is strictly necessary to calibrate the hot wire anemometer under the condition where the temperature and the pressure vary in wide ranges simultaneously. Moreover, we should consider the fact

that the working gas is helium, not air. Figure 2-2 shows the schematic arrangement for the calibration system. The hot wire anemometer is operated in the constant current mode with a heating ratio of 1.4 with respect to the mean gas temperature. The heating ratio of 1.4 means that the temperature difference, ΔT, between the surface of the hot wire T_w and the working gas T_f equals 103 K as described from equation (2-1).

$$\frac{R_h}{R_c} = 1 + \alpha \Delta T \qquad (2\text{-}1)$$

Here, R_h and R_c are electric resistance at T_f and the mean gas temperature, respectively, and α is a temperature coefficient. The pressure of working gas flow is controlled by a pressure regulator, and the temperature is done by heating or cooling the gas line in the heat exchanger kept at a prescribed temperature. The relation between the output voltage of the hot wire anemometer V and the velocity U is expressed on the basis of King's law as follows,

$$V^2 = \left(A + B\sqrt{U}\right)\Delta T \qquad (2\text{-}2)$$

Substituting the relation in the case of zero velocity, $V_0^2 = A\Delta T$, into (2-2) one gets

$$\frac{V^2 - V_0^2}{V_0^2} = \frac{B}{A}\sqrt{U} = C\sqrt{U}, \qquad (2\text{-}3)$$

where, V_0 is the output of the hot wire anemometer when U=0. It is seen from equation (2-3), U can be obtained provided that C and V_0 are empirically given. For this purpose, the temperature and pressure dependencies of C and V_0 are investigated in the ranges of 220 K $\sim$ 320 K and 0.1 MPa $\sim$ 1.5 MPa, covering the whole

present experimental condition.

Figure 2-3 shows the typical example of the temperature dependency of V at 0.1 MPa. Since the heating ratio is kept at a constant value 1.4, at any mean gas temperatures as mentioned above, V becomes almost independent of the gas temperature, and thus all the data are found to follow a single curve. A number of data examples of the pressure dependency of V measured at 300 K are shown in figure 2-4. The output signal is larger in the case of higher pressure at the same velocity. It can be concluded that C is almost independent of the temperature, but strongly depends on the pressure. It is seen from equation (2-3) that the constant C is derived from the slope of the data in a $U^{0.5}$ vs. (V^2/V_0^2-1) diagram as given in figure 2-5. The non-zero x- intercept of the data correlation line in figure 2-5 estimated to be about 0.5 m/sec, indicates the lower bound of the measurement of the velocity imposed by the effect of natural convection. Therefore, in the practical calibration, equation (2-3) may be rewritten in terms of y-intercept, D, instead of the x-intercept, as follows.

$$\frac{V^2 - V_0^2}{V_0^2} = C(p)\sqrt{U} + D \qquad (2\text{-}4)$$

Neglecting heat conduction and radiation, the energy balance around the hot wire element becomes

$$\frac{I^2 \rho_r}{A} = \pi d h \Delta T \qquad (2\text{-}5)$$

where I denotes the electric current, ρ_r is the coefficient of electric resistance, A is the

cross sectional area of the hot wire element, d is the diameter and h is the heat transfer coefficient between the hot wire element surface and gas flow. Eliminating h from equation (2-5) with the aid of the definition of the Nusselt number, $Nu=hd/\kappa_f$, one gets

$$Nu = \frac{I^2 R_s}{\pi l \kappa_f \Delta T}, \qquad (2\text{-}6)$$

where l is the length of the hot wire element, κ_f is the thermal conductivity of the fluid, and $R_s=\rho_r l/A$, is the electric resistance.

On the other hand, an empirical equation of heat transfer for forced convection around circular wire is given by Collins and Williams [23] as

$$Nu\left(\frac{T_m}{T_f}\right) = 0.24 + 0.56\,\mathrm{Re}^{0.45}. \qquad (2\text{-}7)$$

Here T_m is the mean temperature of the fluid and the hot wire element, and Re denotes the Reynolds number. Equation (2-7) is valid in the range of Reynolds number from 0.02 to 44. Combining equations (2-6) and (2-7) to eliminate Nu, one finds

$$V^2 = \left(\frac{T_m}{T_f}\right)^{0.17}\left\{0.24 + 0.56\left(\frac{PUd}{\mu RT}\right)^{0.45}\right\}\pi l \kappa_f R_s \Delta T \qquad (2\text{-}8)$$

It is seen from equation (2-8) that V^2 is proportional to $P^{0.45}$ if other parameters are kept constant. Considering the relation $V^2 \propto P^{0.45}$ and equation (2-4), C(p) is found to be proportional to $P^{0.45}$. Figure 2-6 shows these relations for a number of experimental data. In practice, C(p) may be approximately expressed as a function of $P^{0.5}$ as shown in figure 2-7. The dependency of D is also shown in figure 2-7. D

may be approximated as a constant value in the present experimental pressure range. V_0^2 is found to be almost independent of the pressure as seen from figure 2-6. The only temperature dependency is taken into account for V_0^2. The relation of V_0^2 to the temperature may be regarded to be linear as shown in figure 2-8. Therefore, the final correlation formula for the velocity is obtained from equation (2-9) as follows.

$$U = \left\{ \left(\frac{V^2 - V_0^2(T_f)}{V_0^2(T_f)} - D \right) \Big/ C(P) \right\}^2 \qquad (2\text{-}9)$$

The error of the velocity measurement is estimated from the plot of the reference velocity, U, and the estimated velocity, $U_{es.}$, as shown in figure 2-9, being within about $\pm$ 30 %.

2.3 Experimental procedure.

Two kind of experiments are carried out. One is the experiment to investigate the start-up behavior, and the other to investigate the thermo-physical phenomena in a steady state. The experimental procedure for the start-up experiment is as follows; After repeated evacuation and gas replacement of the whole system, helium gas is charged at the prescribed pressure level. Cooling water is circulated through the heat exchanger at the hot end. The compressor unit is started before introducing high pressure gas into the pulse tube. After confirming the temperature difference is smaller than 1 K along the PT refrigerator, the pressure gas is introduced by opening the stop valve. The pressure ratio and the mean gas pressure are adjusted to be about 1.4, and about 1.4 MPa, respectively. The data are

acquired until a steady state is reached.

For the steady state experiment, after both the wall temperature at the cold end and the heat-out reach steady values, data acquisition is started. Experiments are carried out in the range of the driving frequency between 1 and 18 Hz and the pressure ratio between 1.8 and 3.4 for the basic, the orifice, and the double inlet PT refrigerators.

Chapter 3

Start-up behavior of pulse tube refrigerators

The start-up behavior of a pulse tube refrigerator is investigated by measuring the gas pressure and temperature variations started from a quiescent isothermal state. The purpose of this experiment is : first to discuss whether the presence of the wall temperature distribution in the longitudinal direction which is considered to be one of the necessary conditions for refrigeration action in the thermoacoustic theory [21] is essential for the generation of refrigeration power, and second to grasp various relaxation times in key components and as a whole of a pulse tube which are useful in the engineering applications. Since it was found that the start-up behavior is qualitatively almost same for three types of PT refrigerators, the typical result of a basic PT refrigerator operated at a frequency of 5 Hz is presented and discussed here.

The propagation speed of sound of helium gas is so fast compared with time variations of thermo-fluiddynamic quantities in a PT refrigerator that the pressure variation may be considered to be in phase at all positions through the pulse tube [24]. The time variation of the pressure at the entrance of the pulse tube is

presented as a typical example in figure 3-1 which shows the start-up behavior of the pressure variation after opening the both stop valves at the exit of the compressor. The origin of the abscissa t=0 is taken as the instance when the stop valves are opened. The amplitude of the pressure variation reaches a steady state within a 6 % of deviation from a steady value in as small as 3 sec (15 cycles), though overshoot appears in the very initial stage of the start-up process.

Figure 3-2 shows the start-up behavior of the gas temperature at the cold and the hot ends, which are simultaneously measured together with the pressure variation shown in figure 3-1. It should be noted that the large temperature difference between at the cold and the hot ends appears within a few cycles just after the start-up. Moreover, the mean gas temperature at the cold end significantly decreases from the level before the start even in the second cycle, which indicates the quite fast beginning of refrigeration. In figure 3-3, several initial variations are shown. In addition to the experimental result, the prediction by assuming adiabatic compression and expansion, expressed by the relation (3-1), is also presented as a reference value.

$$T = T_0 \left(\frac{P}{P_0} \right)^{(\gamma-1)/\gamma} \qquad (3\text{-}1)$$

where P_0 and T_0 denote the pressure and temperature levels before start-up, and γ is the ratio of specific heats. It is clearly seen that a large temperature difference between the cold end and the hot end appears only after two cycles from the start-up.

These results indicate that the gas temperature in a PT refrigerator relaxes for rapidly as compared with an over all relaxation time of a pulse tube.

Figure 3-4 and 3-5 show the mean gas and wall temperatures during the period from the start-up till the time when the heat out reaches a steady level, that is about 800 sec. It is seen from figure 3-4 that the gas temperature starts to change immediately after the start-up except inside the regenerator and the temperature difference between at the cold and hot ends increases rapidly to reach over about 65 % of the steady state value as shown in figure 3-4-(b). It is considered that the change of the mean gas temperature is caused mainly by thermo-fluiddynamic process just after the start-up, and after this period the temperature decrease is governed by the heat capacities of tube wall and regenerator. The beginning of gas temperature drop in the regenerator delays as compared with the gas temperature at the cold and hot ends by a quantity decided by the heat capacity of the material of regenerator. Although both the wall temperature and the heat out greatly change along with the gas temperature in the early stage as seen from figure 3-5, their variations are more gradual than that of the gas temperature. As for the change of the wall temperature, it is estimated that times to reach 80 % levels of steady values are about 320 sec for the hot end and 540 sec for the cold end. The heat out reaches 90 % of the steady state value after about 410 sec, which is comparable with the estimated time required for making the temperature gradient over the whole regenerator, and then the constant operating condition of the PT refrigerator is reached.

The results can be summarized as follows:

In the first several cycles remarkable temperature change appears in the gas inside a pulse tube and the temperature difference between the cold and hot ends reaches more than 65 % of a steady temperature difference. After that, the gas temperature changes gradually with the laps of time. The wall temperature distribution does not significantly affect the refrigeration process in the initial stage.

The beginning of temperature drop of the pulse tube wall and the regenerator delay as compared with those of the gas temperature at the cold and hot ends by quantities determined by the heat capacity of materials of the wall and regenerator. The heat out reaches a steady value after the temperature gradient fully develops over the whole regenerator, and then a steady operating state of a PT refrigerator is reached.

Chapter 4

Refrigeration mechanism of a basic pulse tube refrigerator

4.1 Attainable wall temperature.

It is known that there are typical three types of PT refrigerators, that is to say, they are a basic, an orifice and a double inlet types as mentioned in chapter 1. Figure 4-1 shows the results of the lowest attainable refrigerator temperature for the three types recorded in our experiment at the pressure ratio of 1.4, the mean pressure of 1.4 MPa and at the optimum frequency. It has been improved from 280 K by the basic type over 170 K by the orifice type down to 160 K by the double inlet type. Though the performance of the basic type is the worst among three types, the investigation of the basic type is of importance in order to understand the fundamental refrigeration mechanism. Here, the reason how the phase difference being a key for refrigeration can be produced in the basic type is considered on the basis of the gas velocity and temperature measurement results in the radial direction in the pulse tube. The driving frequency dependence of the performance is also investigated.

Figure 4-2 shows the results of the steady state values of the attainable

temperature at the cold end and the heat-out as a function of driving frequency at various pressure ratios. It is seen that the attainable temperature and the heat-out vary depending on the driving frequency, and there exists an optimum working region of the frequency, around 2 Hz, at which the lowest temperature is reached. It is quite natural that the lowest attainable temperature and the heat-out are improved with the increase of the pressure ratio. In figure 4-3 the heat-out is plotted as a function of pressure ratio for a number of driving frequencies. It is seen that the heat-out is roughly proportional to the pressure ratio. The reason for the proportionality is considered as follows. The area encircled in a P-V diagram during a cycle which is equal to the available work is proportional to the pressure ratio and thus so is the heat-out. It is also quite clear in figure 4-2 that the heat-out is in proportion to the driving frequency at lower frequencies ($\leqq$3 Hz). Since it is understood that the pressure ratio is not an essential parameter to investigate the refrigeration mechanism, in what follows, we pay more attention to the driving frequency as an essential parameter rather than to the pressure ratio.

The driving frequency dependence of the attainable temperature at the cold end at the pressure ratio of 1.4 is shown in figure 4-4. It can be considered that there are three regions of the driving frequency, which are the working region 1, 2 and 3 as indicated in figure 4-4. The region 2 is the optimum frequency region, and the regions 1 and 3 are the frequency regions where the attainable temperature decreases and increases, respectively, as the increase of the frequency.

4.2 Measurement of the time-variations of the gas velocity and the temperature.

Figures 4-5-a and 4-5-b show the result of the visualization study by Shiraishi et al. [25] for the working region 2. Figure 4-5-a shows the pressure variation during one cycle, where the numbers from (1) to (8) correspond to those in figure 4-5-b which is observed with the aid of a smoke-wire flow visualization technique. The timings of a smoke emission for visualization are indicated by tc for the compression and by te for the expansion processes, respectively. It is a well known fact that the direction of flow can not be decided from the hot wire signal itself with a single probe. Thus the direction of the velocity measured by the hot wire anemometer is decided on the basis of both the visualization and the pressure measurement results in the present research. Shown in figure 4-6 is time-variation of the velocity measured on the centerline of the pulse tube and the pressure variation. Considering the mass inflow and outflow between the regenerator and the pulse tube described by equation (4-1) and the equation of state for an ideal gas by equation (4-2), an empirical correlation is derived for the gas flow, being the equation (4-3) by Shiraishi [25]. The result is shown by dotted line in figure 4-6.

$$\dot{m} = \rho u A \qquad (4\text{-}1)$$

$$m = \frac{PV}{RT} \qquad (4\text{-}2)$$

$$u = 7.5 \times 10^{-8} \frac{dP}{dt} \qquad (4\text{-}3)$$

Here, m, ρ, u, A, V and R denote the mass, the density, the mean velocity of the gas flow, the cross sectional area of the pulse tube, volume of the pulse tube and the gas constant, respectively. The solid line denotes the data measured by the hot wire anemometer. The positive sign indicates that the flow direction is from the regenerator toward the hot end of the pulse tube. Since figure 4-6 shows a good agreement between the experimental data and the empirical correlation result, it is confirmed that the velocity measurement by the hot wire anemometer is valid and that the velocity variation is governed mainly by the time-derivative of the pressure (dP/dt) in the basic type. Figures 4-7-a through 4-7-g are typical examples of the time-variations of the radial distribution of the axial velocity and of the temperature at 2 Hz. Figure 4-7-a is the pressure variation, and figures 4-7-b ~ 4-7-g are the results of the velocity and the temperature measurements at three locations, the cold end, the middle of the pulse tube and the hot end. The x-axis denotes the time, and the y-axis does the radial location. The origin of the x-axis is defined as a onset of the compression process. The inside wall of the pulse tube is at r=7.8 mm, and thus the centerline of the pulse tube is at r=0 mm. It is also seen from figures 4-7-a through 4-7-g that the velocity variations are roughly proportional to dP/dt, and the amplitude of the velocity variation decreases in the order from figure 4-7-b to 4-7-d, that is, with the distance from the cold end. On the other hand, the amplitude of the temperature variations are found to increase with the distance from the cold end. From figure 4-7-g the profile of the temperature variation near the wall is similar to that of the

pressure variation, but data on the centerline differs from the pressure variation. It is considered that the gas element near the wall can not move owing to the viscosity, so that its temperature variation directly correlates to the pressure variation. However, a gas element on the centerline would be affected by the flow, so that its temperature variation is different from the pressure variation near the wall.

4.3 P-V diagram in the basic type.

Figure 4-8 shows the concept for the estimation of the gas displacement which is necessary to draw a P-V diagram. The y-axis is the axial distance, and the origin of it is the connection point between the pulse tube and the regenerator. The measuring positions are at L=0.03 m ($=x_0$) for the cold end, 0.13 m for the middle point and 0.25 m for the hot end, respectively. Axial velocity distribution along the center line, r=0 mm, shown in figure 4-8 can be constructed by a linear interpolation of the data measured at three positions along the center line. The velocity of an gas element at x_i at the time t_i which is initially at x_0 is calculated from the equation (4-4) and the gas displacement is from the equation (4-5).

$$u_i(x_i,t_i) = \left(\frac{u_{cold}(t_i) - u_{mid}(t_i)}{l_1} \right)(x_i - x_0) + u_{cold}(t_i) \qquad (4\text{-}4)$$

$$x_{i+1} = x_0 + \sum_{i=0}^{n} u_i \Delta t \qquad (4\text{-}5)$$

Here, u_{cold} and u_{mid} denote the velocities measured at the cold end and the middle point, and u_i is the velocity of a gas element at x_i in Lagrange's sense. The distance between

the cold end and the middle point, sampling period and the total number of data are denoted by l_1, Δt and n, respectively. Figure 4-9 shows a kind of P-V diagram derived from the gas displacement result at 2 Hz, where the abscissa denotes the volume per unit cross sectional area, that is, the gas displacement. It is found from this figure that the P-V work near the wall (r=7.3 mm) is larger than that on the centerline (r=0 mm). In order to investigate the reason for this, the amplitude of the gas displacement and the phase difference between the pressure and the displacement variations are evaluated from the data. The phase angle is obtained from the fundamental mode of each variations as shown in figure 4-10, where the solid lines and the dotted lines indicate the experimental data and the approximation by the fundamental mode derived by applying the least square method. The least square result yields estimations of the amplitude and the phase angle. The reason why a gas displacement does not return back to the original position as seen in figures 4-9 and 4-11 is considered to be the result of the total sum of error and the effect of the secondary flow [26],[27]. Figure 4-11 shows the radial profiles of the amplitude of the gas displacement and the phase difference for 0.5 Hz, 2 Hz and 10 Hz that are typical examples of three working regions shown in figure 4-4. The abscissa denotes the normalized radial position, that is to say, $r/r_0=0$ and $r/r_0=1$ correspond to the centerline of the pulse tube and the wall, respectively. The positive sign of the phase difference means that the gas displacement is delayed as compared to the pressure variation. It is found that the phase difference near the wall is large

compared with interior points, and the amplitude decreases rapidly near the wall for all driving frequencies. These results indicate that both of the amplitude and the phase difference change much drastically near the wall owing to the viscous effect. The phase difference, not the amplitude, does directly contribute to P-V work as shown in figure 4-9. It is concluded that the phase difference owing to the viscous effect produces the P-V work mostly near the wall in the basic type. This is clearly seen in figure 4-12 where the radial variations of the P-V work per unit cross sectional area are shown for three driving frequencies. It is seen that the P-V work reaches the maximum near the wall except 0.5 Hz. In the case of the frequency of 0.5 Hz, the velocity of the gas element is so slow that the phase delay owing to the viscous effect becomes small when compared to higher frequencies shown in figure 4-11. Accordingly, the radial variation of 0.5 Hz is different from higher frequencies.

4.4 Driving frequency dependence of the performance.

Integration of the P-V works per unit cross sectional area shown in figure 4-12 in the radial direction gives the P-V work (W). The P-V work thus calculated and the heat-out are plotted as a function of driving frequency in figure 4-13. The P-V work increases almost linearly with the driving frequency, and the magnitude is comparable with the heat-out at higher frequencies (in the working region 3 defined in figure 4-4). It can be considered that the performance of the basic type is improved with the increase of the driving frequency up to the optimum frequency (in the

working regions 1 and 2) because the P-V work increases with the driving frequency. However at higher frequencies friction loss due to the viscosity increases rapidly as the increase of the driving frequency, so that almost all P-V work is converted into heat and thus the net refrigeration power decreases. In order to discuss the dissipation function, the stability diagram of a oscillating flow is examined as shown in figure 4-14 to investigate whether the oscillating flow is laminar or turbulent which is important to evaluate the dissipation. In figure 4-14, the relation between Womerseley number, W_m, and the Reynolds number, R_δ, defined by equations (4-6) and (4-7) is shown.

$$W_m = r_0\sqrt{\frac{\omega}{2\nu}} \tag{4-6}$$

$$R_\delta = \frac{2|U|}{\sqrt{\nu\omega}} \tag{4-7}$$

Here, r_0, ω, μ and $|U|$ denote the radius of the pulse tube, the angular frequency, the kinetic viscosity of helium gas and the amplitude of the velocity variation. The R_δ - W_m -number plane region is divided into same regions according to the experimental result of Hino et al. [28]. This result suggests that the oscillating flow in the basic type is not in a fully developed turbulent state nor in a conditionally turbulent state. Therefore, the term of square of the radial gradient of the velocity is dominant in the dissipation function, Φ, evaluated from equation (4-8).

$$\Phi = \int_0^T \int_0^L \int_0^{r_0} \mu\left(\frac{\partial u}{\partial r}\right)^2 2\pi r\, dr\, dl\, dt \times \frac{1}{T} \tag{4-8}$$

Here, T, and L denote a period of the pressure variation and the total length of the pulse tube. Figure 4-15 shows the evaluation of the dissipation function as a function of driving frequency derived. It is confirmed the dissipation function is negligibly small compared with the heat-out and the P-V work. Next, a number of characteristic times derived from the gas temperature variation are introduced for more detailed discussion on the driving frequency dependency of the performance around the optimum frequency as shown in figure 4-16. Here, τ is the thermal relaxation time that is defined from the experimental data as a time duration from the instance when the temperature rises by gas compression to the temperature peak measured at r=7.3 mm that is the position near the wall, and τ_{BL} , which is estimated from equation (4-9), is defined as a time duration required for reaching the constant temperature over the Stokes's boundary layer thickness.

$$\tau_{BL} = \frac{\left(\sqrt{\frac{2\alpha}{\omega}}\right)^2}{2\alpha} = \frac{1}{\omega} \qquad (4\text{-}9)$$

α is the thermal diffusivity. It is found that the thermal relaxation time, τ, is nearly equal to the time duration to reach the constant temperature over the boundary layer, τ_{BL}, and is too short compared with τ_{BL} at lower frequencies, and is too long compared with τ_{BL} at higher frequencies. It is considered that the heat exchange between the main flow and the boundary layer is took place only near the surface of the boundary layer at higher frequencies because the gas temperature in the boundary layer does not rise within t_{BL} though the heat exchange between the main flow and the

tube wall through the boundary layer is took place at lower frequencies. Therefore it is considered that optimum frequency appears when the whole boundary layer is utilized for the heat exchange between the main flow and the boundary layer. Table 4-1 summarizes the driving frequency dependence of several parameters discussed above.

The results can be summarized as follows:

The P-V work can be estimated from the gas velocity variation in addition to the pressure and the temperature variations measured in the radial and longitudinal directions.

The phase different between the gas pressure and the displacement appears near the tube wall owing to the viscous effect, so that the radial profiles of the P-V work per unit cross sectional area in the basic type has the maximum value near the wall.

The performance of the basic type is improved with the increase of the driving frequency up to the optimum frequency because the P-V work increases with the driving frequency. However, at higher driving frequencies the whole P-V work is almost converted to heat and thus the net refrigeration power is deteriorated.

Chapter 5

Refrigeration mechanism of an orifice pulse tube refrigerator

5.1 Attainable wall temperature.

The driving frequency dependence of the attainable temperature at the cold end at the pressure ratio of 1.4 and the mean pressure of 1.4 MPa is shown in figure 5-1. The orifice valve opening is set at the optimum value at every driving frequency. Figure 5-2 is a similar plot of the attainable temperature as a function of orifice valve opening, V_o (turns), at the frequency of 10 Hz. It is seen that the attainable temperature depends on the orifice valve opening as well as the driving frequency. The attainable temperature lowers with the increase of the driving frequency at low frequencies, and then it becomes constant over 5 Hz. As to the orifice valve opening, there exists an optimum working region around 0.4 turns where the lowest temperature is reached. It can be considered that there are two and three working regions with respect to the driving frequency and the orifice valve opening, which are the working regions D-1 and D-2, and V_o-1, V_o-2 and V_o-3, respectively as indicated in figure 5-1 and 5-2. In what follows, the difference in the performance

between the orifice and the basic types is discussed on the basis of the driving frequency and the orifice valve opening dependencies.

5.2 Difference between the orifice and the basic types.

Figure 5-3-a and 5-3-b show the result of the visualization study for the orifice type at 2 Hz conducted by Shiraishi et al. [25]. Figure 5-3-a shows the pressure variation during one cycle, where the numbers from (1) to (8) correspond to those in figure 5-2-b which is observed with the aid of a smoke-wire flow visualization technique. The timings of smoke emission for visualization are indicated by tc for the compression and by te for the expansion processes, respectively. Though the gas displacement in the orifice type is larger than that in the basic type as seen from figure 4-5-b, the oscillating flow at the cold end in the orifice type is qualitatively similar to that in the basic type. On the other hand, the smoke-line at the middle point in the photograph (4) in figure 5-3-b, in which a spin-up is observed, is different from that of the basic type. Moreover, during the expansion process ((5) through (8)) a jet injected into the main body of the pulse tube from the reservoir is observed and even the formation of a vortex ring is recorded near the entrance to the reservoir. Therefore, it is concluded that the gas simply flows not only in the longitudinal direction like the basic type but also in the radial direction especially near the hot end. However, it may be regarded that the gas velocity in the radial direction is so small that the main flow is primarily in the longitudinal direction.

Thus the direction of the velocity measured by the hot wire anemometer can be decided on the basis of both the visualization and the pressure variation results. The velocity variations measured on the centerline of the pulse tube in the orifice (V_o=0.36 turns) and the basic types at 10 Hz are compared in figure 5-4. Pressure variation in the reservoir is also shown together with that inside of the pulse tube. It is seen that the decrease in the amplitude and the occurrence of the phase delay of the pressure variation in the reservoir are due to the flow impedance of the orifice valve and the finite volume of the reservoir. It is also found from this figure that the velocity in the orifice type does not vanish during the pressure plateau phase unlike the basic type. This result indicates that the flow in the orifice type is caused not only by dP/dt but also by the pressure difference between the pulse tube and the reservoir, and so that the magnitude of the phase difference in the orifice type to the refrigeration is considerably improved as compared with the basic type. Figures 5-5-a through 5-5-g are typical examples of the time-variations of the radial distribution of the axial velocity at 10 Hz and at V_o=0.36 turns. Figure 5-5-a shows the pressure variations inside of the pulse tube and the reservoir, and figures 5-5-b through 5-5-g are the results of the velocity and the temperature measured at three locations, the cold end, the middle of the pulse tube and the hot end. The amplitude of the velocity variation decreases with the distance from the cold end, in particular it decreases drastically between the middle point and the hot end and it is kept nearly constant between the cold end and the middle point. The amplitude of the

temperature variation at the middle point becomes the largest among three measuring points. The peak of the velocity variation measured on the centerline at the middle point (figure 5-5-c) appears just after the onset of the expansion process and shifts backward about 70 degree compared to that at the cold end (figure 5-5-b), while the peak of the temperature variation at the same point (figure 5-5-f) appears just after the onset of the compression process. It is considered that just after the onset of the compression process the temperature at the middle point increases largely because of the additional compression by the inflow from the reservoir, and the velocity at the middle point becomes small by the collision of flows in the orifice type. Then after the flow driven by dP/dt overcomes the flow from the reservoir, the velocity begins to increase. It is seen from figure 5-5-d the flow is much disturbed in the expansion process at the hot end. The detail discussion on disturbances is presented later on the basis of turbulence level of the velocity data. Figure 5-6 shows the radial profiles of the amplitude of the gas displacement and the phase difference between the pressure and the gas displacement. The refrigerator would work as a basic type at V_o=0 turns. The orifice valve opening, V_o =0.36 turns is selected as a typical value of the performance of the orifice type. It is found that both of the amplitude and the phase difference are improved in the orifice type compared with the basic type. These improvement can be considered to be made by the effect of the orifice valve-reservoir combination. Figure 5-7 shows the comparison of the radial profiles of the P-V work per unit cross sectional area at 10 Hz between the orifice and basic types.

It is seen that the P-V work per unit cross sectional area of the orifice type decreases near the wall and is constant elsewhere while that in the basic type becomes maximum near the wall. Moreover, it should be noted that the P-V work of the orifice type is far larger than that of the basic type. This is the explanation why the refrigeration performance is improved in the orifice type compared with the basic type.

5.3 The dependence of the performance on the driving frequency.

Figure 5-8 shows the P-V work per unit time variation as a function of driving frequency. The P-V work increases with the increase of the driving frequency up to 10 Hz, and decreases above 10 Hz. It is seen from figures 5-1 and 5-8 that the performance is improved with the increases of the driving frequency for lower frequencies (in the working region D-1 defined in figure 5-1) because the P-V work increases with the frequency. On the other hand, the P-V work becomes small over 10 Hz, nevertheless the attainable temperature is kept almost constant as seen from figure 5-1. In figure 5-9 the amplitude of gas displacement and the phase difference are plotted as a function of driving frequency. It is seen that both of the amplitude and the phase difference decrease with the increases of the frequency over 5 Hz and thus so does the area encircled in a P-V diagram during a cycle. However, the P-V work per unit time still increases up to 10 Hz as shown in figure 5-8 because the increase in the driving frequency overcomes the reduction of both of the amplitude and the phase difference. The reduction of P-V work above 10 Hz is resulted from

further reductions of the amplitude and the phase difference. It should be noted that the amplitude decreases with the increase of the driving frequency because the high pressure ratio can not be maintained at high frequencies in the present experimental set-up. The compressor unit does not have the capability of driving the PT refrigerator at high frequencies enough to maintain the constant pressure ratio at high frequencies because the higher flow velocity of gas at high frequencies causes the higher pressure drop. The dependence of the performance on the driving frequency may be summarized as follows; the performance is improved up to 10 Hz because the P-V work per unit time increases with the increase of the driving frequency. On the other hand, the P-V work decreases over 10 Hz. The dream pipe effect, Q_d, which is defined as the irreversible heat flow from the high temperature to low temperature sides as expressed by equation (5-1), decreases as the increase of the frequency above 10 Hz.

$$Q_d = F_s \chi'' \omega C_p \nabla T_m \frac{1}{2} \xi^2 \qquad (5\text{-}1)$$

This equation is given by Tominaga [29] where, $F_s\chi''$, ω, C_p, ΔT_m and ξ denote the dimensionless quantity indicating the degree of irreversible process, the angular frequency of pressure variation, the specific heat at constant pressure, the temperature gradient on the wall and the amplitude of gas displacement, respectively. The dream pipe effect is plotted as a function of driving frequency in figure 5-10, where the dream pipe effect is normalized by the value at 10 Hz and at V_o=0.36 turns. It is seen from this figure that the dream pipe effect, which is the negative effect to the

refrigeration, decreases with the increase of the frequency over 10 Hz. Accordingly, the wall temperature keeps constant level over 10 Hz despite of the decrease of the P-V work as shown in figure 5-8.

5.4 The dependence of the performance on the orifice valve opening.

Figure 5-11 shows the P-V work variation as a function of orifice valve opening, V_o (turns). The P-V work increases with the increase of the valve opening up to V_o=1 turn, and decreases above V_o=1. It is seen from figures 5-2 and 5-11 that the performance is improved with the increases of the valve opening for rather small values of the valve opening (in the working region V_o-1 and V_o-2 defined in figure 5-2) because the P-V work increases with the valve opening. On the other hand, the attainable temperature even rises up though the P-V work is almost constant in the working region V_o-3. It is seen from figure 5-12 that both of the amplitude and the phase difference increase with the increase of the valve opening in the working regions V_o-1 and V_o-2, and they reach constant values in the working region V_o-3. Since C_v value of the orifice valve, that is the inverse of the flow resistance, increases rapidly with the valve opening at smaller values and does not increase so rapidly at higher values in the present experimental set-up, both of the amplitude and the phase difference vary largely only in the regions V_o-1 and V_o-2 and reach constant values in the working region V_o-3. The dependence of the performance on the orifice valve

opening may be summarized as follows; the performance is improved in the working regions V_o-1 and V_o-2 because the P-V work increases in these working regions. In the working region V_o-3, the wall temperature rises up though the P-V work increases. In this region the increase of dream pipe effect, Q_d, defined by equation (5-1), is considered as one of reasons to the refrigeration temperature rise because the effect is proportional to the square of the amplitude of gas displacement. The dream pipe effect normalized by the value at 10 Hz and at V_o=0.36 is shown as a function of valve opening in figure 5-13. It is seen that the normalized dream pipe effect in the working region V_o-3 is larger than those in regions V_o-1 and V_o-2. It should be noted that the effect in region V_o-3 keeps constant though the attainable temperature gradually rises up with the increase of the valve opening as shown in figure 5-2. In order to investigate this in more detail, the negative effect to the refrigeration, turbulent disturbance, is also considered.

Figure 5-14 shows the R_δ-W_m plot of oscillating flow, according to the result by Hino et al. [28], in the orifice type in the present experiment. It is seen from this plot that in the orifice type the oscillating flow is not in the fully turbulent state nor in the conditionally turbulent state. However, turbulence at the hot end in the orifice type becomes significant compared with that of the basic type in particular during the expansion process owing to the diverging inflow from the regenerator as seen from the comparison between the results shown in figure 5-15-a and 5-15-b. In these figures the ordinate is the r.m.s value of the turbulent velocity fluctuation during

a cycle defined by equation (5-2).

$$r.m.s(i) = \sqrt{\sum_{k=1}^{N}\left[u_{hot}(k, i+n\times(k-1)) - \overline{u_{hot}}(k,i)\right]^2} \Big/ N \qquad (5\text{-}2)$$

Here, $u_{hot}(k, i+n\times(k-1))$ is the time sequence of the velocity measured at the hot end at the i-th sampling of k-th cycle and the upper bar denotes the ensemble average of the velocity variation. N is the total number of cycles measured. It is found from 5-15-b that the flow disturbance becomes large just after the onset of the flow driven by the pressure difference between the pulse tube and the reservoir at 180 deg. Figure 5-16 shows the valve opening dependency of the turbulence level. The value of turbulence level is evaluated by equation (5-3).

$$turbulence\ level = \sqrt{\frac{\sum_{i=0}^{n} r.m.s(i)}{n-1}} \Big/ \left|\overline{u_{hot}}(i)\right| \qquad (5\text{-}3)$$

Here, n and | | mean total number of data for one cycle and the amplitude, respectively. Since the turbulence level increases with the increase of the valve opening, the disturbance which can be considered as a negative effect to the refrigeration increases with the increase of the opening. This negative effect contributes slightly to the performance of the orifice type. Table 5-1 and 5-2 summarize the dependency of the driving frequency and the orifice valve opening with several parameters discussed above.

The results can be summarized as follows:

The P-V work of the orifice type is much larger than that of the basic type, and consequently the refrigeration performance of the orifice type is superior to the basic type

The performance of the orifice type is improved with the increase of the driving frequency in lower and optimum driving frequency regions because the P-V work increases with the driving frequency.

The performance is also improved with the increase of the orifice valve opening in smaller opening region because of the P-V work increase. However, at larger value openings irreversible effects such as the dream pipe effect and turbulence of the oscillating flow increases, so that the net refrigeration power is deteriorated.

Chapter 6

Refrigeration mechanism of a double inlet pulse tube refrigerator

6.1 Attainable wall temperature.

Figure 6-1 shows the results of the steady state value of the attainable wall temperature measured at the cold end as a function of double inlet valve opening, V_d, (turns) at the driving frequency of 10 Hz. The pressure ratio is about 1.4 and the mean gas pressure is about 1.4 MPa. The orifice valve opening is set at V_o=0.36 turns which is in the optimum working region V_o-2 of figure 5-1 for the orifice type. The refrigerator would work as an orifice type at the double inlet valve opening, V_d=0, which means the value is closed. It is seen that the attainable temperature slightly goes down with the increase of the double inlet valve opening, and it reaches a constant value over 1 turns of V_d. The difference in the attainable temperatures between the double inlet and orifice types is found to be at most 10 K. In the followings, the difference in the performance between the double inlet and orifice types will be discussed from the thermo-fluid dynamic point of view.

6.2 Difference in the refrigeration performance between the double inlet and orifice types.

Figure 6-2 shows a typical example of the time-variations of the radial distributions of the axial velocity and the temperature in the double inlet type in the case of V_o =0.36, V_d =2 and 10 Hz. The amplitude of the gas velocity variation decreases with the distance from the cold end similarly to the basic type (figures 4-7-b. ~ figure 4-7-d.). The amplitude of the gas temperature variation is the largest at the middle point among the three measuring points, and this feature is similar to that of the orifice type. The amplitudes of the velocity and the temperature variations at the middle point of the double inlet type are smaller than those of the orifice type, though they are almost same at the cold end for both types. The difference in the velocity and the temperature between the double inlet and orifice types appears significantly at the middle point. Figure 6-3 shows the variation of the P-V work at the cold end as a function of double inlet valve opening. It seems strange that the attainable temperature is lower for the double inlet type rather than for the orifice type though the P-V work of the double inlet type is smaller than that of the latter. Figure 6-4 shows the V_d dependency of the amplitude of the gas displacement and the phase difference between the gas pressure and displacement variations at the cold end, both of which are the averaged values over the cross section. It is seen that the phase difference is almost independent of the double inlet valve opening, 65 deg., but the amplitude decreases with the increase of the valve opening up to V_d =1 turns and

it becomes almost constant over 1 turns. From the results in figures 6-1, 6-3 and 6-4, it is considered that the dream pipe effect, Q_d, being the irreversible heat flow from the hot side to the cold side, becomes small in the double inlet type compared with the orifice type (V_d=0) because the dream pipe effect, Q_d, is proportional to the square of the amplitude descried by equation (5-1). Figure 6-5 shows the normalized dream pipe effect, Q_d, as a function of valve opening. It is seen that the dream pipe effect, Q_d, decreases with the increase of the double inlet valve opening up to V_d =1 turns and then becomes constant. Therefore, it can be concluded that the dream pipe effect, Q_d, is smaller for the double inlet type than for the orifice type and that the refrigeration performance in the double inlet type is improved in spite of the smaller amplitude of gas movement. Figure 6-6 shows the turbulence level, the averaged turbulent fluctuation normalized by the amplitude of the velocity variation, calculated from equation (5-3) as a function of valve opening. It is found that the turbulence level also decreases with the increase of valve opening up to V_d =1 turns, and becomes constant over 1 turns. It may be considered that the oscillating flow is closer to the laminar flow in the double inlet type than that in the orifice type in the sense that the disturbance becomes small in the double inlet type. This feature slightly contributes to improved performance in the double inlet type compared to the orifice type.

It may be concluded that the performance in the double inlet type is better than that of the orifice type, because the irreversible effects such as the dream pipe effect and turbulent disturbance of the oscillating flow are reduced in the double inlet

type though the P-V work in the double inlet type is a little bit smaller than that in the orifice type. The results as discussed above is summarized in table 6-1.

Chapter 7

Concluding remarks

Measurement.

It becomes possible in the present study to measure the velocity and temperature of helium gas inside a pulse tube simultaneously at the same position by the use of a probe composed of a set of a hot wire element and a thin sheathed thermocouple. Owing to the simultaneous measurement, the velocity of working gas of which temperature varies in a wide range can be measured with a hot wire. The temperature and pressure dependencies of a hot wire anemometer are investigated in the ranges of 220 K $\sim$ 320 K and 0.1 MPa $\sim$ 1.5 MPa covering the whole present experimental condition for calibration. The error of the velocity measurement is estimated to be within about $\pm$ 30 %.

Start-up behavior of a pulse tube refrigerator.

A detailed experimental investigation of a start-up behavior was first carried out in the present study. In the first several cycles remarkable temperature change appears in the gas inside a pulse tube and the temperature difference between the cold and hot ends reaches more than 65 % of a steady value. After that, the gas

temperature changes very slowly with the laps of time. The wall temperature distribution does not significantly affect the refrigeration process in the initial stage.

The beginning of temperature drop of the pulse tube wall and the delay in the temperature drop in the regenerator as compared with the gas temperature at the cold and hot ends can be estimated in terms of quantities determined by the heat capacity of material of the wall and regenerator. The heat-out reaches a steady value after the temperature gradient fully develops over the whole regenerator, and then a steady operating state of a pulse tube refrigerator is reached.

The thermo-fluid dynamic phenomena in a steady state.

In the present study a reliable estimation of the P-V work was first made from the direct gas velocity measurement data in addition to those of the pressure and the temperature in the radial and longitudinal directions.

It is first experimentally confirmed that in the basic type the phase difference owing to the viscous effect produces the P-V work mostly near the wall. It can be, accordingly, concluded that the gasdynamic process over most cross sectional area of a pulse tube except just the vicinity of tube wall, say in the boundary layer, is wasted in stead to produce the P-V work for refrigeration.

The performance of the basic type is improved with the increase of the driving frequency up to the optimum frequency because the P-V work increases with

the driving frequency. However, at higher driving frequencies the P-V work is almost converted to dissipative heat and thus the net refrigeration power is deteriorated.

It is experimentally confirmed that the P-V work of the orifice type is far larger than that of the basic type. Therefore, the refrigeration performance is far better in the orifice type than in the basic type.

The performance of the orifice type is improved with the increase of the driving frequency at lower and optimum driving frequency regions because the P-V work increases with the driving frequency.

The performance is also improved with the increase of the orifice valve opening in a region of smaller opening because of the increase of the P-V work. However, at larger values of opening irreversible effects such as the dream pipe effect and turbulence of the oscillating flow, which are first experimentally estimated, increases so that the net refrigeration power is deteriorated.

It may be concluded that the performance in the double inlet type is better than that of the orifice type, because the irreversible effects such as the dream pipe effect and turbulent disturbance of the oscillating flow are reduced in the double inlet type though the P-V work in the double inlet type is a little bit smaller than that in the orifice type.

It is considered that the reduction of irreversible effects such as secondary flow and turbulence in a pulse tube can contribute to the improvement of the refrigeration performance. For example, eliminating the structure of rapid diverging around the hot end which is a trigger producing turbulence of the oscillating flow, is one of the improvements of the refrigeration performance in the orifice and double inlet types.

References

[1]. Masahide Murakami, "Progress in Space Cryogenics" , Cryogenic Engineering (in Japanese), Vol.25 (1990) pp.373.

[2]. Genshiro FUJII and Yoshiro ISHIZAKI, "Recent State of Development of Cryocoolers for Space Application" , Cryogenic Engineering (in Japanese), Vol.27 (1992) pp.9.

[3]. W.E.Gifford and R.C.Longsworth, "Pulse -Tube Refrigerator", ASME paper, (1963) No.63-WA-290.

[4]. R.C.Longsworth, "An Experimental Investigation of Pulse Tube Refrigeration Heat Pumping Rate", Advances in Cryogenic Engineering, Vol.12 (1967) pp.608.

[5]. W.E.Gifford and G.H.Kyanka, "Reversible Pulse Tube Refrigeration", Advances in Cryogenic Engineering, Vol.12 (1967) pp.619.

[6]. W.E.Gifford and R.C.Longsworth, "Pulse Tube Refrigeration progress", Advances in Cryogenic Engineering, Vol.10B (1965) pp.69.

[7]. E.L.Mikulin, A.A.Trasov and M.P.Shkerbyonock, "Low-Temperature Expansion Pulse Tubes, Advances in Cryogenic Engineering, Vol.29 (1984) pp.629.

[8]. R.Radebaugh, J.Zimmerman, D.R.Smith and B.Louie, "A Comparison of Three Types of Pulse Tube Refrigerators : New Methods for Reaching 60 K", Advances in Cryogenic Engineering, Vol.31 (1986) pp.779.

[9]. S.Zhu, P.Wu, Z.Chen, W.Zhu, and Y.Zhou, "A Single Stage Double Inlet Pulse Tube Refrigerator Capable of Reaching 42 K", Cryogenics, Vol.30 September Supple., (1990) pp.257.

[10]. J.L.Gao and Y.Matsubara, "Experimental Investigation of 4 K Pulse Tube Refrigerator", Cryogenics, Vol.34 (1994) pp.25.

[11]. Y.Matsubara and J.L.Gao, "Novel Configuration of Three-Stage Pulse Tube Refrigerator for Temperatures below 4 K", Cryogenics, Vol.34 (1994) pp.259.

[12]. Y.Matsubara, J.L.Gao, K.Tanida, et al., "An Experimental and Analytical Investigation of 4 K Pulse Tube Refrigerator ", Proc. 7th Int. Cryocooler Conf., (1992) pp.166.

[13]. R.N.Richardson, "Pulse tube refrigerator - an alternative cryocooler ?", Cryogenics, Vol.26 (1986) pp.331.

[14]. D.David and J.C.Marechal, "How to Achieve the Efficiency of a Gifford-Macmahon Cryocooler with a Pulse Tube Refrigerator", Cryogenics, Vol.30 September Supple., (1990) pp.262.

[15]. E.Taward, C.K.Chan and W.W.Burt, "Pulse Tube Refrigerator Performance" Advances in Cryogenic Engineering, Vol.35 (1990) pp.1207.

[16]. W.E.Gifford and R.C.Longsworth, "Surface Heat Pumping", Advances in Cryogenic Engineering, Vol.11 (1966) pp.171.

[17]. G.W.Swift, "Thermoacoustic Engines", J. Acoust. Soc. Am., vol.84 (1988) pp.1145.

[18]. P.J.Storch and R.Radebaugh, "Development and Experimental Test of an Analytical Model of the Orifice Pulse Tube Refrigerator, Advances in Cryogenic Engineering, Vol.33 (1988) pp.851.

[19]. R.Radebaugh, "A Review of Pulse Tube Refrigerator, Advances in Cryogenic Engineering, Vol.35 (1990) pp.1191.

[20]. N.Rott, "Damped and Thermally Driven Acoustic Oscillations in Wide and Narrow Tubes", Z. Angrew. Math. Phys. Vol.20 (1969) pp.230.

[21]. A.Tominaga, "Thermodynamic Aspects of Thermoacoustic Theory", Cryogenics, Vol.35 (1995) pp.427.

[22]. J.H.Xiao and X.T.Wang, "Regenerator Irreversibility Analysis Based on Thermoacoustic Theory", Proc. of 4th Joint Sino-Japanese Seminar on Cryocoolers and Concerned Topics, Beijing (1993) pp.242.

[23]. D.C.Collins and M.J.Williams, "Two Dimensional Convection from Heated Wires at Low Reynolds Numbers", J. Fluid. Mech. (1959) pp.357.

[24]. K.Seo, M.Shiraishi and M.Murakami, "Influence of Driving Frequency on Temperature Oscillations in a Pulse Tube Refrigerator" , Cryogenic Engineering (in Japanese), Vol.31 (1996) pp.9.

[25]. M.Shiraishi, N.Nakamura, K.Seo and M.Masahide, "Velocity Profiles and Displacements of an Oscillating Flow Inside a Pulse Tube Refrigerator", Proc. 9th Int. Cryocooler Conf., to be published.

[26]. E.S.Jeong, "Secondary Flow in Basic Pulse Tube Refrigerators", Cryogenics, Vol.36 (1996) pp.317.

[27]. N.Rott, "The Influence of Heat Conduction in Acoustic Streaming", J. Appl. Math. Phys., vol.25 (1974) pp.417.

[28]. M.Hino, M.Sawamoto and S.Takasu, "Experiments on Transition to Turbulence in an Oscillatory Pipe Flow", J. Fluid. Mech. (1976) pp.193.

[29]. A.Tominaga, "Thermoacoustic Theory of Dream Pipe", Cryogenic Engineering (in Japanese), Vol.25 (1990) pp.300.

Acknowledgments

All of this research work have been conducted and analyzed under the supervision of Dr. M. Shiraishi, Thermodynamic Division, Department of Energy, Mechanical Engineering Laboratory, Agency of Industrial Science and Technology, Ministry of International Trade and Industry, Japan. I would like to acknowledge the great contributions of Dr. M. Shiraishi for fruitful suggestions and discussions on the present study.

I would like to express my sincere appreciation to Prof. M. Murakami for all of the things he has done for me including beneficial information, disciplinary, encouragement, and initiative instruction.

I would like to express my appreciation to the members of the dissertation committee, Prof. Y. Yoshizawa, Prof. K. Matsuuchi and Assc. Prof. H. Ishiguro for their effort to have judged the dissertation.

Finally, I thank all the people who helped me both in tangible and intangible ways to finish the research, all students in Murakami laboratory, Institute of Engineering Mechanics.

This research was partly supported by the Japan Society of Promotion of Science.

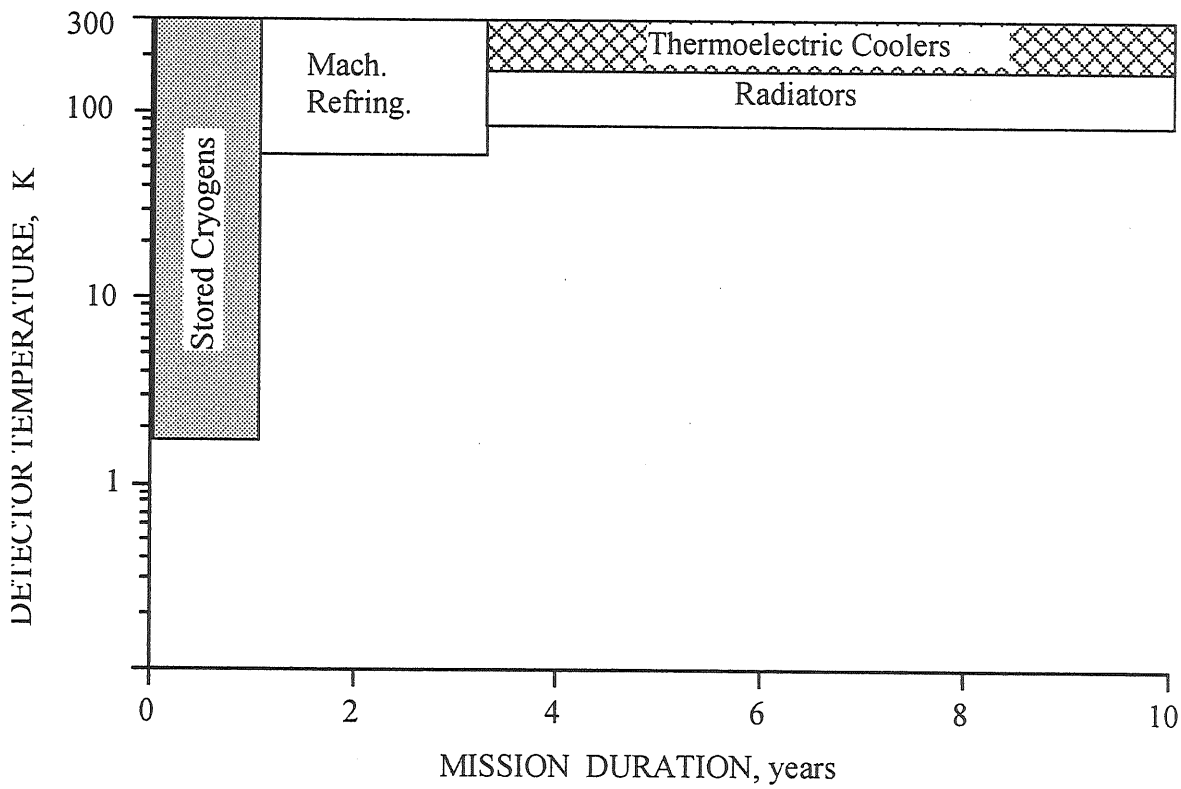

Figure 1-1. Present cooling technique .

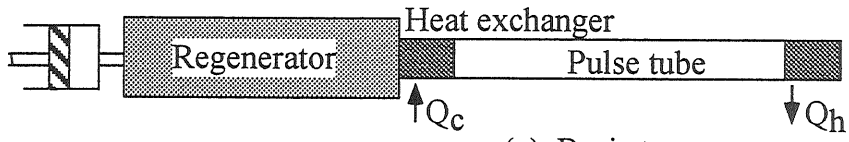

(a) Basic type.

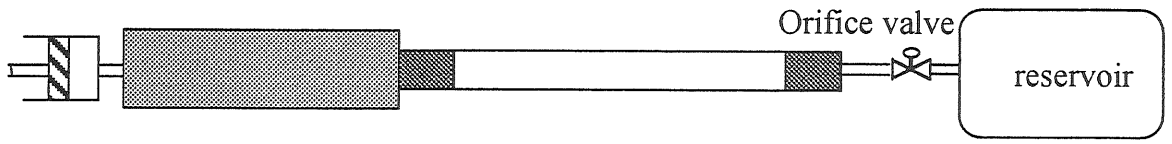

(b) Orifice type.

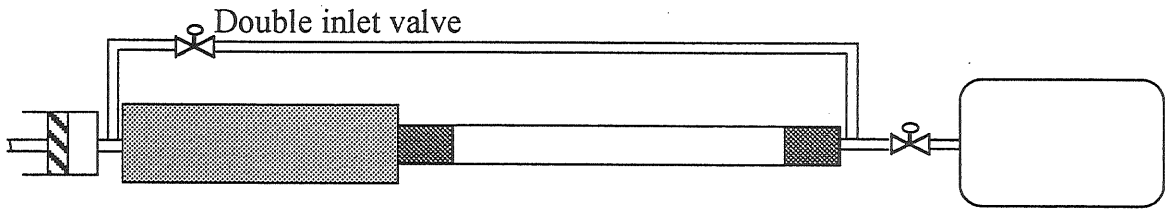

(c) Double inlet type.

Figure 1-2. Three types of pulse tube refrigerators.

Table 1-1. Chronology of pulse tube refrigerators.

	Number of Cooling Stage						
year	■ 1	▲ 2	● 3	× 4		Type	pre-cooled
1963	124				Gifford	B	
1964		79			Longsworth	B	
1965				30	Longsworth	B	65K→30K
1984	105				Mikulin	O	
1987	60				Radebaugh	O	
1988		31			Y.Zhou	O	77K→20K
1989	49				Liang	O	
1990	42				S.W.Zhu	D	
1990		26			E.Tward	O	
1991			11.5		C.K.Chan	O	20K→7.3K
1992	30				Tanida	4	
1992	28				Ravex	D	
1992	23				Ishizaki	P	
1993		17			J.L.Gao	D	20K→4.0K
1993			3.6		J.L.Gao	D	15K→3.5K

B;Basic, O;Orifice, D;Double inlet, 4;4 valves, P;2nd piston

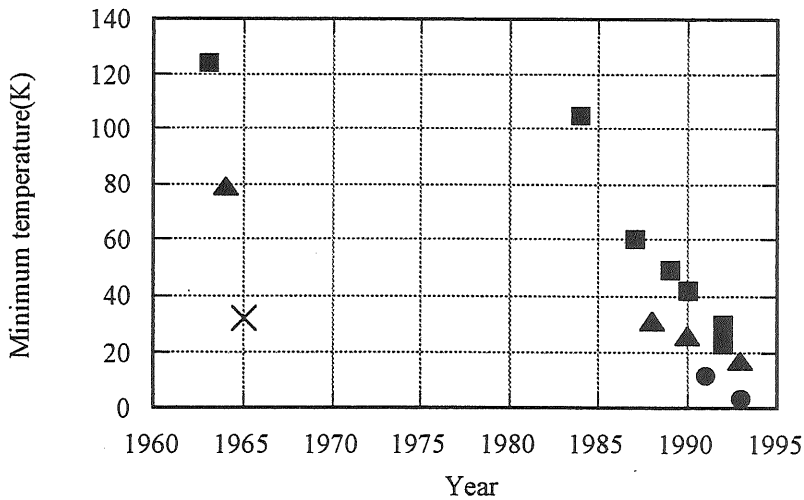

Figure 1-3. Historical Background of Pulse Tube Refrigerator.

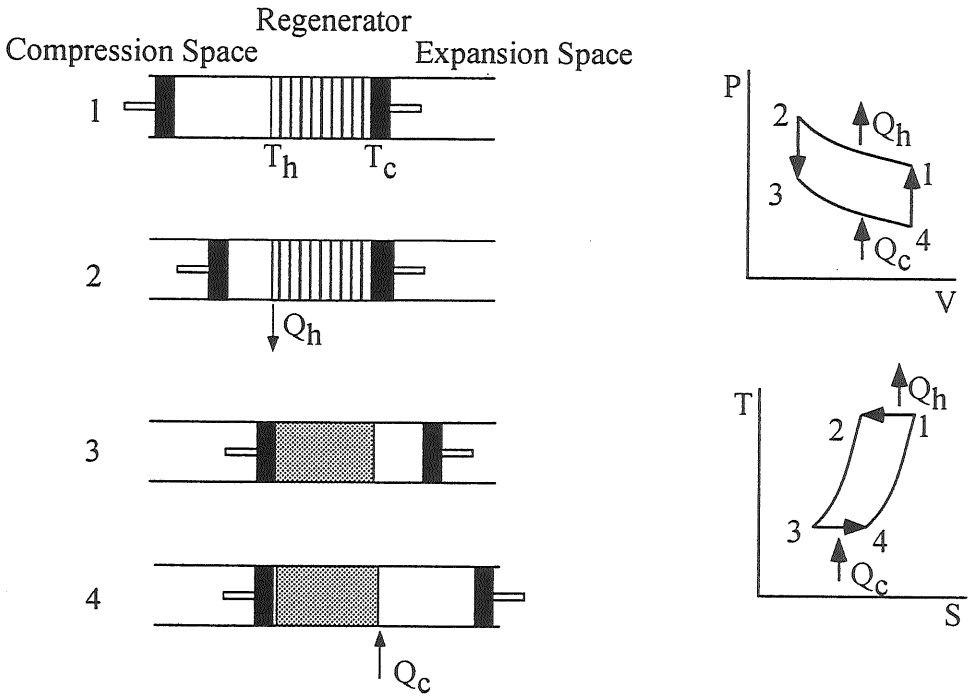

Figure 1-4. Stirling cycle, and P-V, T-S diagram.

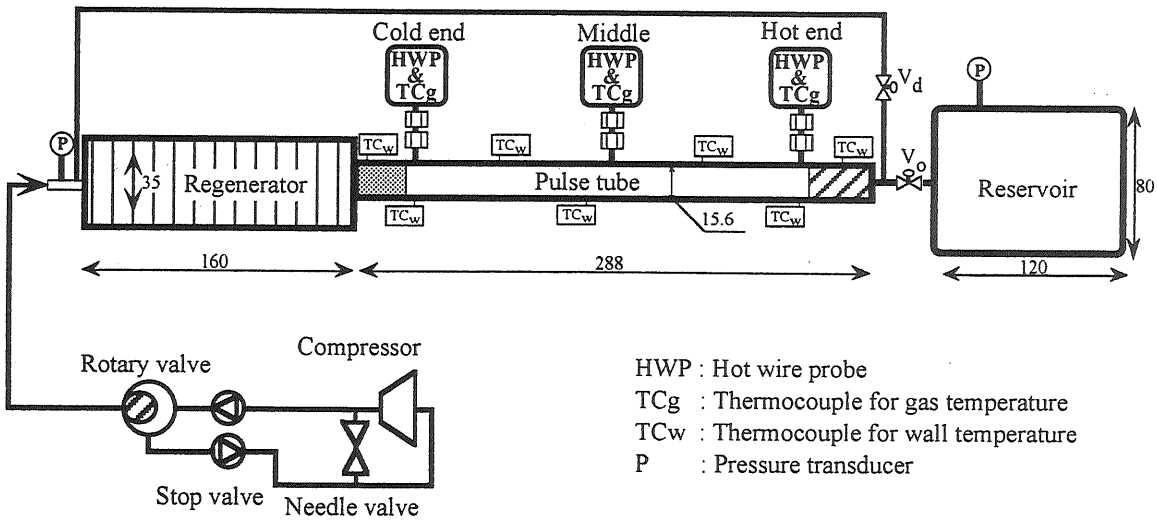

Figure 2-1. Experimental apparatus.

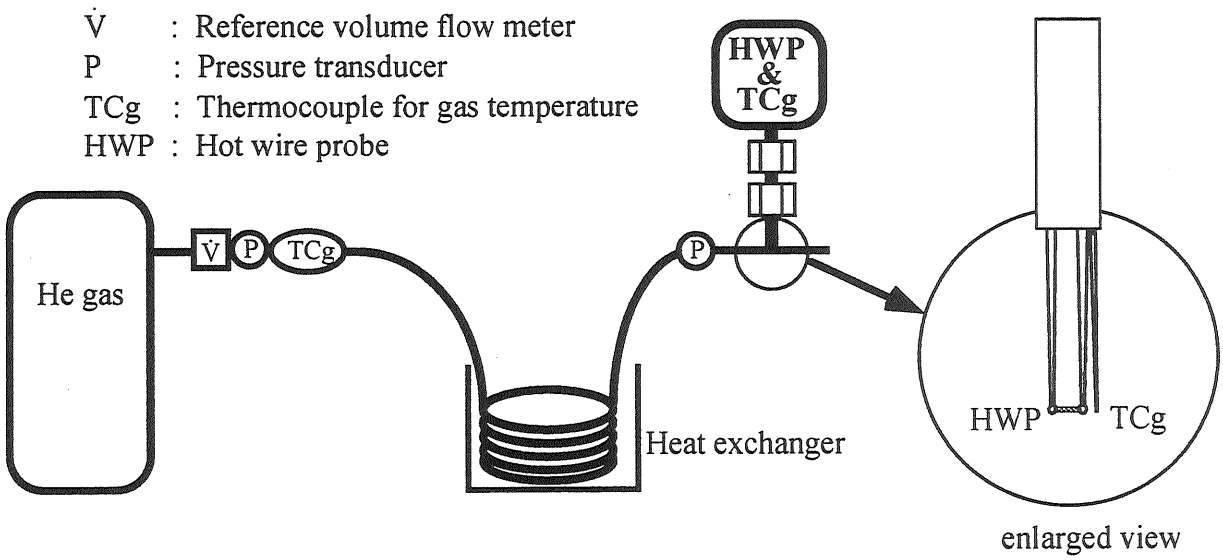

Figure 2-2. Calibration system for a hot wire under the condition that the temperature and pressure vary in wide ranges simultaneously.

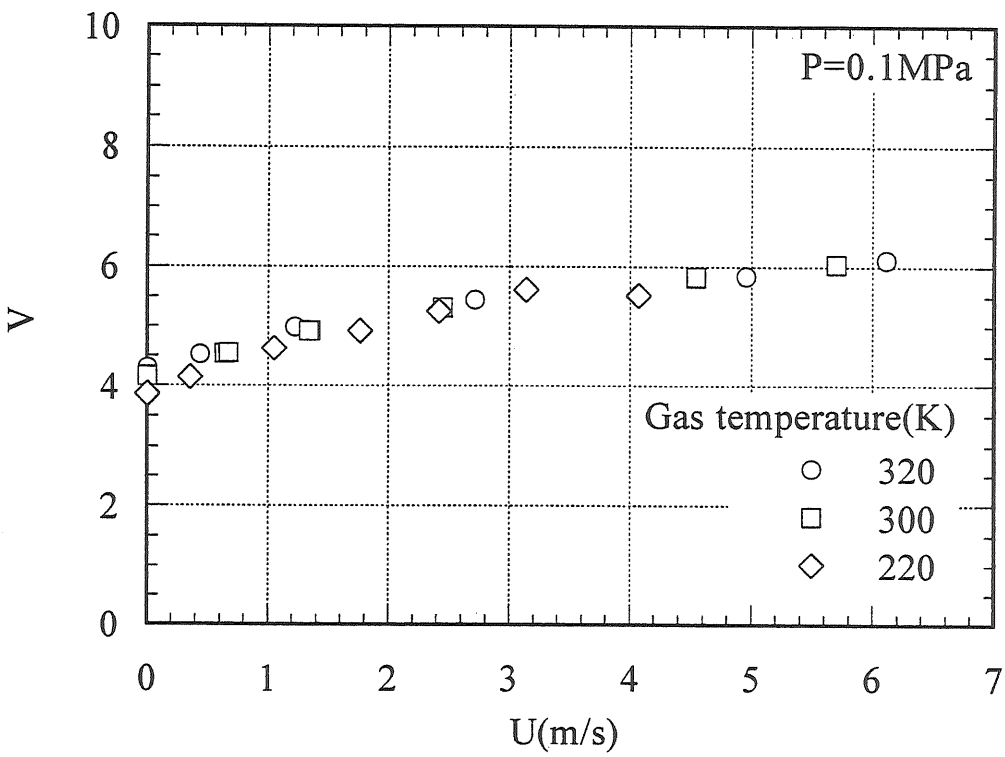

Figure 2-3. Temperature dependency of the output voltage of the hot wire anemometer,V.

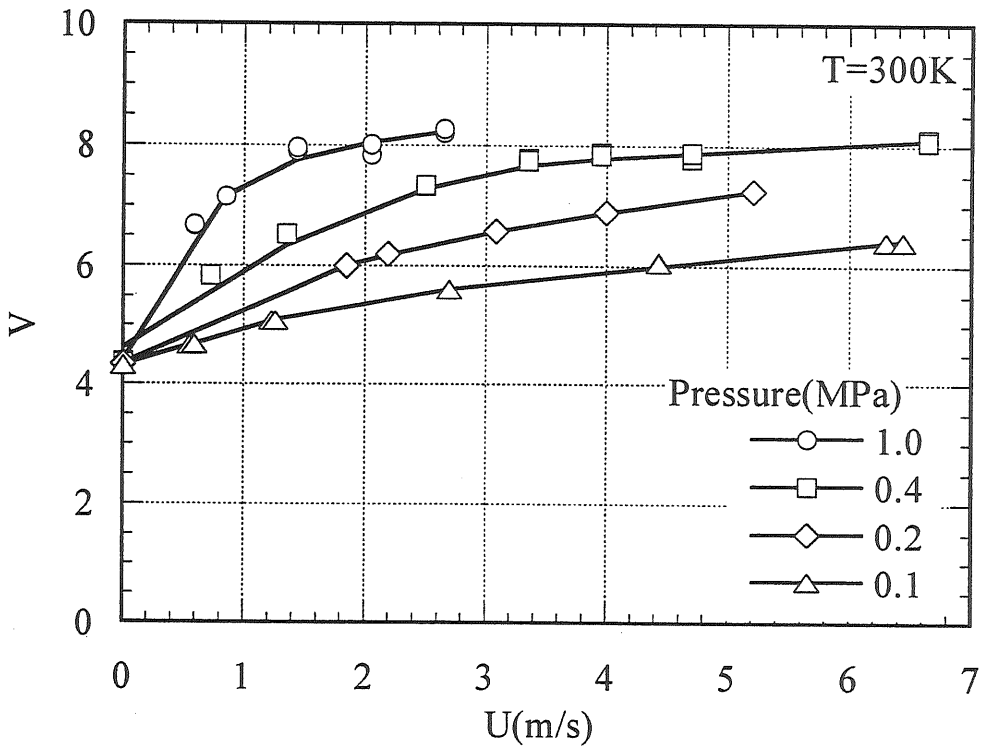

Figure 2-4. Pressure dependency of the output voltage of the hot wire anemometer, V.

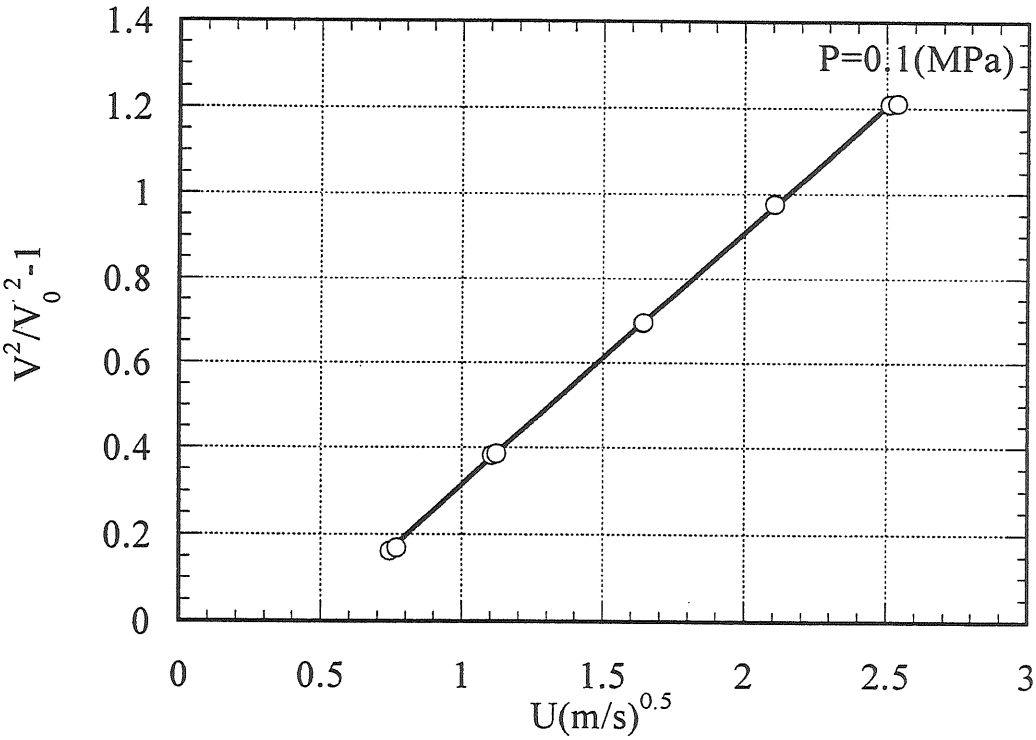

Figure 2-5. The relation of V^2 and $U^{0.5}$ for an experimental result on the basis of King's law.

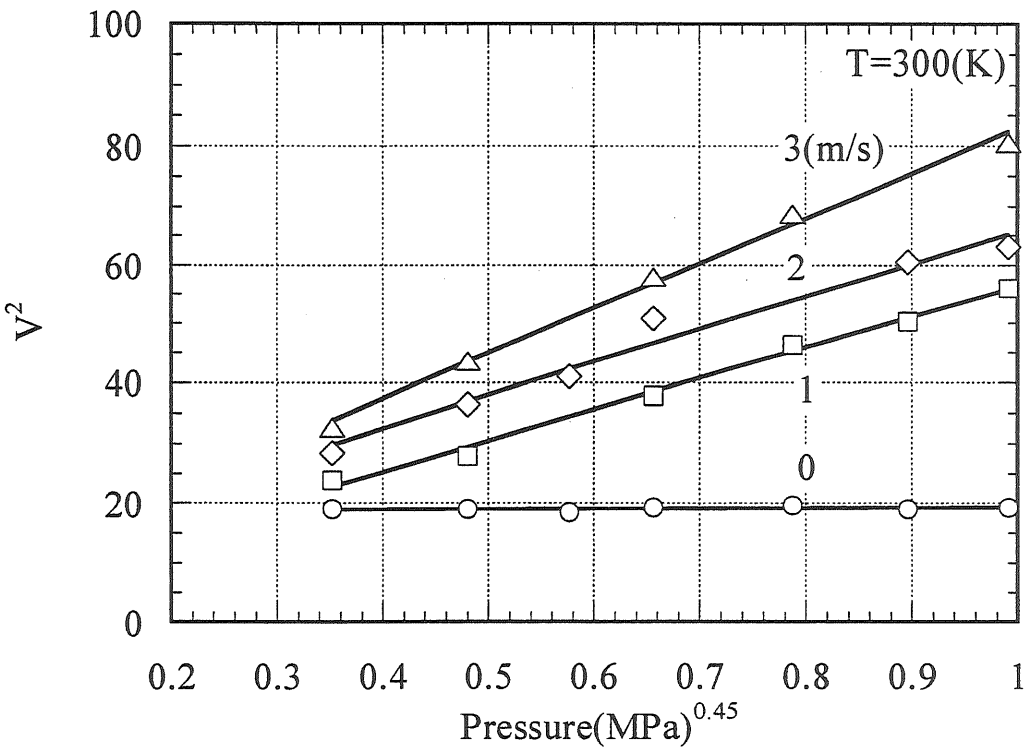

Figure 2-6. V^2 vs. $P^{0.45}$ relations for a number of values of the velocity U.

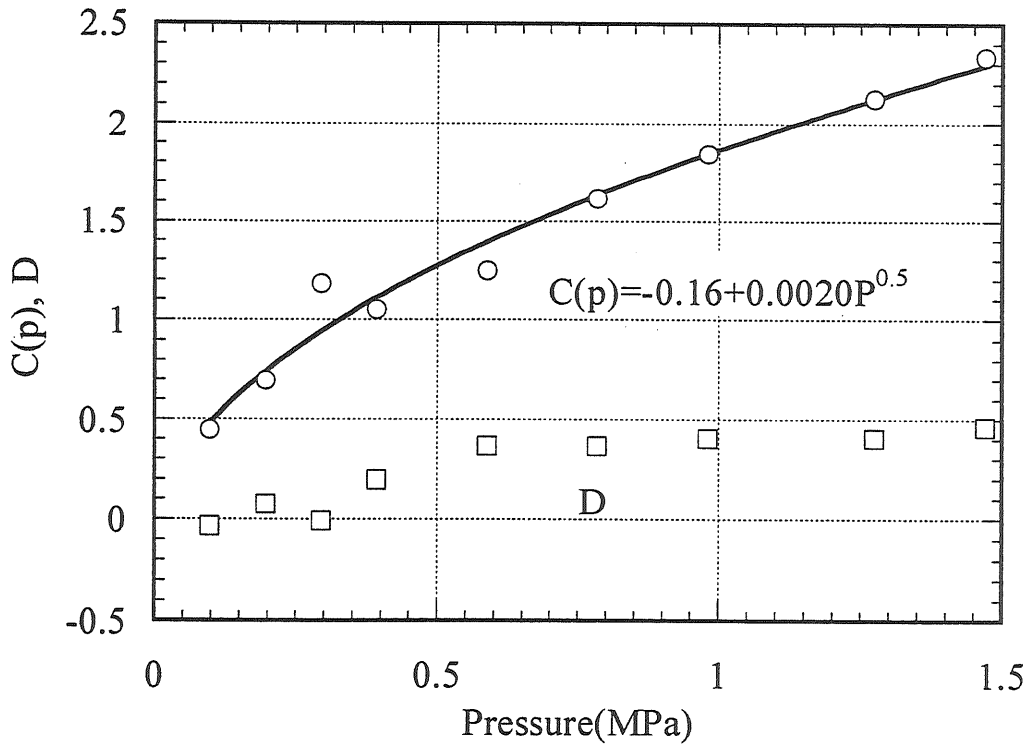

Figure 2-7. C(p) and D as a function of the pressure.

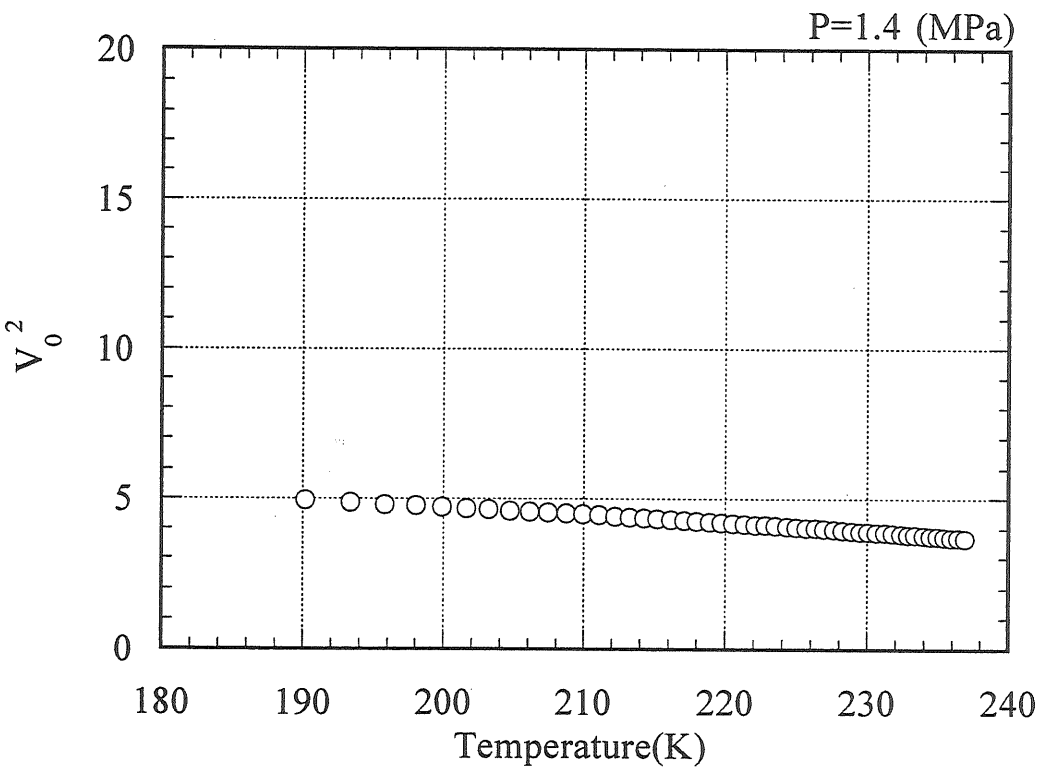

Figure 2-8. Temperature dependency of V_0^2.

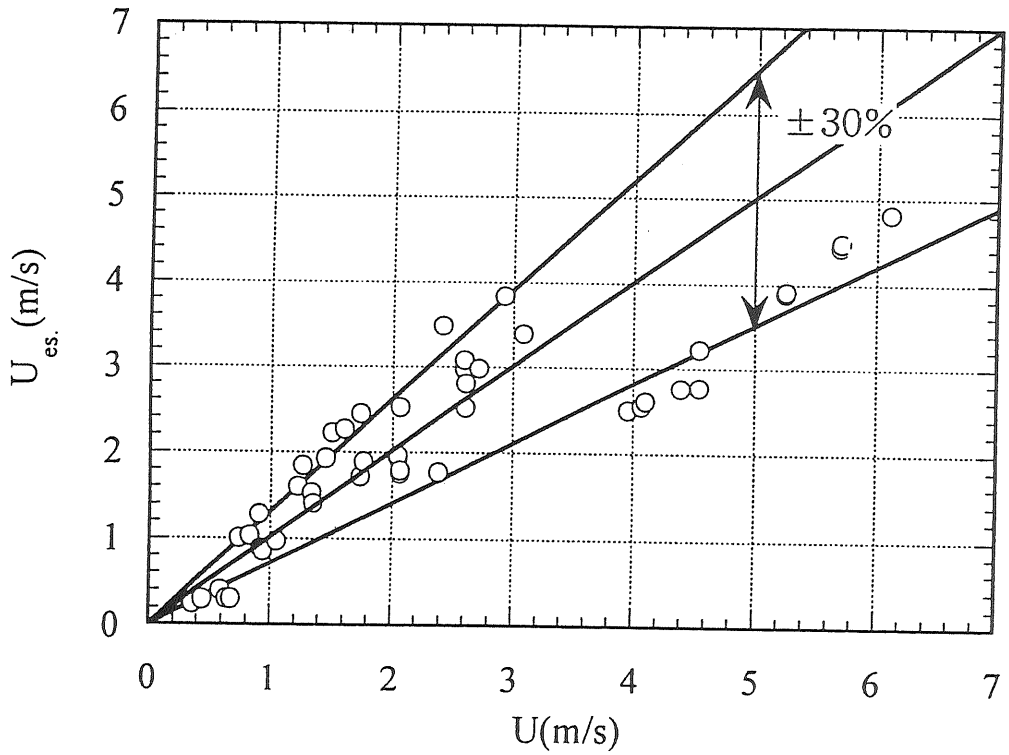

Figure 2-9. Comparison of the estimated velocity, $U_{es.}$, with the reference velocity, U for the estimation of the measurement error.

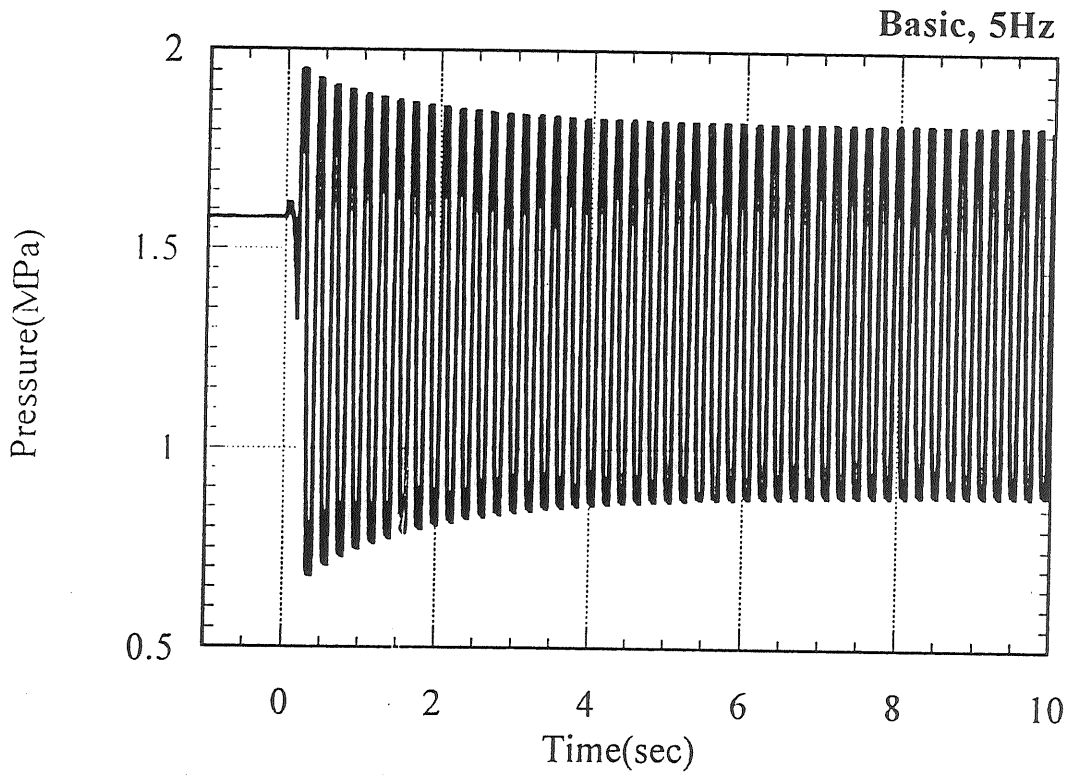

Figure 3-1. The start-up behavior of the pressure variation in a basic pulse tube refrigerator at 5 Hz for 10 sec.

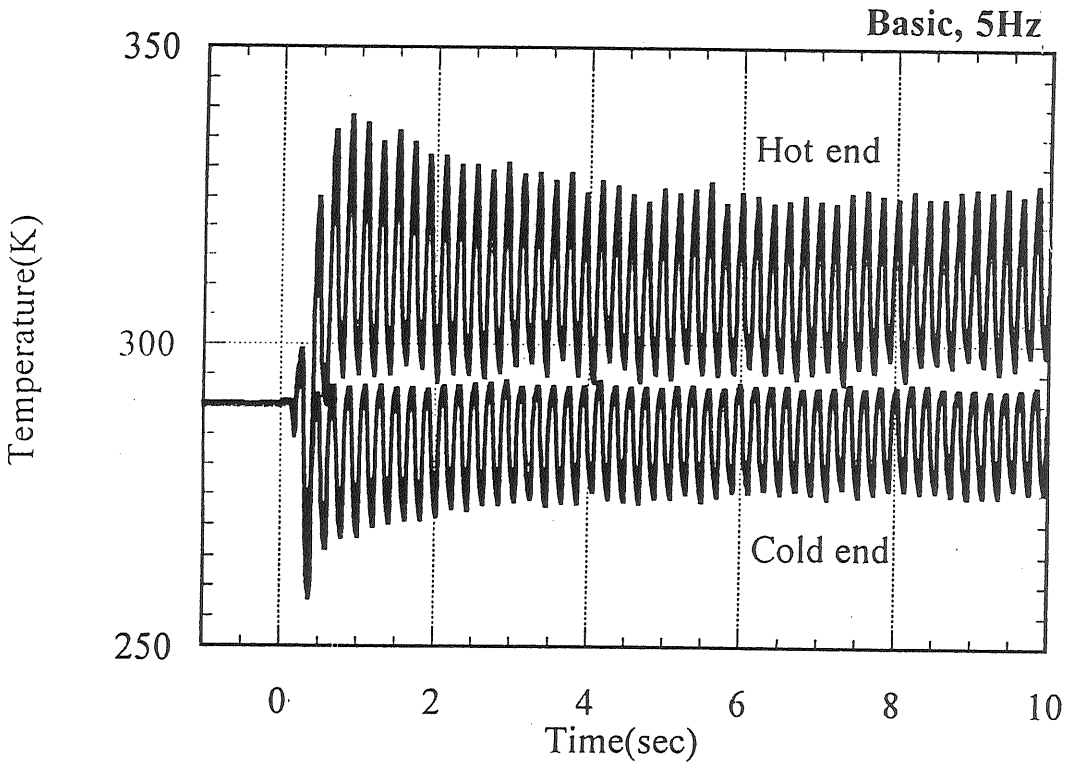

Figure 3-2. The start-up behavior of the gas temperature variation in a basic pulse tube refrigerator at 5 Hz for 10 sec.

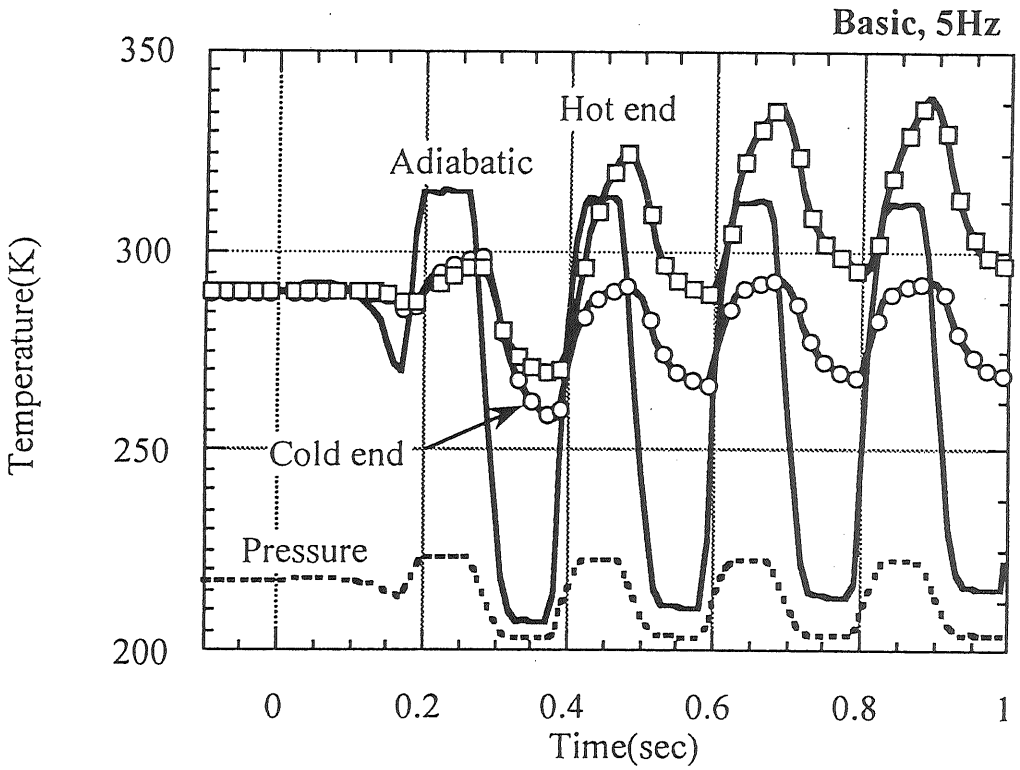

Figure 3-3. The start-up behavior of the gas temperature variation during several cycles; □ for hot end temperature, ○ for cold end temperature. The plain solid line is the adiabatic temperature variation calculated from the pressure data indicated by the dotted line.

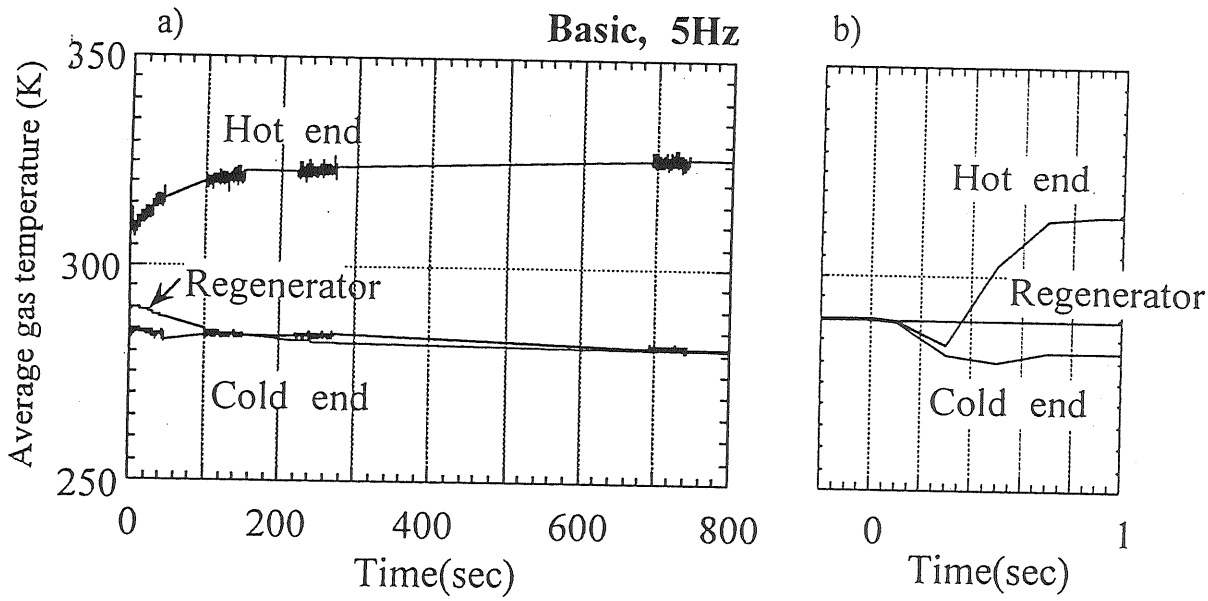

Figure 3-4. The start-up behavior of average gas temperatures during the cooling-down process. a) during 800sec, b) during 1sec immediately after the start-up.

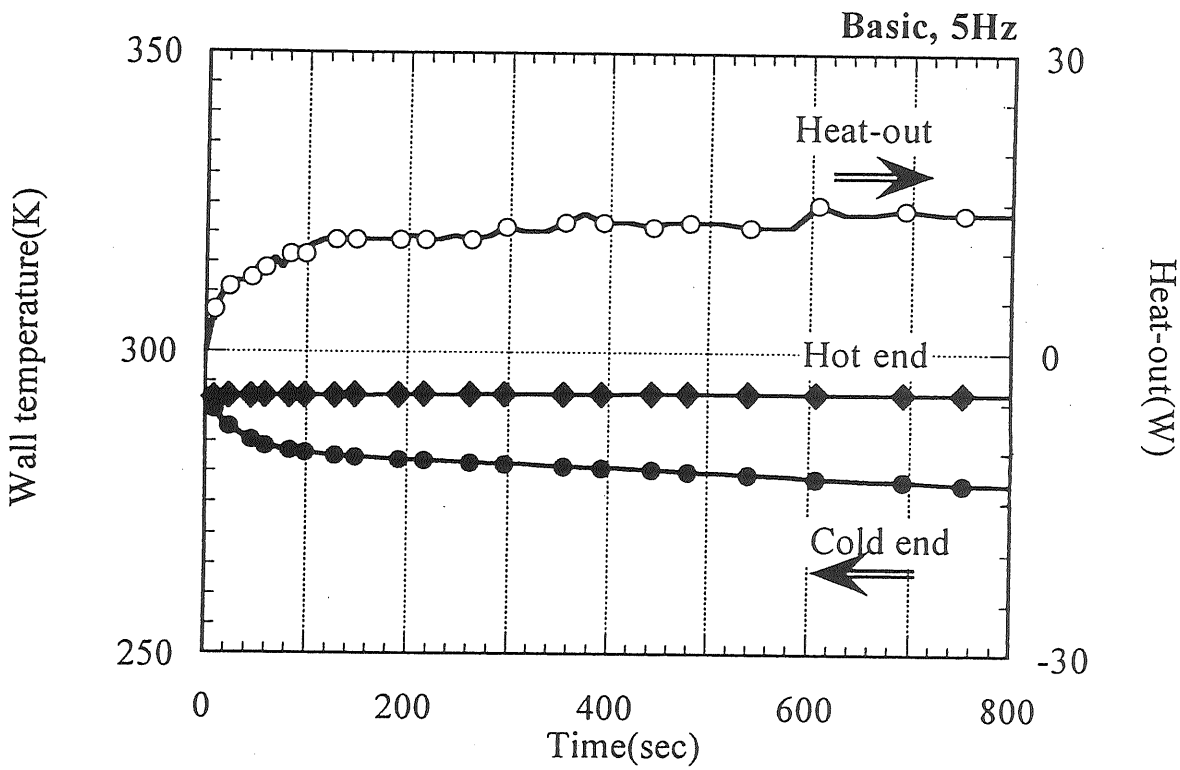

Figure 3-5. The start-up behavior of the wall temperatures and heat out during the cooling-down process.

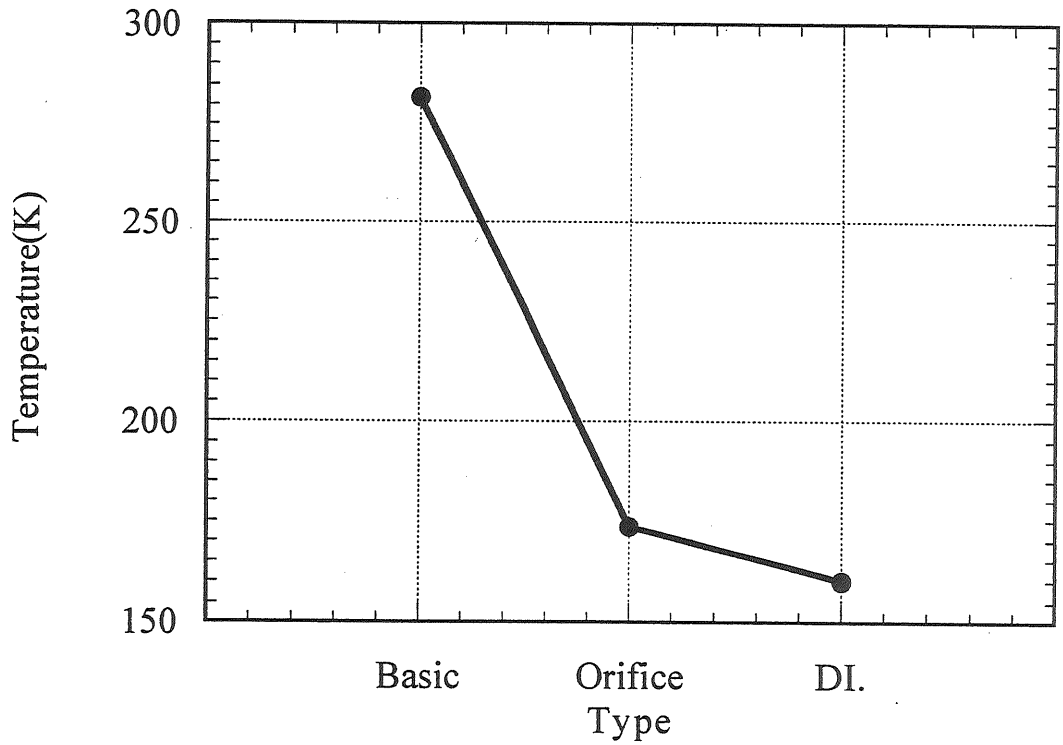

Figure 4-1. The lowest attainable wall temperature at the cold end for the three types. Pressure ratio; 1.4, mean gas pressure; 1.4 MPa, and without thermal vacuum inslation.

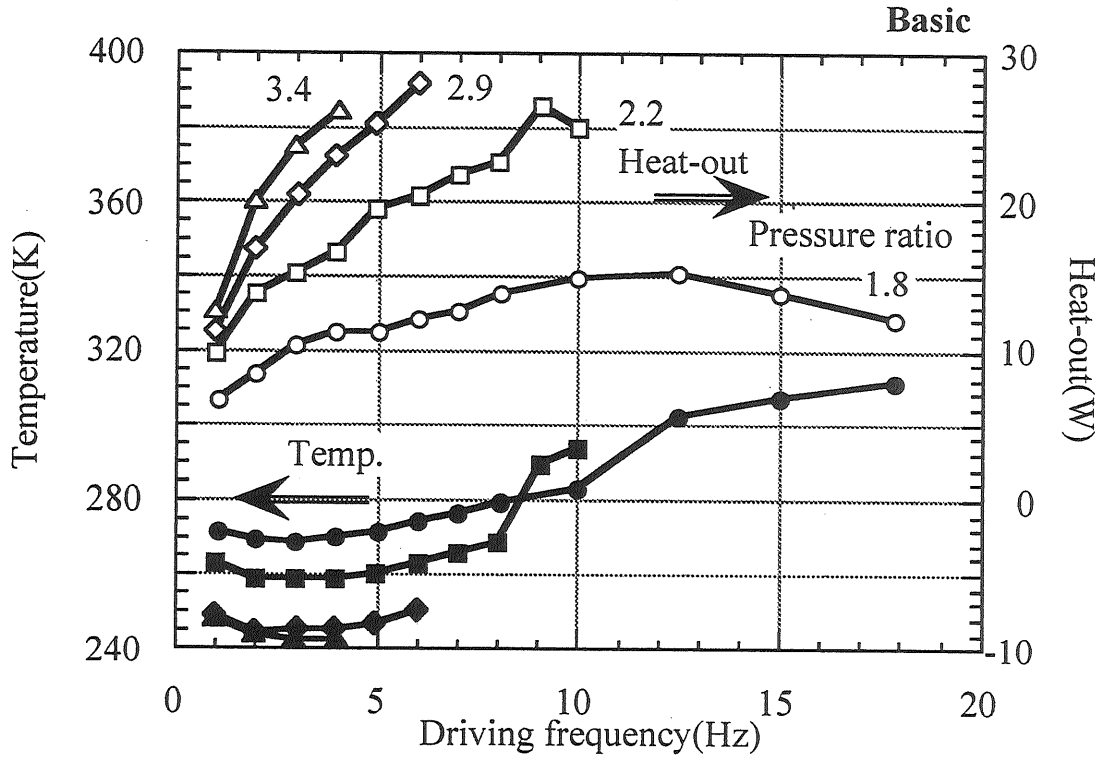

Figure 4-2. The attainable temperature at the cold end and the heat-out as a function of driving frequency in the basic type. Pressure ratio 1.8; ● and ○, 2.2; ■ and □, 2.9; ◆ and ◇, 3.4; ▲ and △.

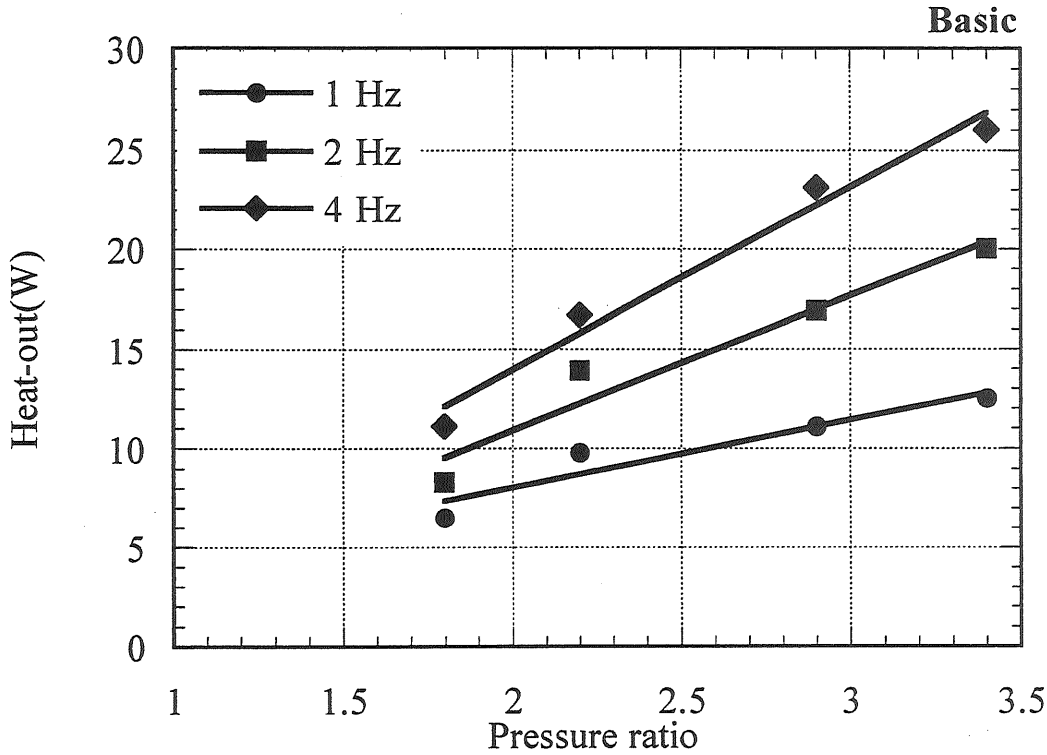

Figure 4-3. The heat-out as a function of pressure ratio at three driving frequencies.

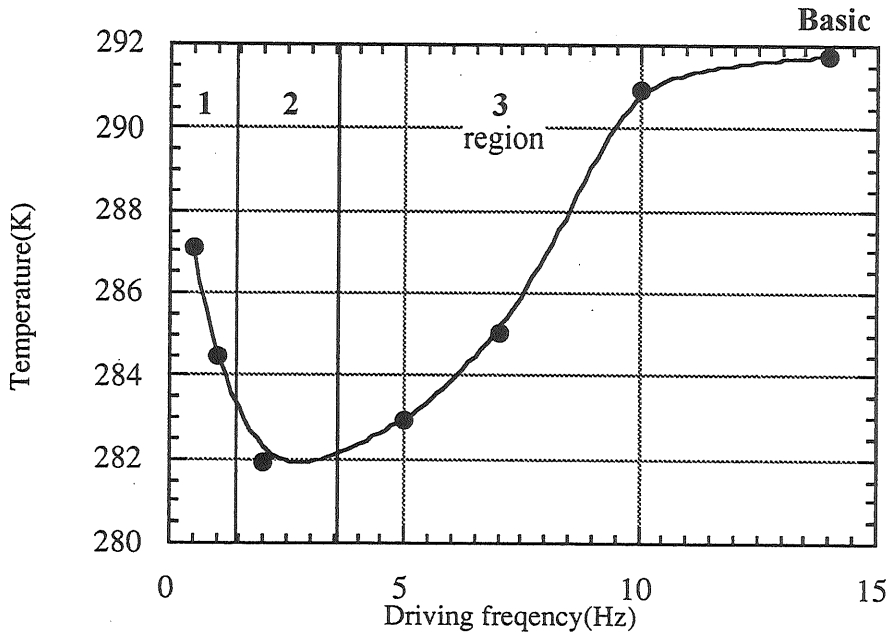

Figure 4-4. The attainable temperature at the cold end as a function of driving frequency. Pressure ratio;1.4, mean gas pressure; 1.4 MPa. The fundamental performance is divided into three regions as indicated by numbers 1, 2 and 3.

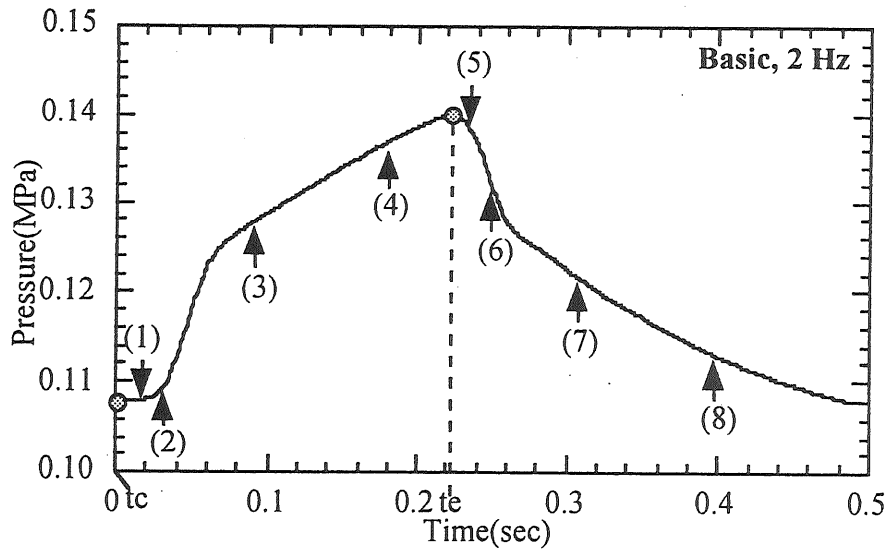

Figure 4-5-a. Pressure variation during typical one cycle for the basic type, 2 Hz. The timing of visualization and smoke emission are indicated by the numbers (1) through (8) for visualization and tc and te for smake emission. (Ref. [25])

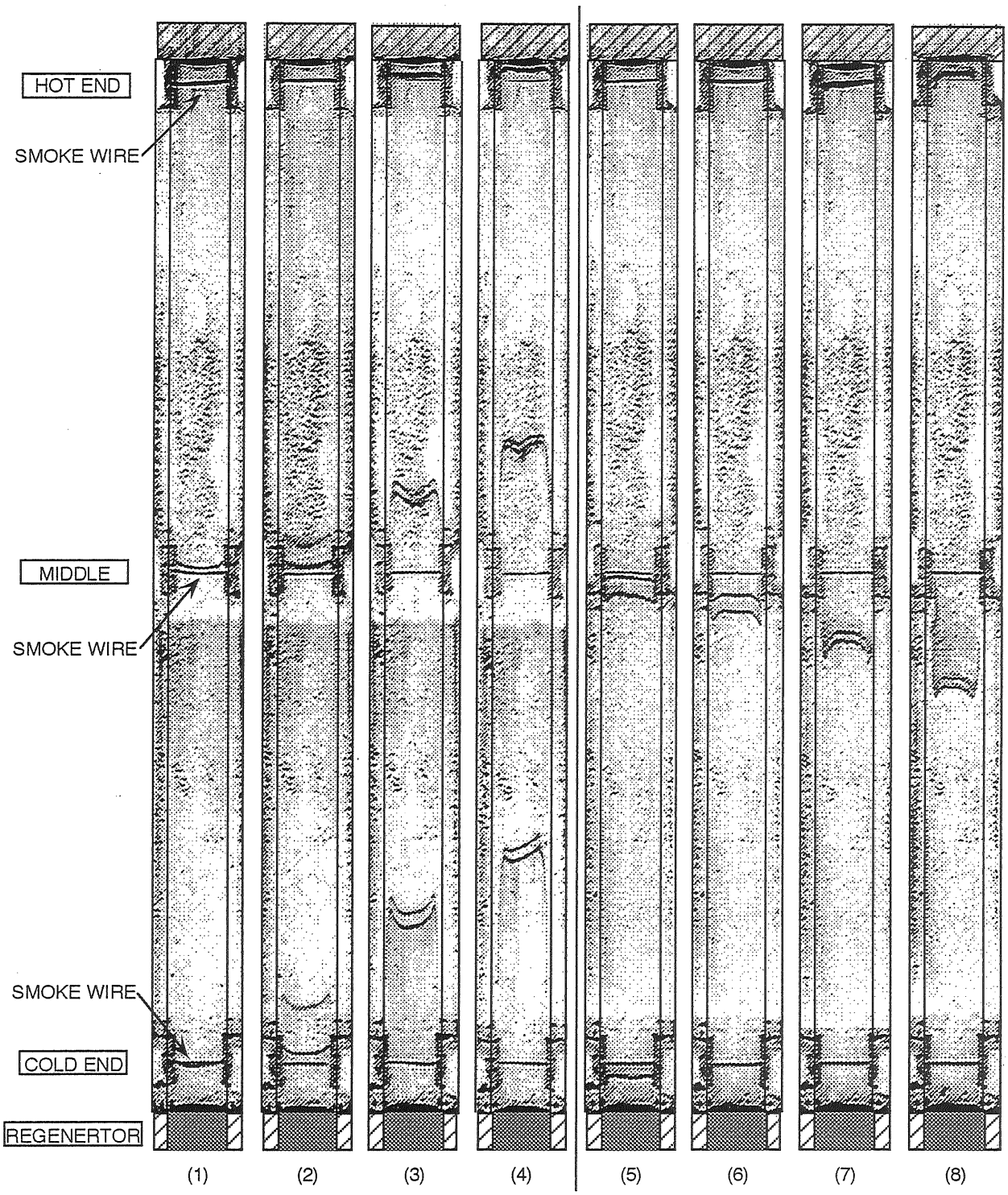

Figure 4-5-b. Smoke-wire flow visualization photographs in the basic type. The numbers (1) through (8) correspond to those indicated in figure 4-5-a. (Ref. [25])

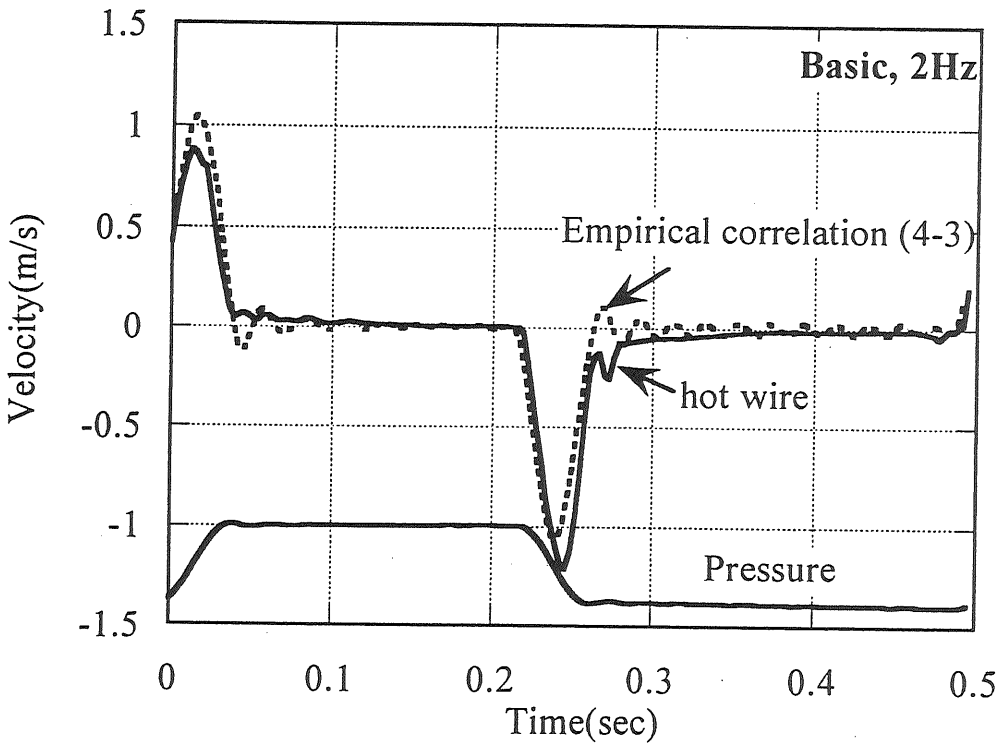

Figure 4-6. The comparison of the velocity variations between the experimental data and the result derived from the empirical correlation drawn by a dotted line equation (4-3), 2 Hz, r=0 mm.

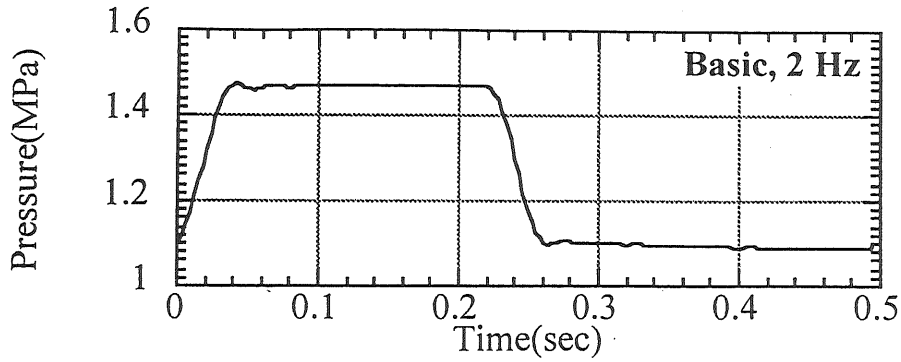

Figure 4-7-a.

Velocity

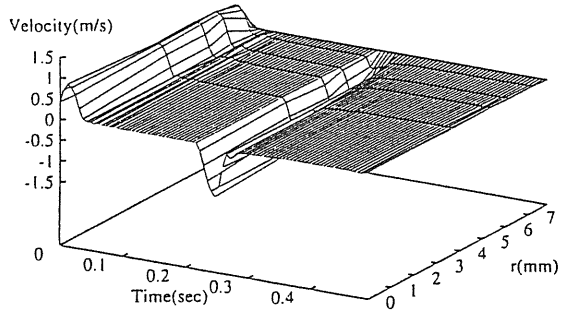

Figure 4-7-b..

Temperature

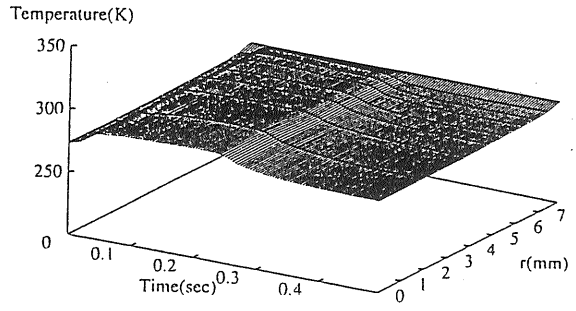

Figure 4-7-e..

Cold

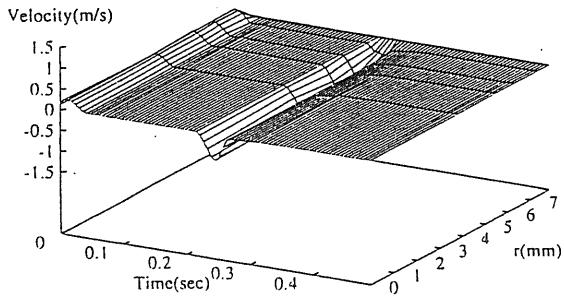

Figure 4-7-c.

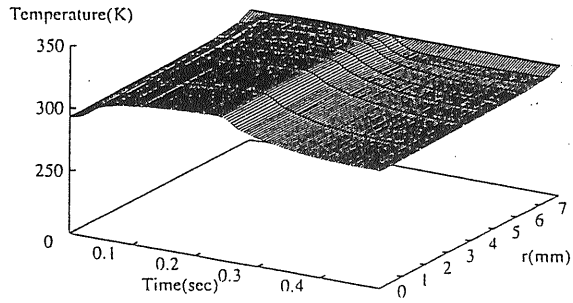

Figure 4-7-f.

Middle

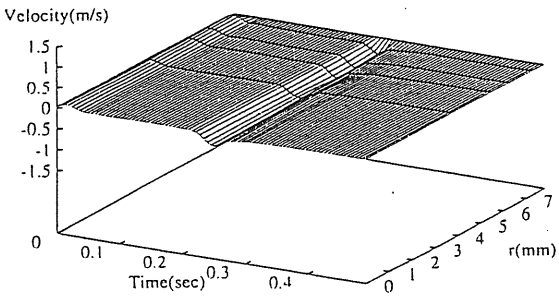

Figure 4-7-d.

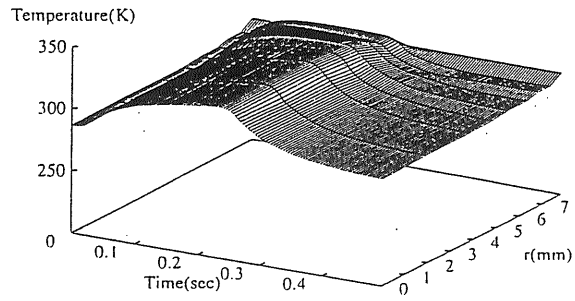

Figure 4-7-g.

Hot

Figure 4-7. Time variations of the radial distribution of the axial velocity and the temperature in the basic type. Pressure ratio; 1.4, mean gas pressure; 1.4 MPa driving frequency; 2 Hz.

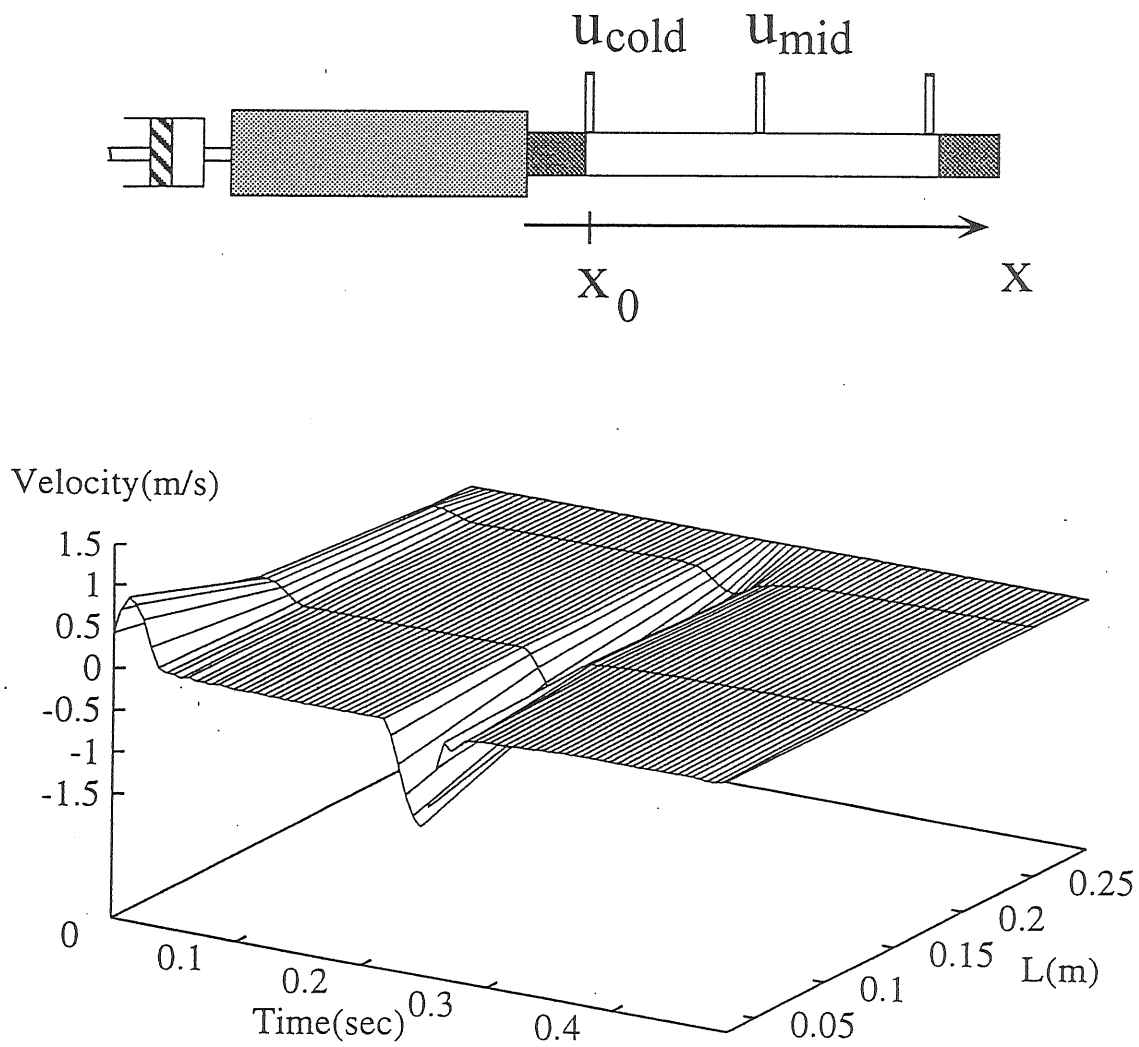

Figure 4-8. Geometrical model for the estimation of the gas displacement. Time variation of the velocity distribution in the axial direction.

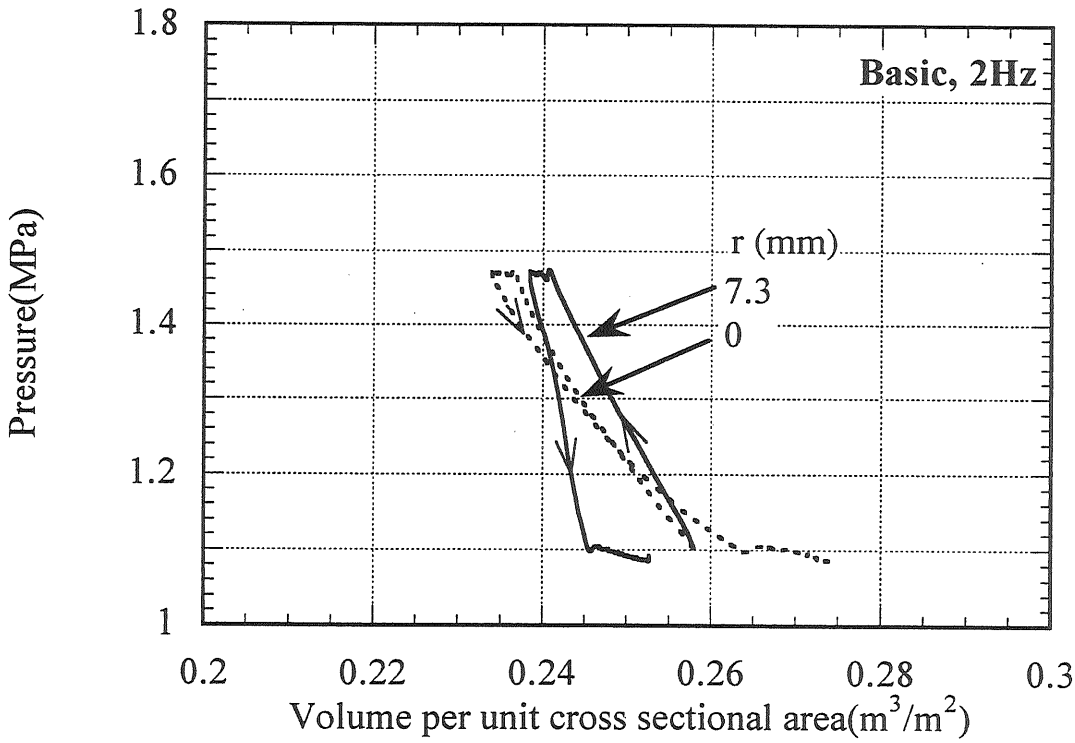

Figure 4-9. The P-V diagram per unit cross sectional area at two radial position; r/r_0=0 and 0.94. Driving frequency is 2 Hz.

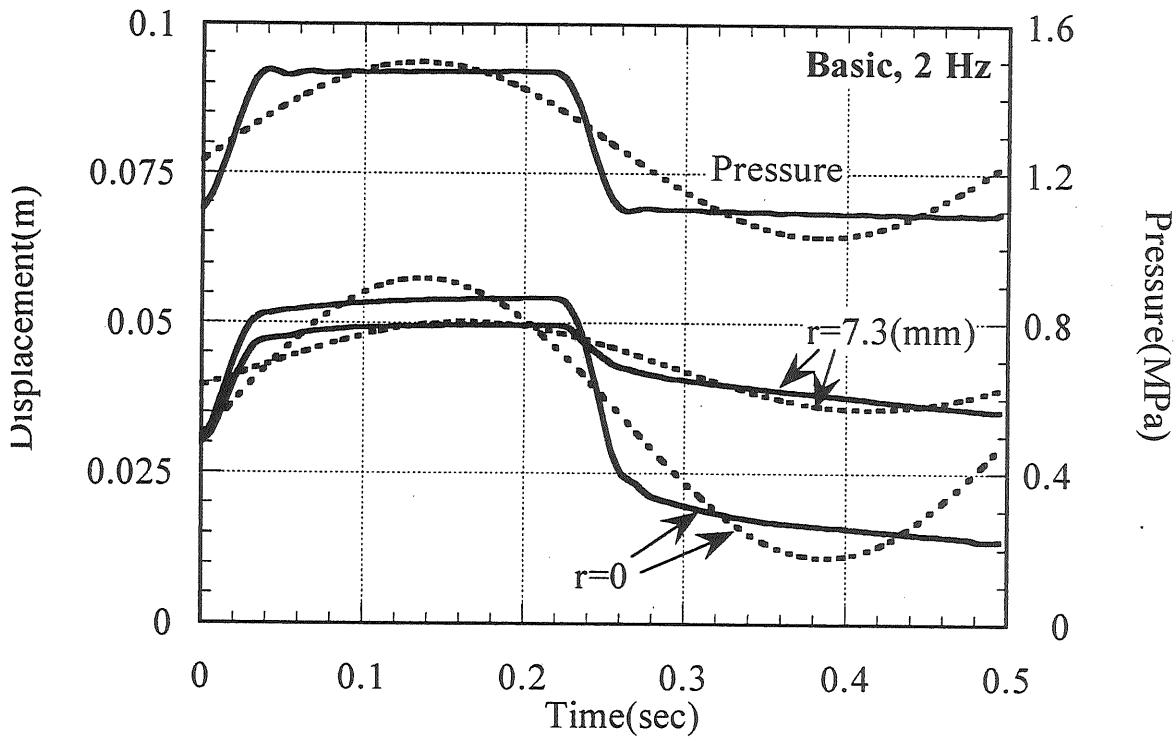

Figure 4-10. The comparison of variations between the experimental data and the approximation by the fundamental mode only.
——— Experimental data, - - - - Approximation

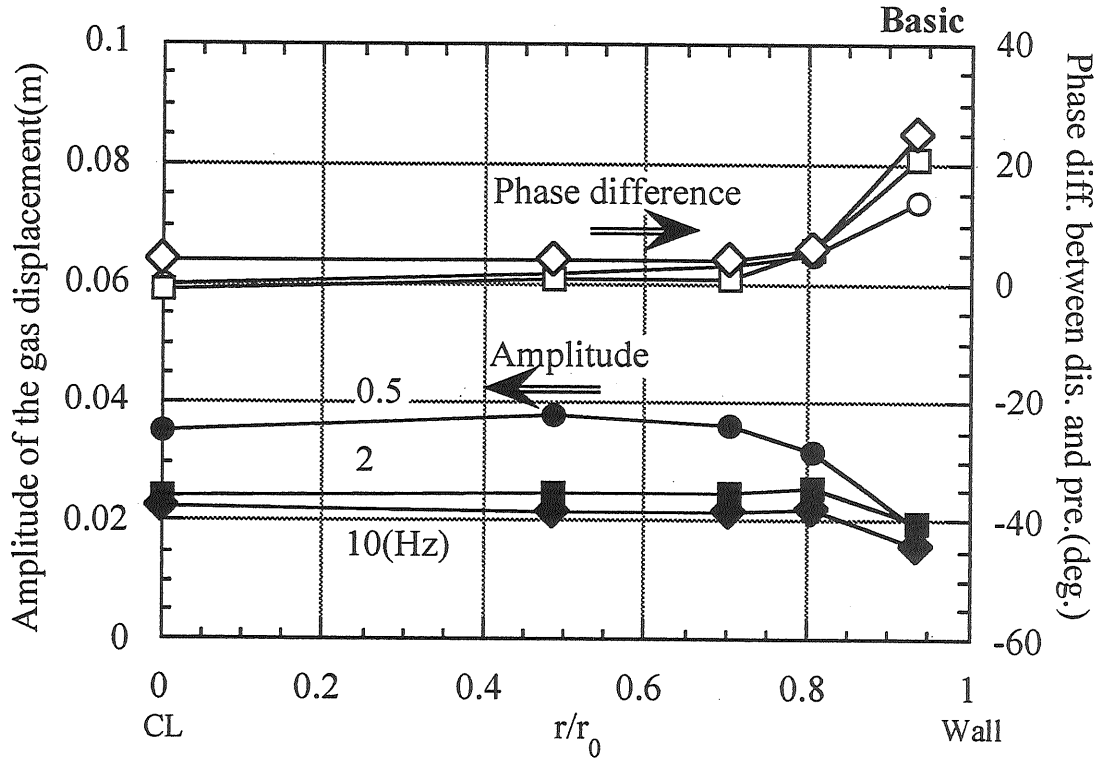

Figure 4-11. Radial profiles of the amplitude of the gas displacement and the phase difference between the gas pressure and the displacement . 0.5 Hz; ● and ○ , 2 Hz; ■ and □, 10 Hz; ◆ and ◇.

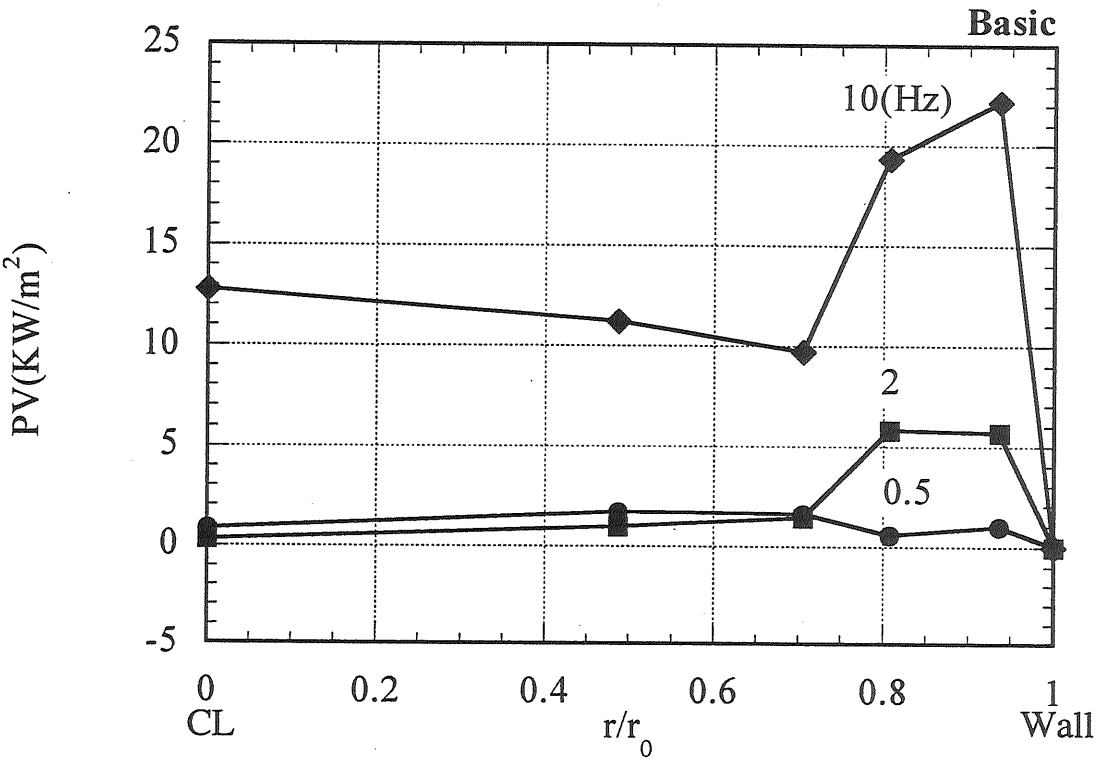

Figure 4-12. Radial profiles of P-V works per unit cross sectional area for three driving frequencies. Pressure ratio; 1.4, mean gas pressure;1.4 MPa

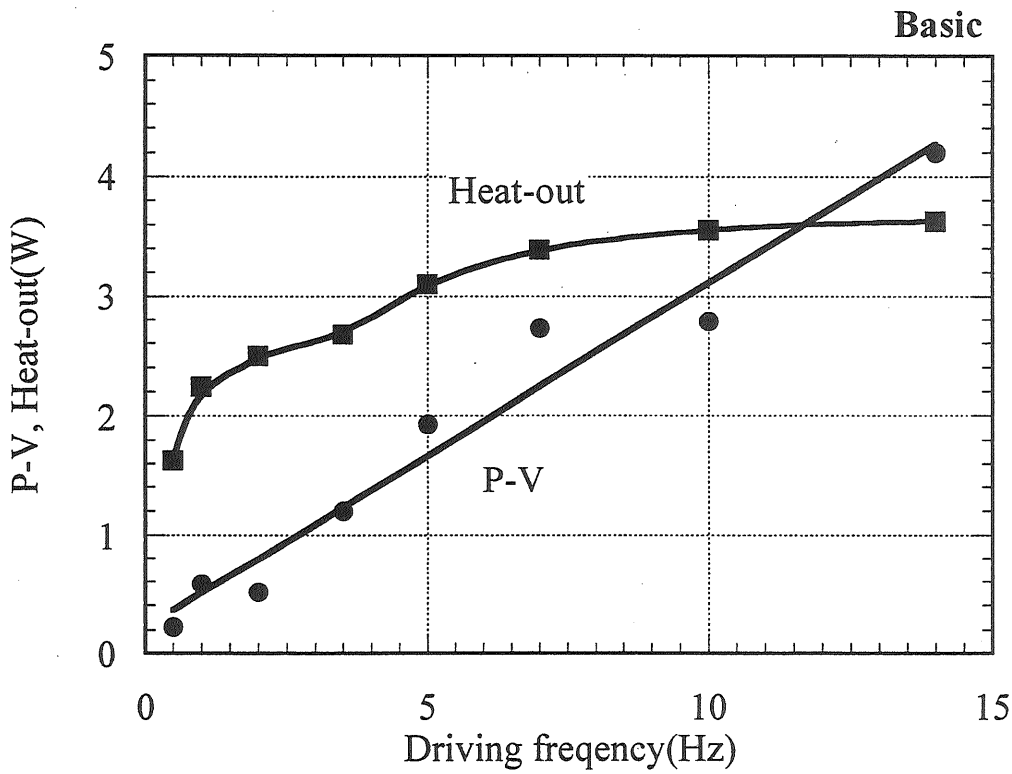

Figure 4-13. The P-V work and the heat out as a function of driving frequency.

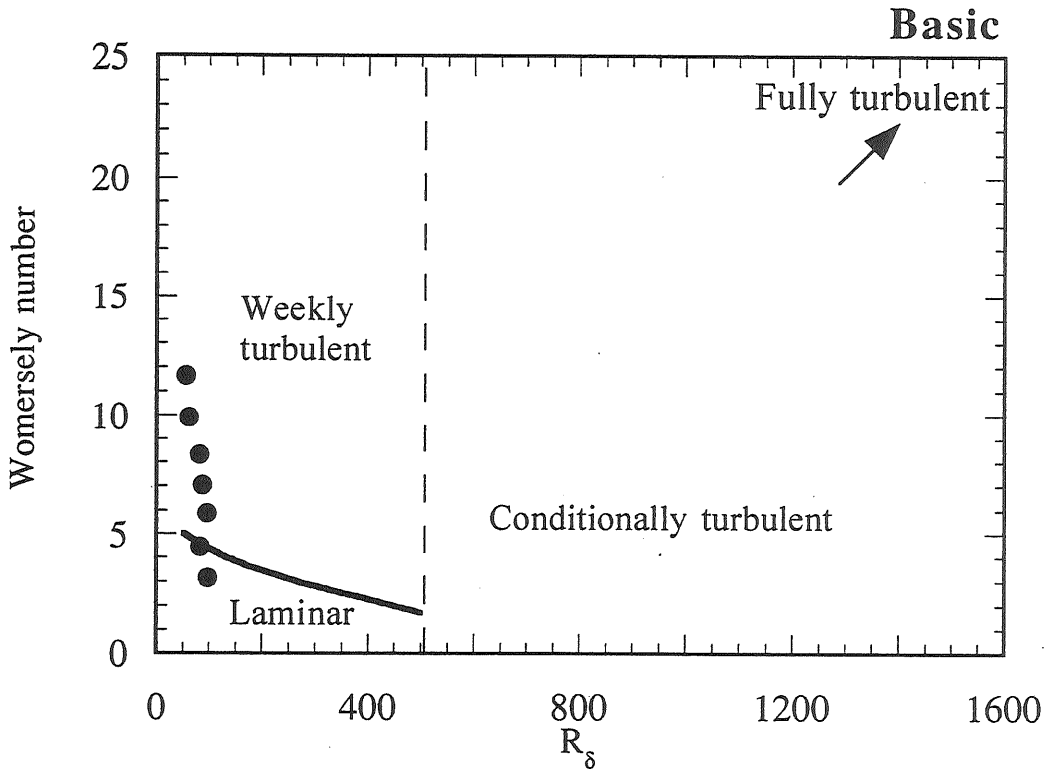

Figure 4-14. The stability diagram for the oscillating flow according to the result by Hino et al.

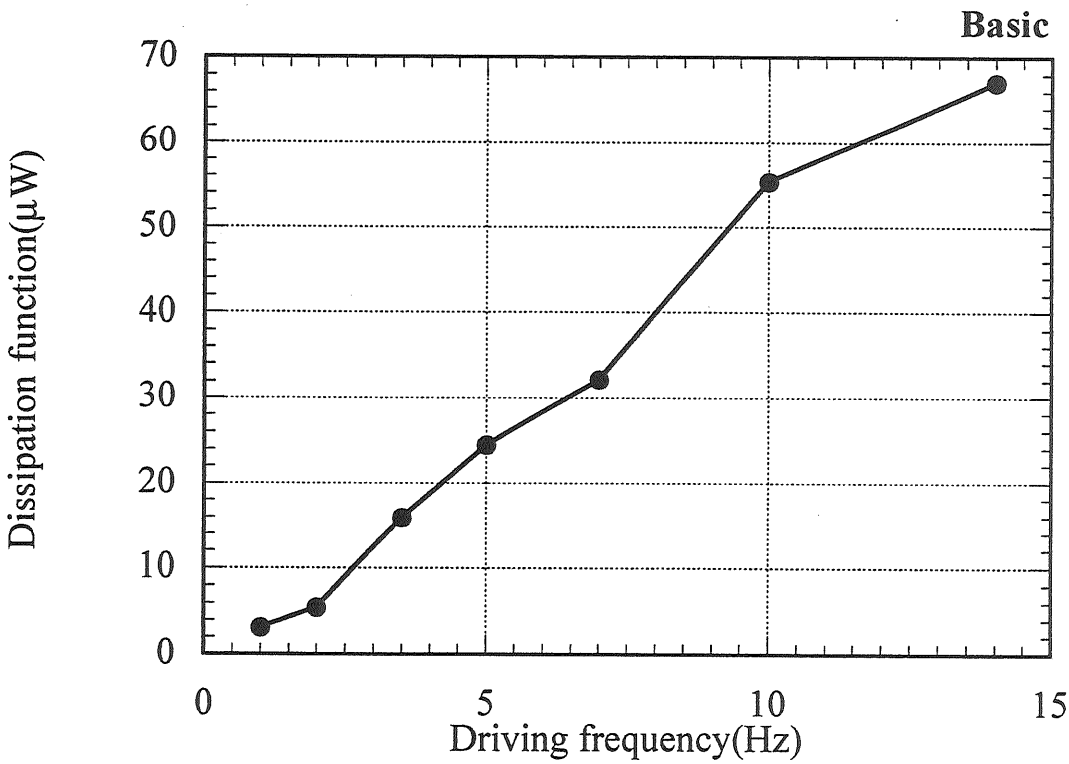

Figure 4-15. Dissipation function as a function of driving frequency.

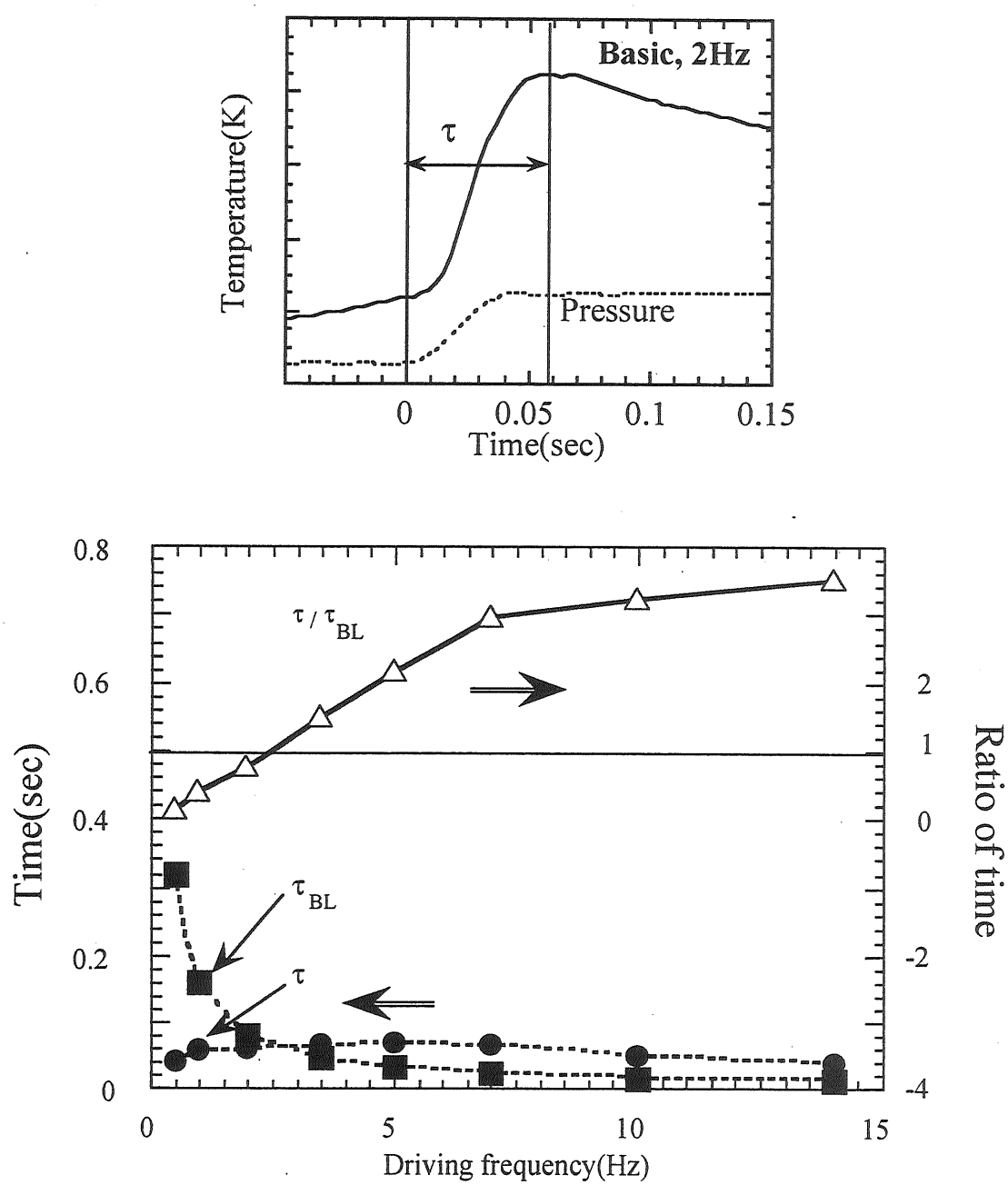

Figure 4-16. Characteristic times and ratio of characteristic times as a function of driving frequency.

Table 4-1. Summary of the driving frequency dependence.

Frequency	Attainable temperature	P-V work	ϕ	τ/τ_{BL}
Region 1	High	Small	Small	<1
Region 2	Low	Medium	Medium	$\fallingdotseq$1
Region 3	High	Large	Large	>1

ϕ : Dissipation function

τ/τ_{BL} : Ratio of thermal relaxation time to the time duration reaching the constant temperature over the boundary layer

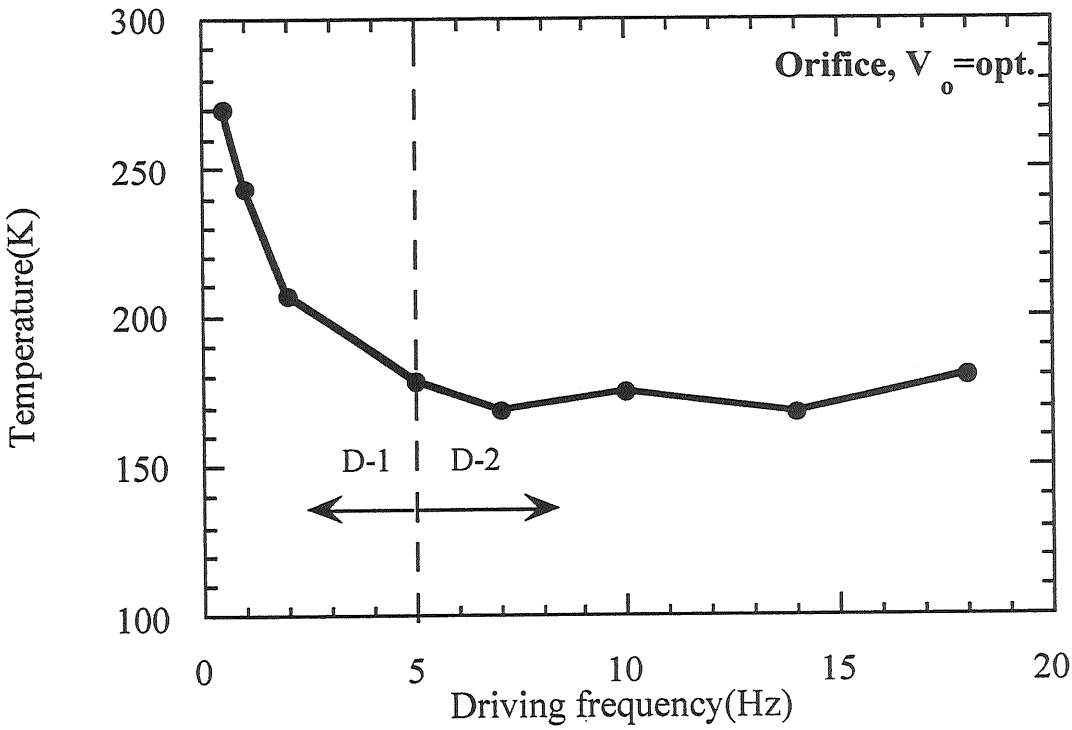

Figure 5-1. The attainable temperature at the cold end as a function of driving freqency for the orifice type. The pressure ratio of 1.4, the mean pressure of 1.4 MPa. The optimum valve opening is set for every driving frequency. The fundamental performance is divided into two regions as indicated by D-1 and D-2.

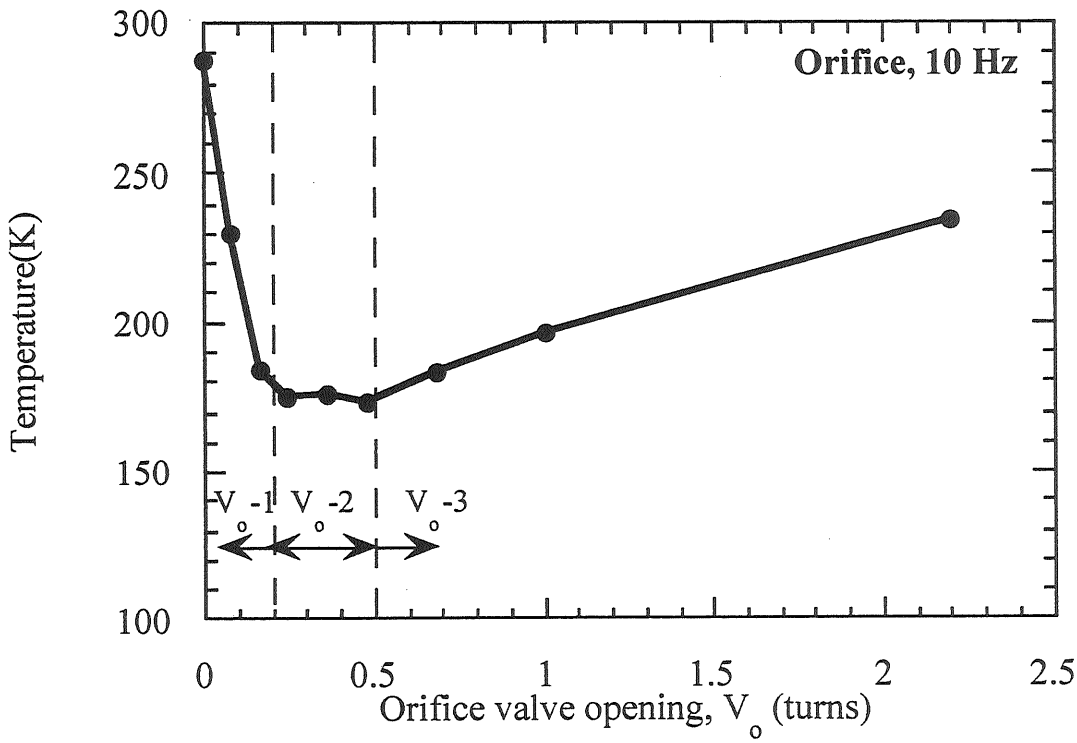

Figure 5-2. The attainable temperature at the cold end as a function of orifice valve opening for the orifice type at 10 Hz. The pressure ratio of 1.4, the mean pressure of 1.4 MPa. The fundamental performance is divided into three regions as indicated by V_o-1, V_o-2 and V_o-3.

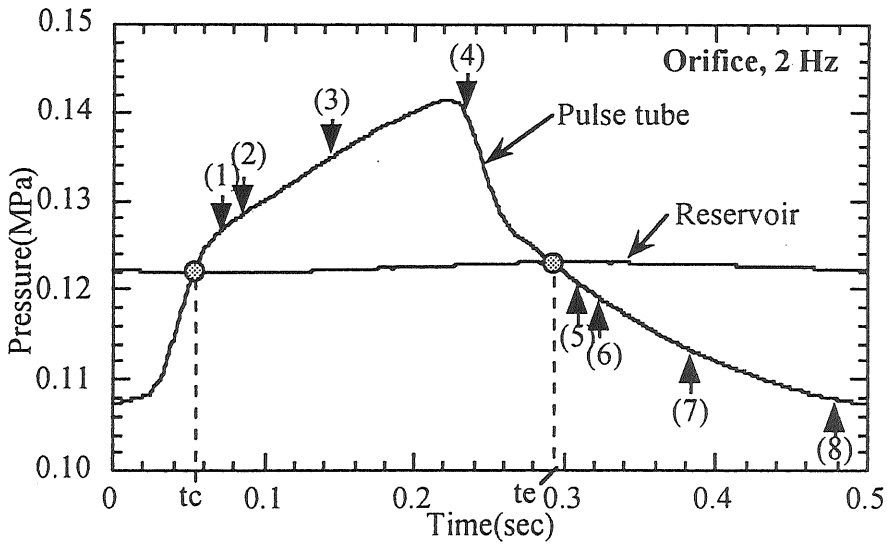

Figure 5-3-a. Pressure variation during typical one cycle for the orifice type, 2 Hz. The timing of visualization and smoke emission are indicated by the numbers (1) through (8) for visualization and tc and te for smoke emission. (Ref. [25])

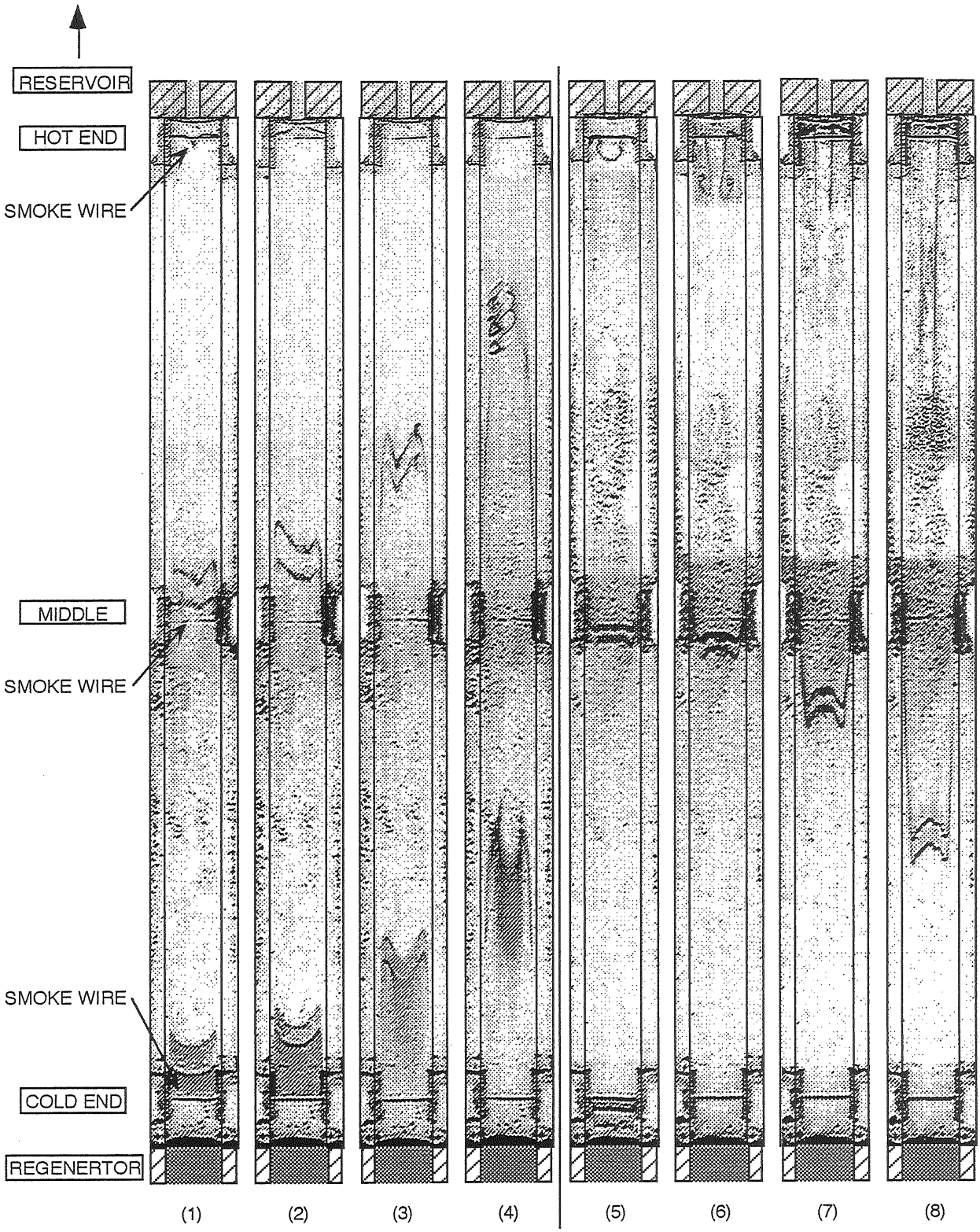

Figure 5-3-b. Smoke-wire flow visualization photographs in the orifice type. The numbers (1) through (8) correspond to those in figure 5-2-a. (Ref. [25])

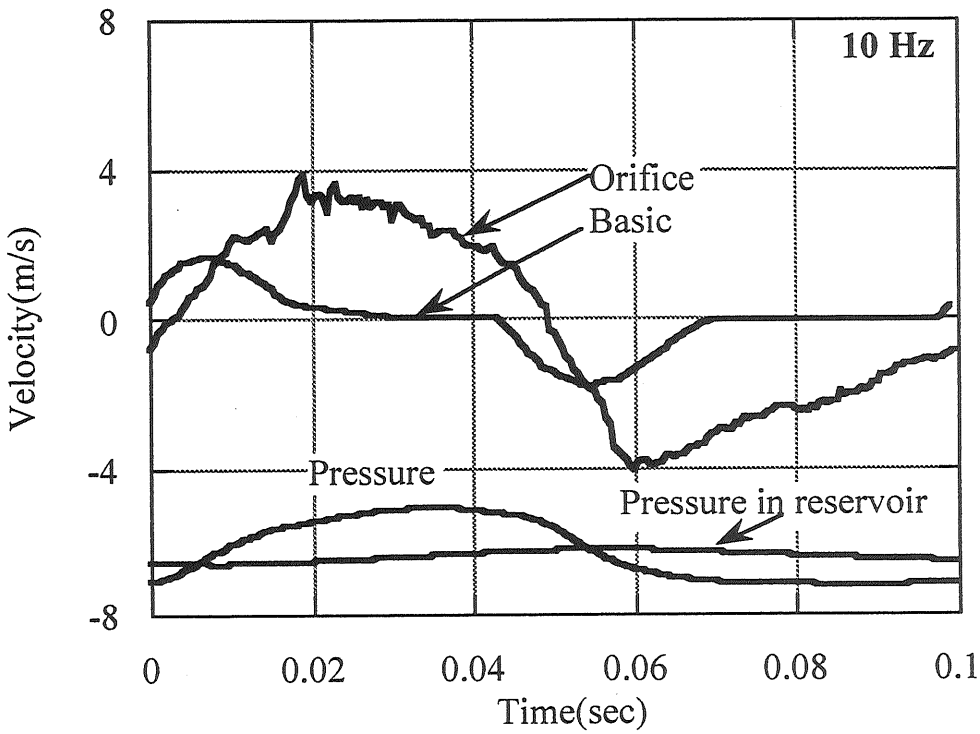

Figure 5-4. The comparison of the velocity variations on the centerline between the orifice and the basic types at 10 Hz. The pressure variation in the pulse tube and in the reservoir are also shown. The pressure ratio of 1.4, the mean pressure of 1.4 MPa.

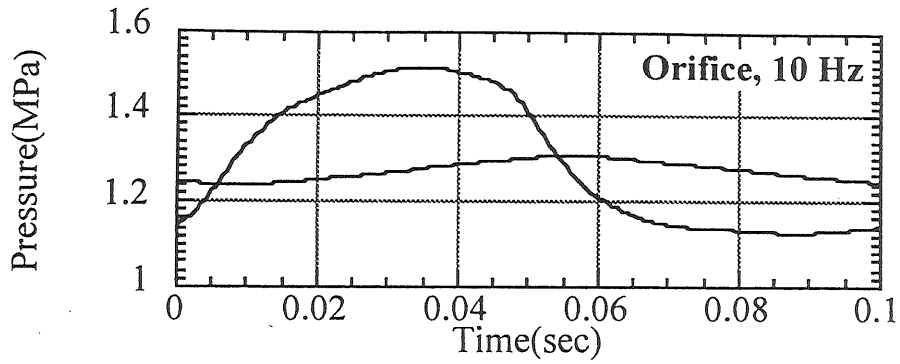

Figure 5-5-a.

Velocity **Temperature**

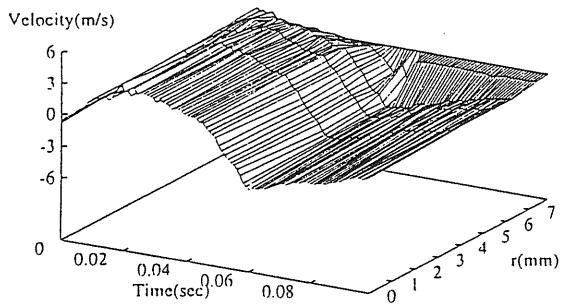

Figure 5-5-b.

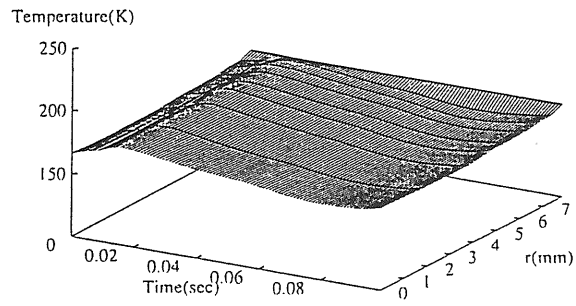

Figure 5-5-e.

Cold

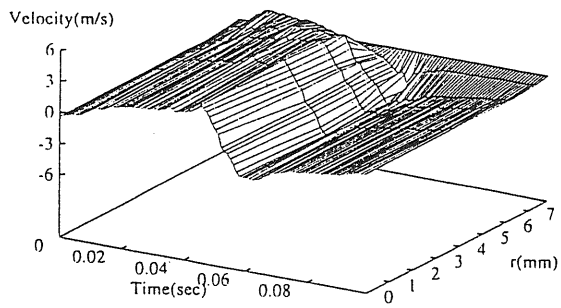

Figure 5-5-c.

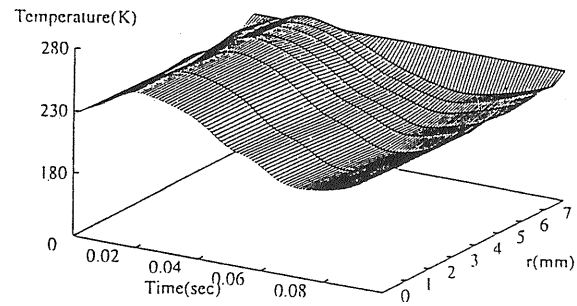

Figure 5-5-f.

Middle

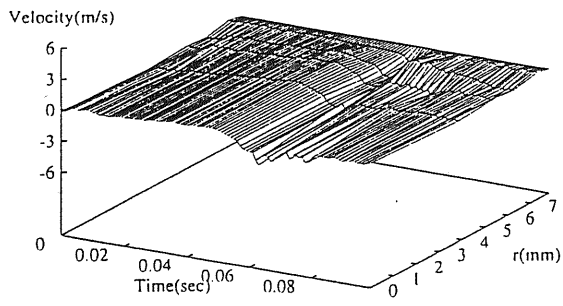

Figure 5-5-d.

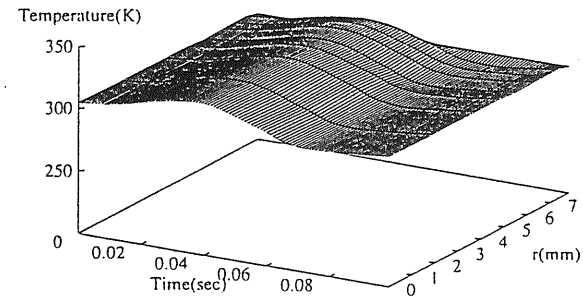

Figure 5-5-g.

Hot

Figure 5-5. Time variations of the radial distribution of the axial velocity and the temperaturein the orifice type, 10 Hz, V_o=0.36.

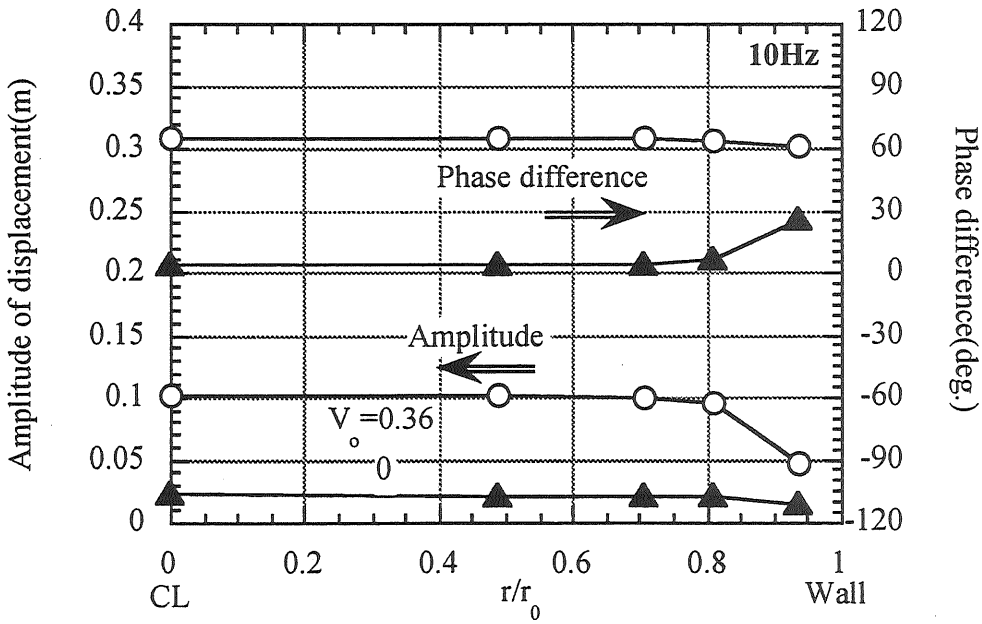

Figure 5-6. Radial profiles of the amplitude of the gas displacement and the phase difference between the pressure and the displacement variations. V_0=0; ▲, V_0=0.36; ○ .

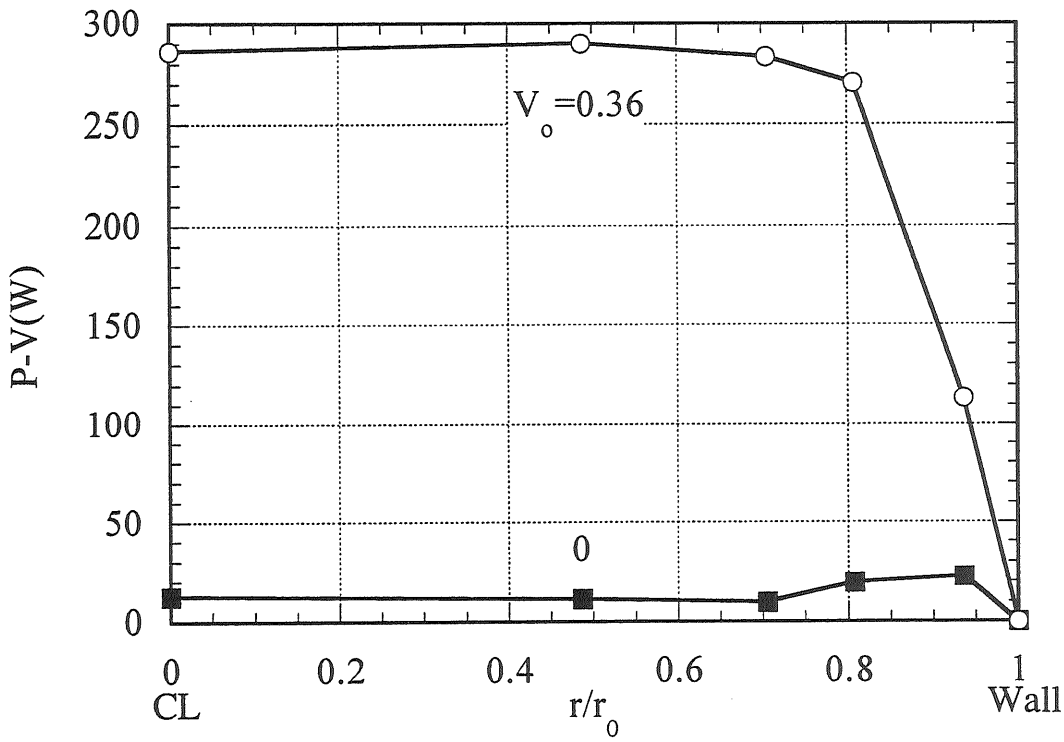

Figure 5-7. Radial profiles of P-V works per unit cross sectional area in the orifice and basic types. The pressure ratio of 1.4, the mean gas pressure of 1.4 MPa.

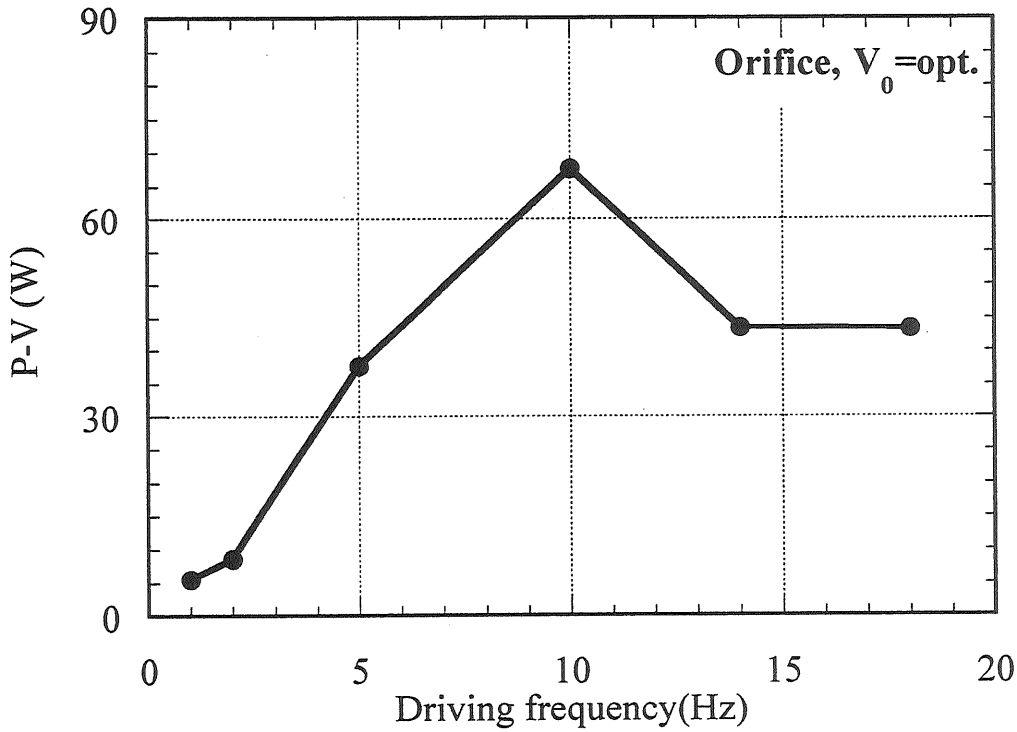

Figure 5-8. The variation of P-V work as a function of driving frequency. The orifice valve opening is set at the optimum value for every frequency.The pressure ratio of 1.4, the mean gas pressure of 1.4 MPa.

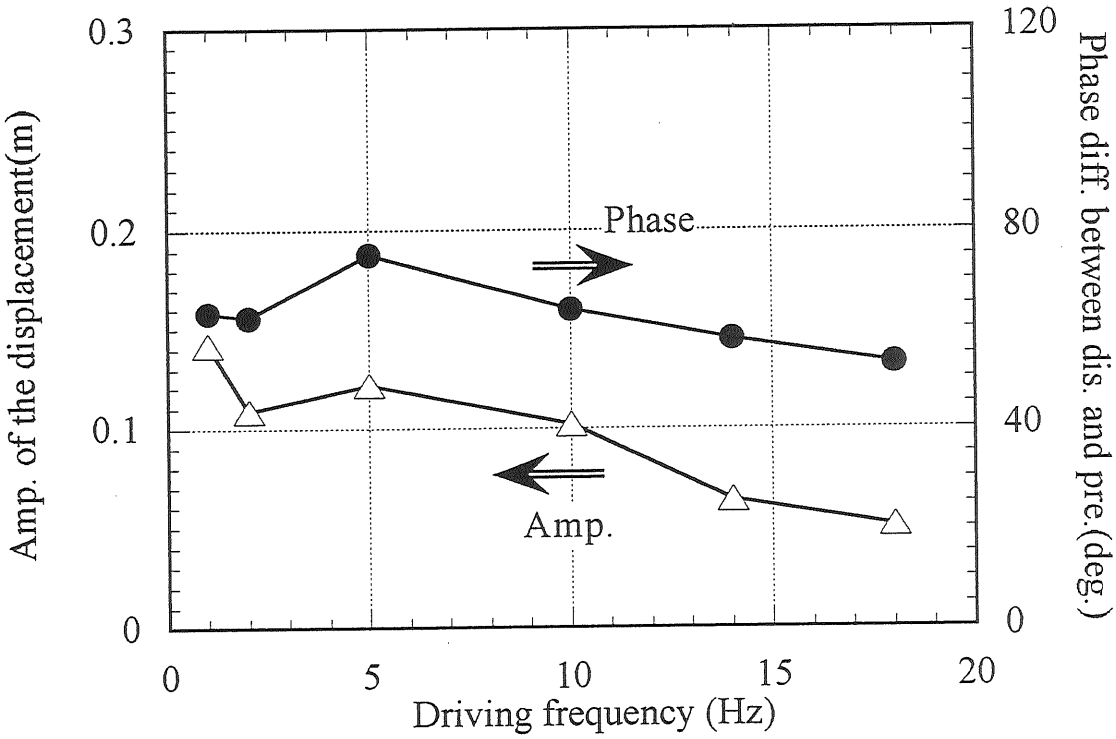

Figure 5-9. The amplitude of the gas displacement and the phase difference as a function of driving frequency at 10 Hz. The pressure ratio of 1.4, the mean gas pressure of 1.4 MPa.

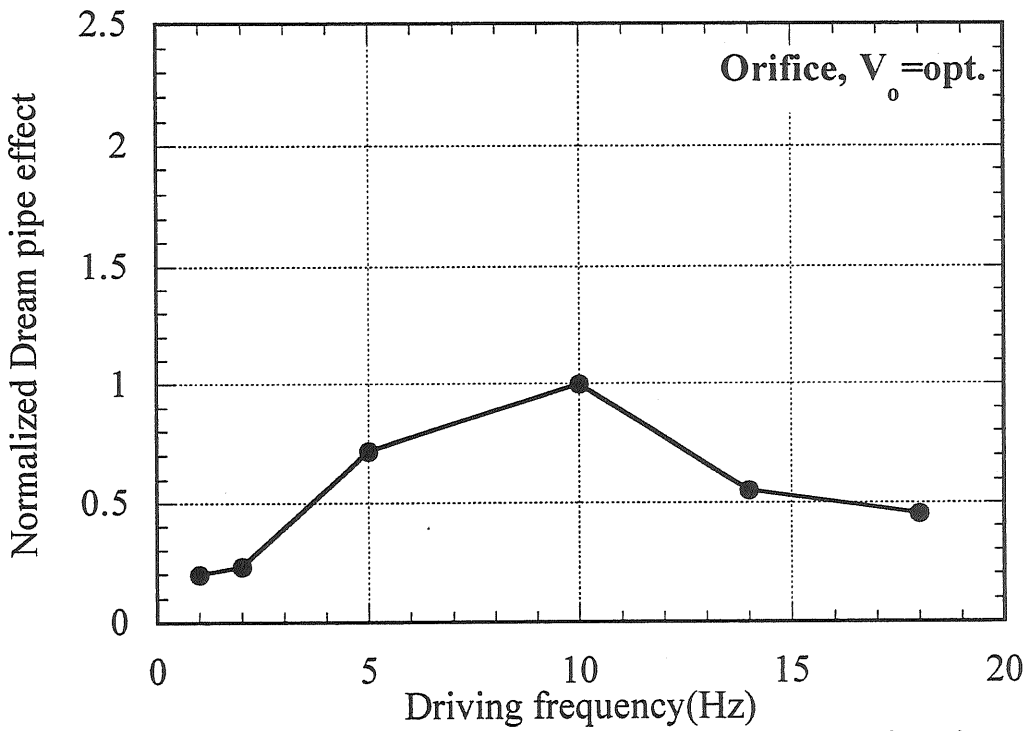

Figure 5-10. Normalized dream pipe effect as a function of driving frequency. The dream pipe effect is normalized by the value at 10 Hz and at V_o=0.36 turns. Pressure ratio; 1.4, mean gas pressure;1.4 MPa.

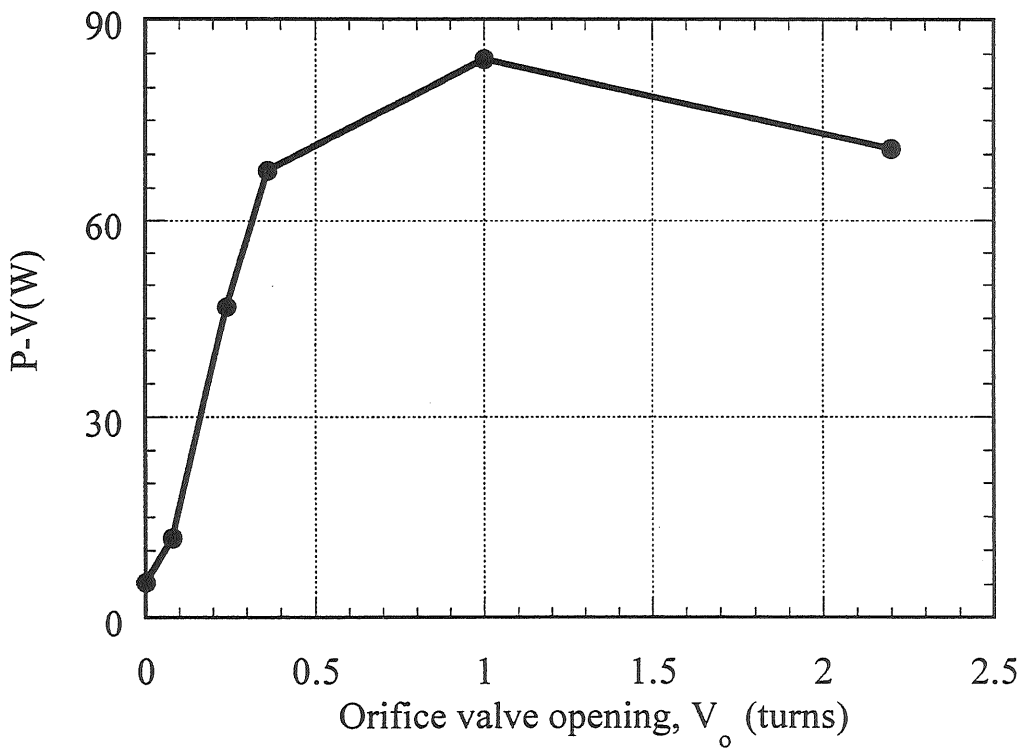

Figure 5-11. The variation of P-V work as a function of orifice valve opening at 10 Hz. The pressure ratio of 1.4, the mean gas pressure of 1.4 MPa.

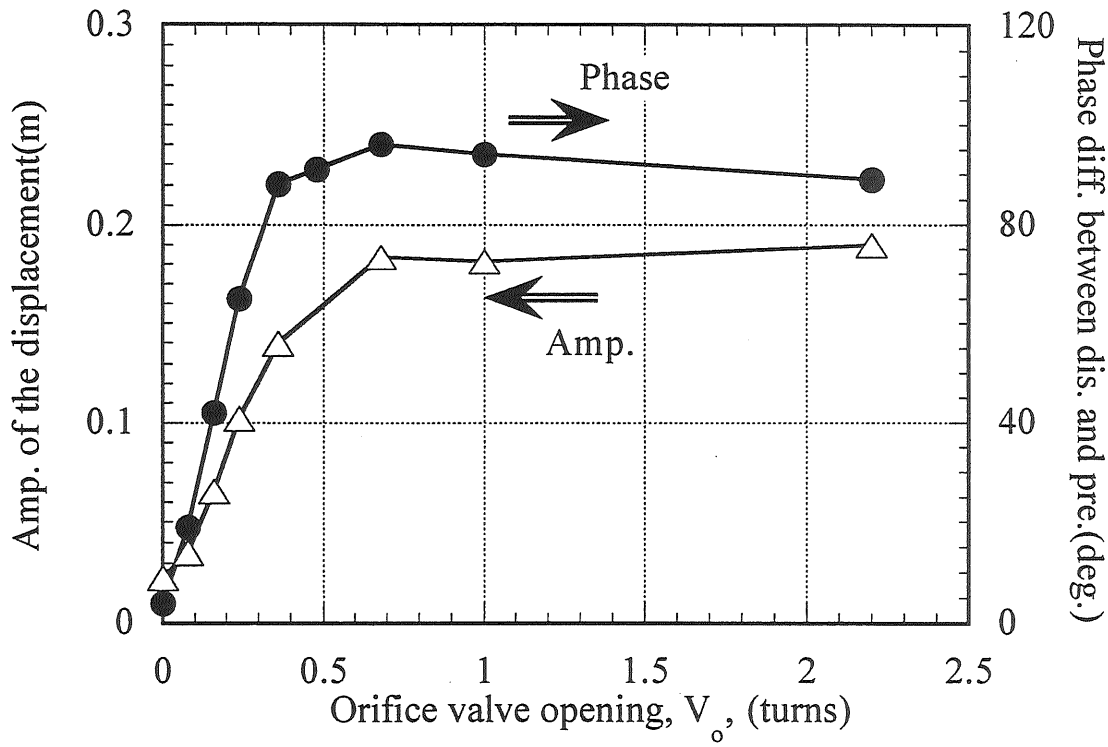

Figure 5-12. The amplitude of the gas displacement and the phase difference as a function of orifice valve opening at 10 Hz. The pressure ratio of 1.4, the mean gas pressure of 1.4 MPa.

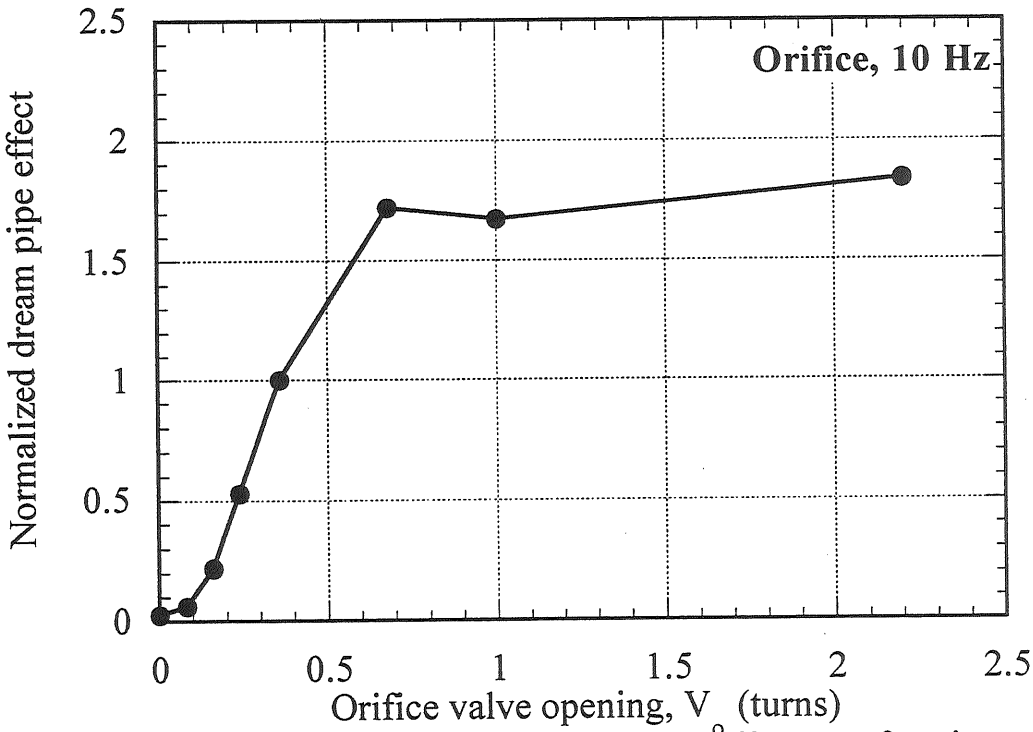

Figure 5-13. Normalized dream pipe effect as a function of orifice valve opening. The dream pipe effect is normalized by the value at 10 Hz and at V_o=0.36 turns.Pressure ratio;1.4, mean gas pressure;1.4 MPa.

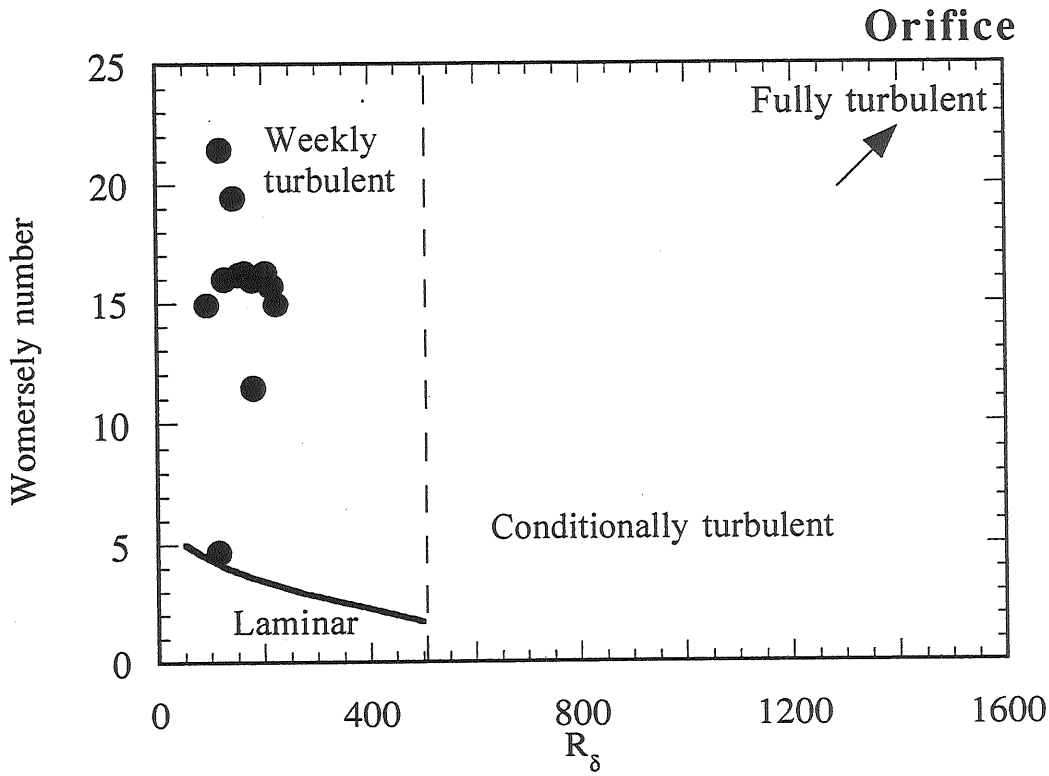

Figure 5-14. The stability diagram in the orifice type according to the result by Hino et al.

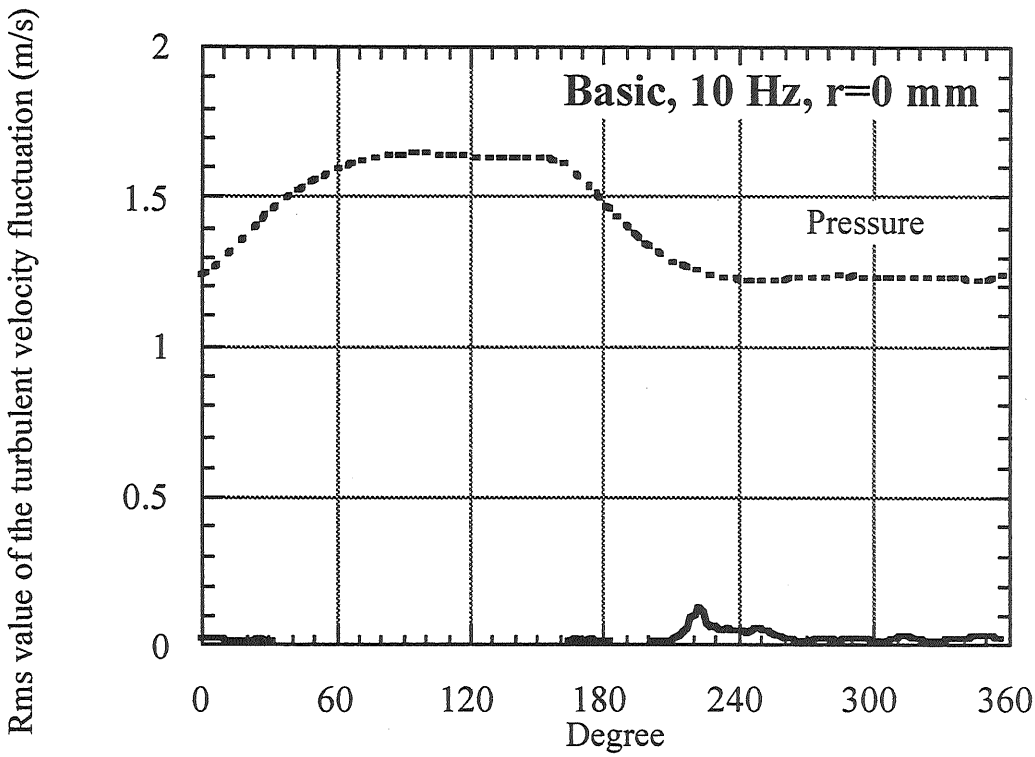

Figure 5-15-a. The r.m.s value at the hot end on the centerline in the basic type. The pressure variation in the pulse tube is also shown by dotted line. Pressure ratio; 1.4, mean gas pressure; 1.4 MPa.

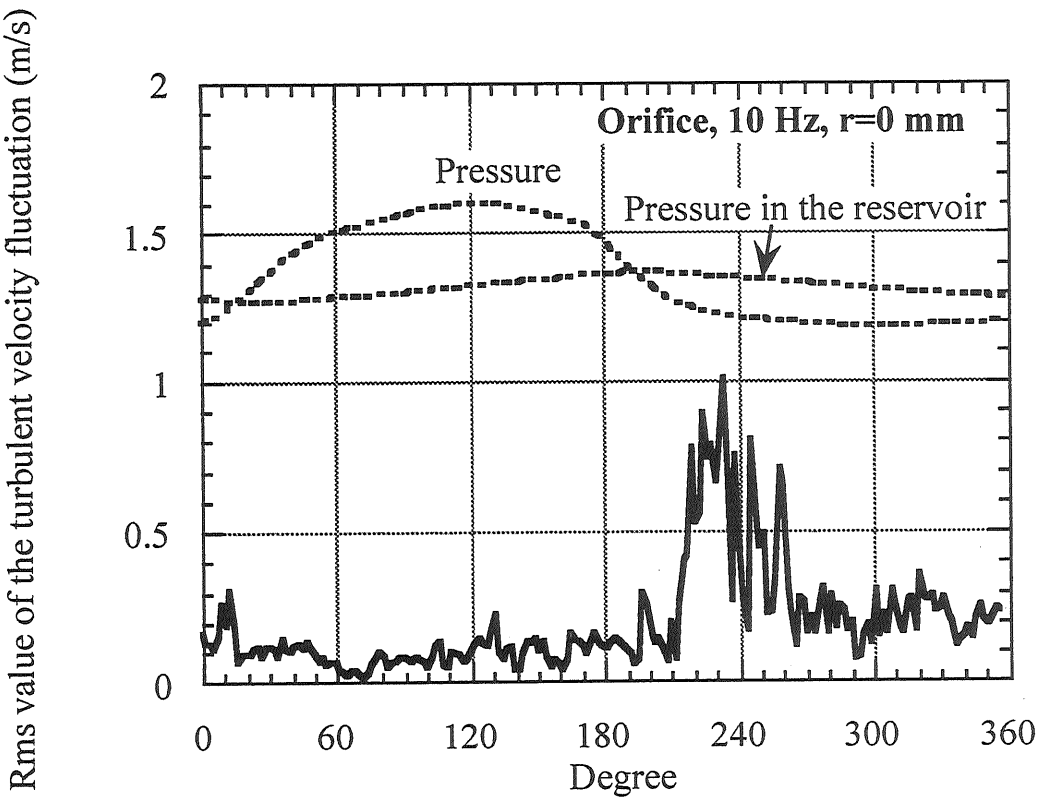

Figure 5-15-b. The r.m.s value at the hot end on the centerline in the orifice type. The pressure variation in the pulse tube is also shown by dotted line. Pressure ratio; 1.4, mean gas pressure; 1.4 MPa.

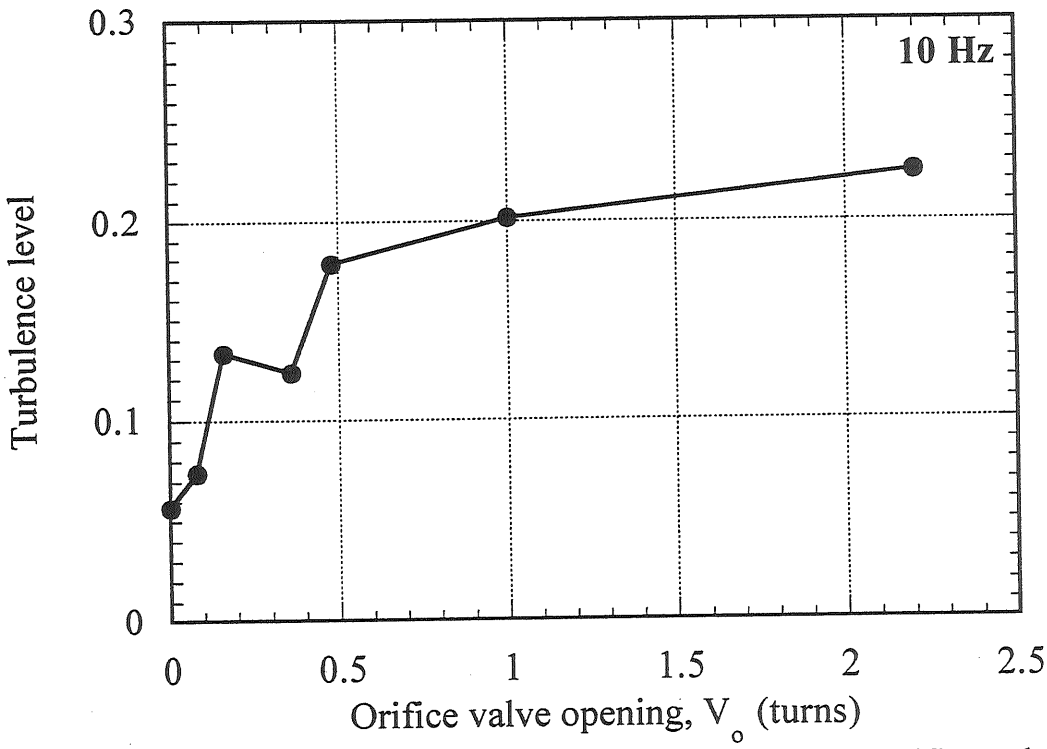

Figure 5-16. Turbulence level as a function of orifice valve opening, 10 Hz. The pressure ratio of 1.4, the mean gas pressure of 1.4 MPa.

Table 5-1. Summary of the dependencies of parameters on driving frequency.

Frequency	Attainable temperature	P-V work	Q_d
Region D-1	High	Small	Small
Region D-2 (5~10 Hz)	Low	Large	Large
(over 10 Hz)		Medium	Medium

Q_d : Dream pipe effect

Table 5-2. Summary of the dependencies of parameters on orifice valve opening.

V_o	Attainable temperature	P-V work	Q_d	Turbulence level
Region V_o-1	High	Small	Small	Small
Region V_o-2	Low	Large	Medium	Medium
Region V_o-3	Medium	Large	Large	Large

V_o : Orifice valve opening

Q_d : Dream pipe effect

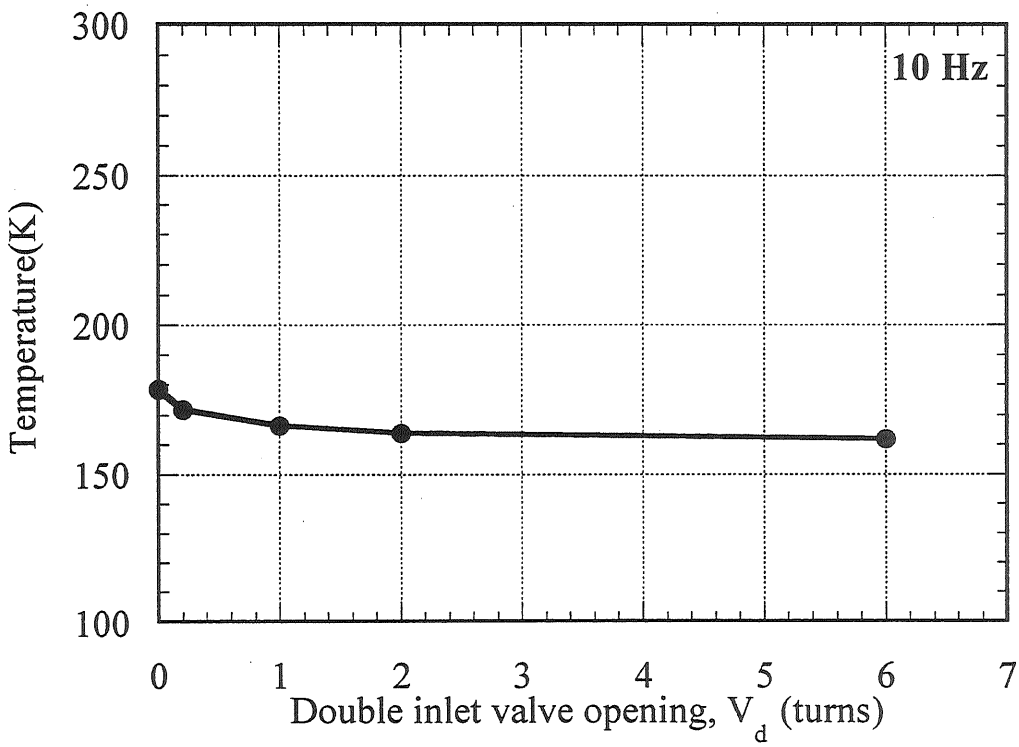

Figure 6-1. The attainable wall temperature as a function of double inlet valve opening. Pressure ratio;1.4, mean gas pressure;1.4 MPa, driving frequency;10 Hz.

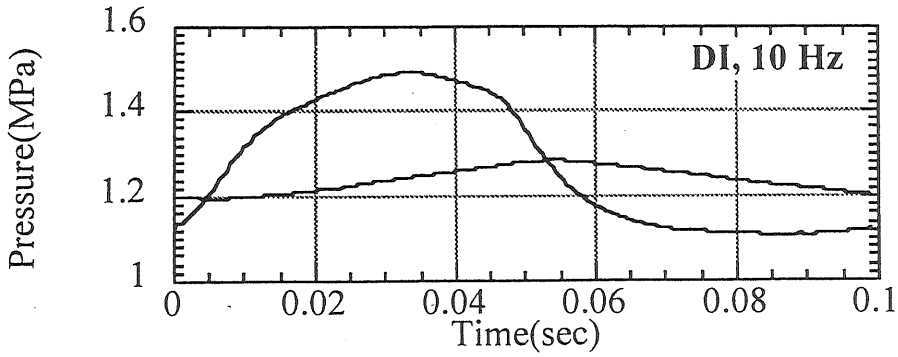

Figure 6-2-a.

Velocity **Temperature**

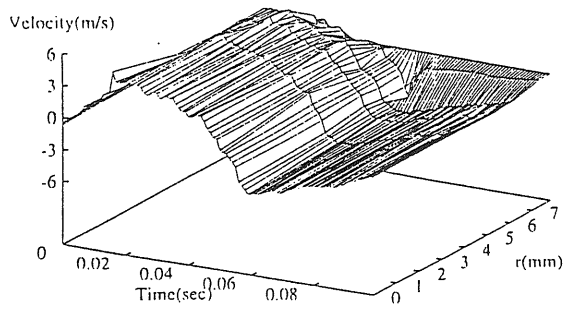

Figure 6-2-b..

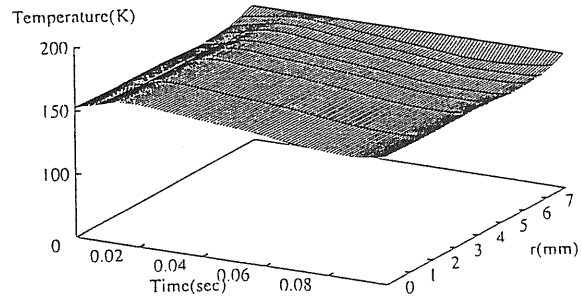

Figure 6-2-e..

Cold

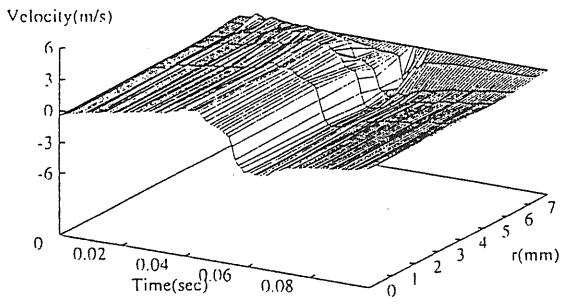

Figure 6-2-c.

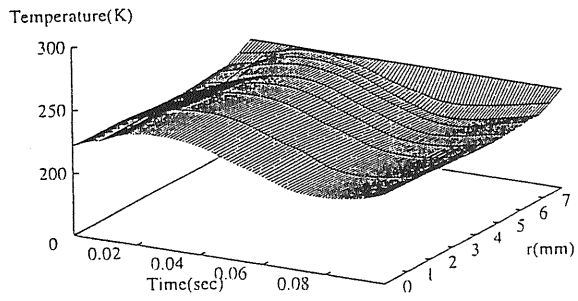

Figure 6-2-f.

Middle

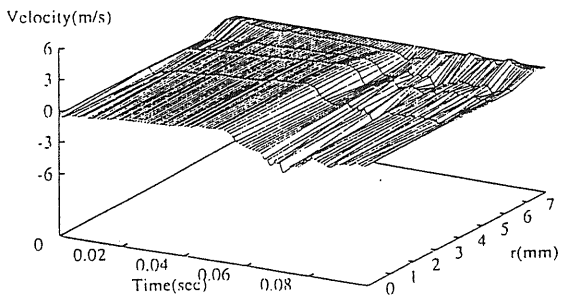

Figure 6-2-d.

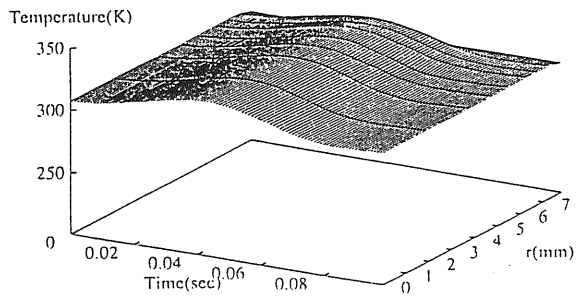

Figure 6-2-g.

Hot

Figure 6-2. Time variations of the radial distribution of the axial velocity and the temperature in the double inlet type; 10 Hz, V_o=0.36, V_d=2.

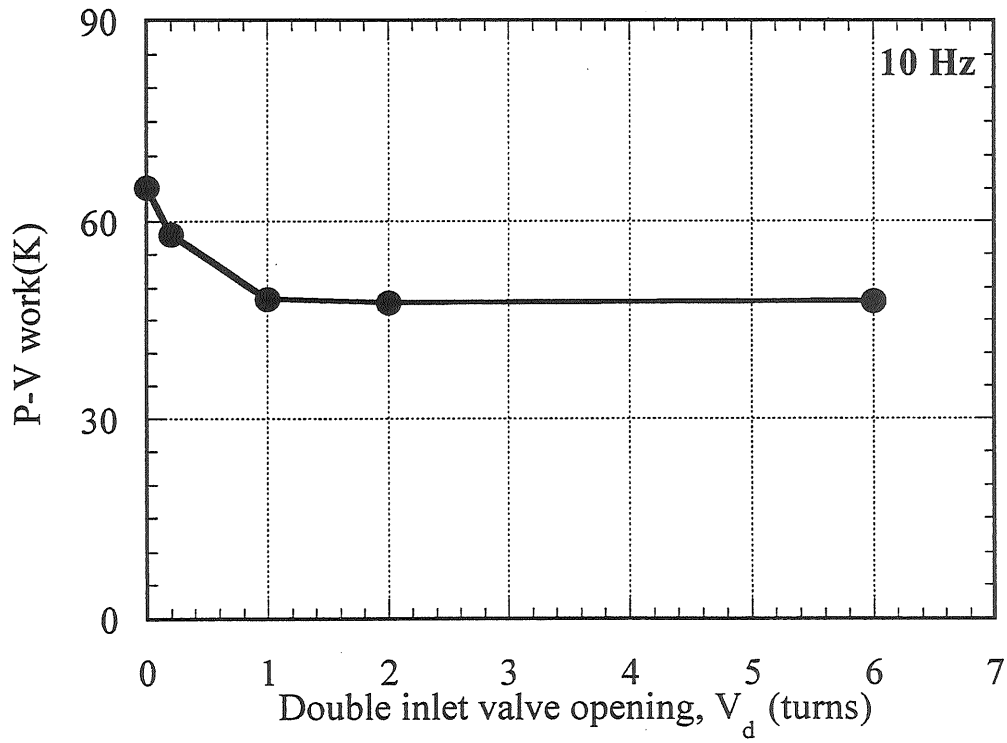

Figure 6-3. The variation of P-V work as a function of double inlet valve opening. Pressure ratio;1.4, mean gas pressure; 1.4 MPa, driving frequency;10 Hz.

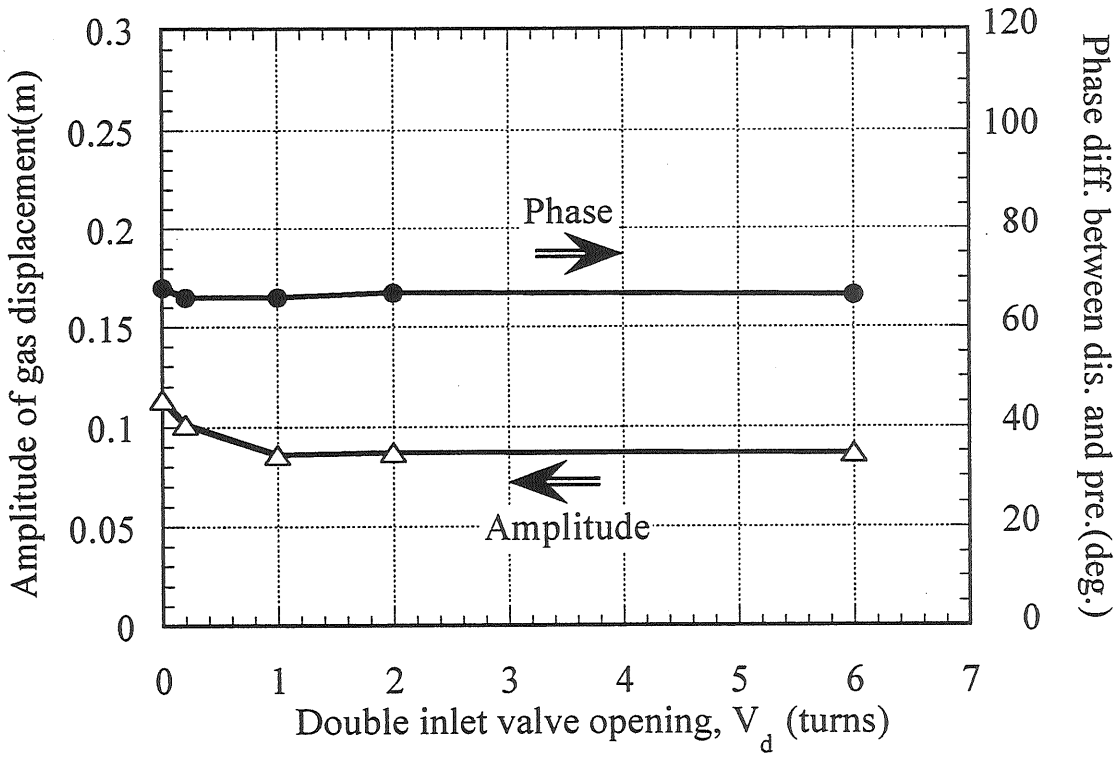

Figure 6-4. The amplitude of the gas displacement and the phase difference as a function of double inlet valve opening. Pressure ratio;1.4, mean gas pressure;1.4 MPa, driving frequency;10 Hz.

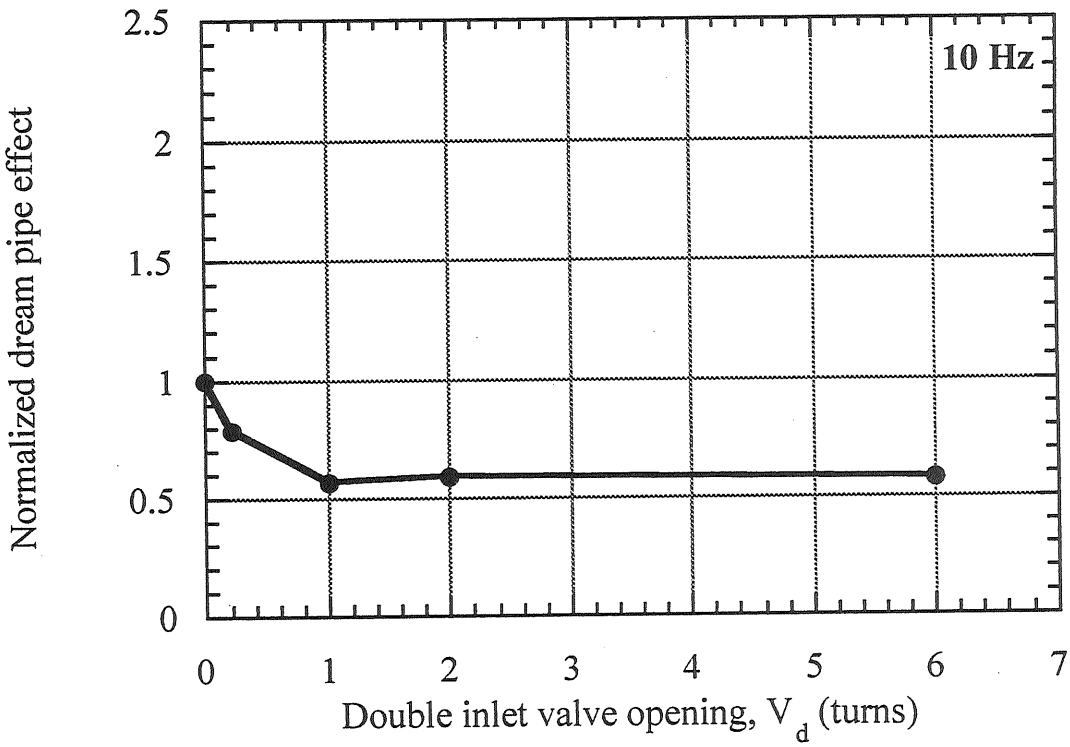

Figure 6-5. Normalized dream pipe effect as a function of double inlet valve opening. The reference is taken for the case of V_d=0, that is the effect for the orifice type.

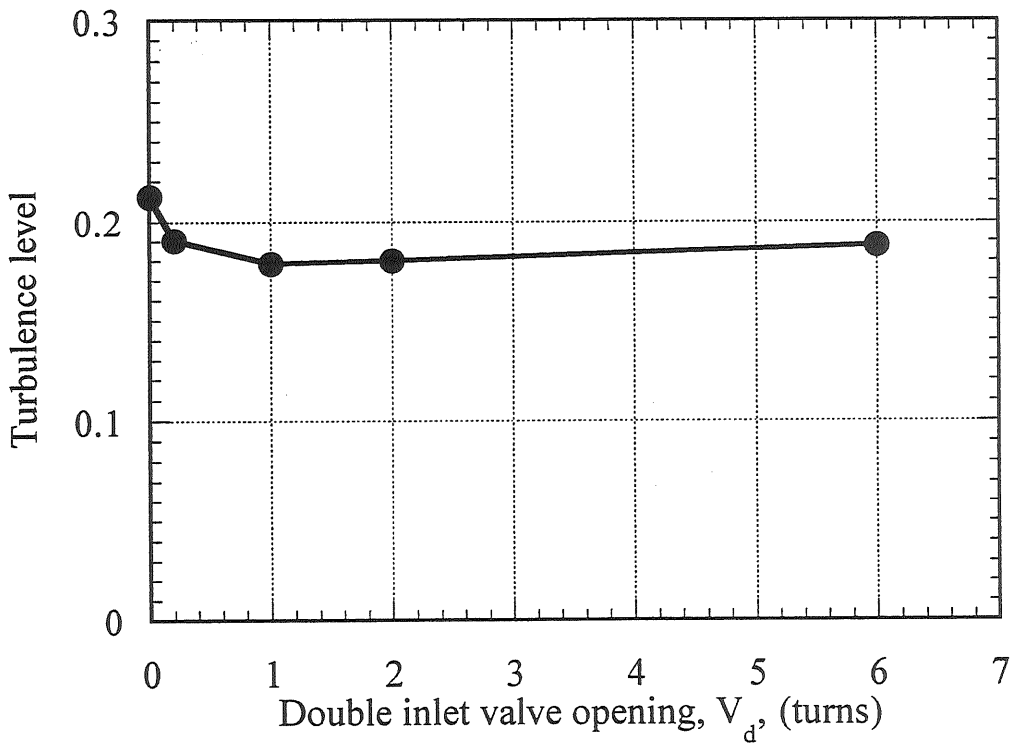

Figure 6-6. Turbulence level at the hot end as a function of double inlet valve opening. Pressure ratio;1.4, mean gas pressure;1.4 MPa, driving frequency;10 Hz.

Table 6-1. Summary of the defference in the refrigeration performance between the double inlet and the orifice types.

Type	Attainable temperature	P-V work	Q_d	Turbulence level
Orifice	High	Large	Large	Large
Double inlet	Low	Small	Small	Small

Q_d : Dream pipe effect